SISSA  ISAS

SCUOLA INTERNAZIONALE SUPERIORE DI STUDI AVANZATI
INTERNATIONAL SCHOOL FOR ADVANCED STUDIES

Improving molecular-dynamics simulations of simple ionic systems

Thesis submitted for the degree of
Doctor Philosophiæ

Candidate:
Paul Tangney

Supervisor:
Prof. Sandro Scandolo

October 2002

To my parents.

Contents

Chapter 1

Introduction

Although the fundamental interactions responsible for the macroscopic properties of materials have been known for some time, our ability to use this knowledge in order to quantitatively map microscopic properties onto macroscopic observables is still very limited. The goal of theoretical condensed matter physics is twofold : to understand microscopic mechanisms - the interactions of electrons and ions - and how they relate to experimental observables, and to quantitatively predict the properties of materials. Theory has had many successes in explaining experimentally observed phenomena and some notable failures. Good examples are the explanation, more than forty years ago, of the phenomenon of superconductivity in a wide class of materials as being the result of electron-phonon coupling[1] and the more recent failure of theorists to fully explain higher temperature superconductivity in a different class of materials despite intensive effort. The quantitative prediction of macroscopic properties is extremely desirable as it would allow the design of new materials which could be tailored to suit a specific purpose and it would also allow one to gain knowledge about materials under conditions inaccessible to experiment. However, despite very rapid progress in the field of materials modelling in the last thirty years, it has not yet developed to the point where it can proceed without recourse to empiricism or experimental verification.

The fundamental problem is that although we can state the principles by which electrons and ions interact, the nature of these interactions and the large number of such interactions present in real materials means that apart from extremely simple systems such as the isolated hydrogen atom it is not possible to solve the relevant equations in order to see how the macroscopic system behaves as a whole. It is necessary to use computers to help solve the many-body problem, but unfortunately despite enormous increases in computational power in the last three decades, it is simply not possible to solve the equations exactly except in an extremely limited number of cases. In fact, one can show that to solve exactly the Schrödinger equation in its standard form for even ten electrons is beyond any conceivable computer.

A more practical goal therefore is to re-express the many-body problem in a way which is easier to solve, by making reasonable approximations wherever possible. There are many different approaches to this and the best approach to use depends on a wide range of factors such as the material of interest, the conditions under which the material is to be

studied, the computational resources available and the man-hours required to implement the solution. Here the focus is on two of the most widely used approaches for atomistic materials modelling, namely, the molecular dynamics technique and density functional theory within the local or semilocal density approximations. Density functional theory (DFT)[2, 3] , which is discussed in more detail in chapter 4, allows one to calculate the ground-state probability density of a system of electrons in a given potential. As a result it may be used to calculate the energy and forces of a system of atoms which is large enough to approximate certain properties of the bulk material. Central to the application of this method is the use of what is known as the *local density approximation*, or LDA, which has produced very accurate results for a wide range of materials. The molecular dynamics (MD) technique was historically a tool for exploring the statistical mechanical behaviour of idealized systems. Given a known, or calculable interaction potential between a system of atoms it evolves the atoms in time according to the forces via Newton's equations of motion. Since most atoms are large enough to be considered classical particles, this allows one to model the behaviour of a system at arbitrary temperatures or pressures. The necessity of repeatedly calculating the forces between atoms has meant that the majority of molecular dynamics simulations have used very simplified phenomenological interaction potentials and that these simulations are qualitative rather than quantitative in nature.

In 1985, in a landmark paper[4], Car and Parrinello married density functional theory with molecular dynamics for the first time to allow the increased accuracy of the DFT interaction potential and the finite temperature real-time system evolution of MD in the same simulation. Now known simply as *Car-Parrinello Molecular Dynamics* (CPMD), this method has become one of the most widely used techniques for the calculation of dynamic and electronic properties of condensed matter with the original paper being cited many thousands of times to date. Although this method represents a vast improvement over the simplified potentials which existed beforehand, it is extremely computationally expensive relative to these potentials and even with a modern parallel supercomputer one is generally confined to system sizes of the order of one hundred atoms and simulation times of only a few picoseconds. This is a major problem as it severely limits the range of properties which one can calculate and the range of phenomena which can be simulated. The larger the system size that is simulated the closer one gets to the dimensions observed by experiment and to the human scale on which most materials are encountered. The longer that one can run a real-time simulation, the closer one gets to experimental time scales and to the human time scale of minutes, hours, days, and years on which materials are generally used. In practice simulation can never even approach the relevant size and timescales and it generally fails by many orders of magnitude in each case. However, the error introduced in this way can be minimized by having as large and as long a simulation as possible. For example, the larger and longer a simulation is the more precision one can achieve in the calculation of thermodynamic observables such as pressure, temperature or density. At present, the fact that CPMD and other DFT based MD techniques are so limited by computational expense means that the precision with which many properties are calculated is poor. On the other hand, simplified phenomenological potentials which allow increases in size and time scale of three to five orders of magnitude, provide a very poor description of interatomic interactions.

The practical goal of this thesis is to find a way in which the properties of bulk ionic systems under conditions of low symmetry and high temperatures and pressures can be predicted with accuracy and a reasonable degree of precision. The motivation for this work is the desire to be able to quantitatively simulate systems of geophysical interest such as the minerals that are found deep in the earth's mantle which are mostly ionic in nature. The extreme conditions of temperature and pressure make it very difficult for the properties of such minerals to be constrained by direct measurement and up to now the results of simulation have been of variable quality. Properties, such as the elastic properties of some of the major constituents of the earth's lower mantle[5, 6, 7], have been simulated with state-of-the-art first-principles methods. Although such simulations frequently have not been verified experimentally, it is likely that they are reasonably accurate. The range of problems that can be tackled in a purely first-principles way is very limited however. Other problems, a prime example being the melting behaviour of oxides under pressure, have been tackled with a range of force-fields in a molecular dynamics framework and the results have been extremely poor. An example, which will be discussed in detail in chapter 6 is the melting line of MgO. There have been at least five separate simulations of the pressure dependence of the melting temperature published. Of these, all have disagreed with experimental measurements of the slope of the zero-pressure melting curve by factors of between 2.5 and 8. There has also been little agreement between different simulations, even between those using the same method of calculating the slope. This level of disagreement clearly signifies problems with existing force-fields.

In this thesis we tackle the general problem of simulating ionic systems such as oxides under arbitrary thermodynamic conditions. Although we have a clear practical goal in mind, we approach the problem in a very general way and most of the methodology that is developed is applicable to almost any system for which accurate simulations of simple ionic systems are required.

We begin, in chapter 2 by looking in detail at Car-Parrinello molecular dynamics as the most widely used dynamical *ab initio* technique and discuss some theoretical issues which have not previously been fully addressed. We show that the standard understanding of the method is incomplete and we describe in a more rigorous way its theoretical underpinning. Most importantly, our theoretical investigations show that contrary to popular belief, the electronic orbitals do not take their ground-state values on average during a Car-Parrinello simulation. This means that there are errors intrinsic to the method and we show how these errors may be partially corrected for many systems, but particularly effectively for simple ionic systems.

The computational expense involved in *ab initio* molecular dynamics means that for most of the problems in which we are interested, an alternative solution is required. We would like to find a compromise between accuracy and precision in our calculations so that thermodynamic properties can be computed with more confidence than has been done in the past. The approach that we take to finding this compromise is to look for force-fields with functional forms which capture phenomenologically more of the dynamical electronic effects which contribute to interionic forces and which are therefore capable of providing more accuracy. The compromise lies in the fact that this capacity for improved accuracy

is generally at the expense of computational efficiency. The improved accuracy is achieved with a give functional form by using data from density functional theory simulations in a general and well-controlled parametrization procedure.

The problem of finding a good functional form for ionic systems is discussed in detail in chapter 3. Many force-fields over many years have been proposed for ionic systems but none of these fully meet the criteria that we set. All are either too simple to be accurate, too slow to be precise or too specific to be useful. We introduce a novel general force-field for ionic systems which is physically well motivated but orders of magnitude faster than CPMD.

In chapter 4 we build on previous work and describe how these force-fields are parametrized using first-principles data. The resulting force-field is shown in chapters 5 and 6 to provide thermodynamic and dynamic properties of an extremely high quality while still allowing the simulation of much larger systems over much longer timescales than can possibly be tackled within a fully first-principles approach. Our method is clearly shown to provide precision far surpassing that of *ab initio* methods and an accuracy far surpassing that of simple empirically-parametrized force-fields.

In chapter 6 this method is applied to the outstanding problem of the melting temperature of MgO under pressure.

Chapter 2

Car-Parrinello Molecular Dynamics

In 1985, in a seminal paper [4], Roberto Car and Michele Parrinello showed how it was possible to perform a molecular dynamics simulation whilst calculating the forces within density functional theory. In other words, the electrons were treated explicitly in an *ab initio* way in the calculation for the first time. The importance of this cannot be overstated. Even apart from the fact that density functional theory can be much more accurate than effective parameter-based force-fields, any MD simulation which does not treat electrons explicitly requires one to make a choice *a priori* about the nature of the system. We show in chapters 5 and 6 how it is possible to make very good effective force-fields for ionic systems. However, if the bonding in the system changes due to changes in pressure, temperature or phase, the accuracy of the force-field suffers. Moreover, we are biasing the system from the start by the phenomenology that we include in the potential form, and apart from the ingredients that we include, nothing else can play a role. Physics and chemistry are full of surprises and many effects and structures occur due to delicate balances between many different factors. It is simply not possible to predict with any degree of certainty *a priori* what effects may become important under a given set of conditions.

Explicitly treating the electrons means that, in principle, one does not make assumptions about the bonding of the system and this allows surprises to occur. Spontaneous changes in bonding can take place without loss of accuracy. This means that one can simulate changes of phase with much more confidence. *Ab initio* molecular dynamics can also allow one to model chemical reactions. This is something that effective force fields are unable to do because, by definition, chemical reactions involve changes in the bonding and when they occur it is the electrons which play the dominant role. Unless the dependence of electrons on ionic positions is explicitly calculated, the reaction cannot be modeled.

The method of Car and Parrinello, in its original and most widely used form, works within the Born-Oppenheimer approximation. This means that at any instant the state of the electronic system can be well described by the electronic ground-state calculated for the ionic positions at that instanti and that it responds instantaneously to changes in ionic positions. For many systems this is an extremely good approximation given the mass of the electron relative to that of the ions, which for hydrogen, the lightest element, is approximately 1/1836. When the electronic ground-state is close to degenerate, which

frequently occurs, it can be said that the Born-Oppenheimer approximation breaks down. However it should be valid before and after the occurrence of such degeneracies and the time during which degeneracies are relevant is generally small.

The Car-Parrinello MD method started the field of *ab initio* molecular dynamics and remains the most widely used method for coupling density functional theory with molecular dynamics. It is not the only method however. A number of other techniques[8, 9, 10, 11] have been developed which are based on minimization of the electronic (Kohn-Sham [3]) orbitals to their ground state at each time step. These techniques will be referred to from now on as Born-Oppenheimer (BO) methods to distinguish them from the Car-Parrinello (CP) method which does not put the orbitals to their ground state at each time step, as we will see below.

Despite widespread application of the CP method to many areas of physics, chemistry and biology and despite rapid development of many aspects of the methodology, no serious testing of the accuracy of the method has ever been published to our knowledge. A number of people [4, 12, 13], including the inventors of the method, have shown that it reproduces ground-state forces and energies in simple systems, such as toy-models of crystalline silicon or germanium, extremely well, but silicon and germanium are particularly easy systems to treat with most electronic structure methods, and the ability to achieve high accuracy for these systems is no guarantee that the method works well in other systems.

In this chapter, we begin by explaining the Car-Parrinello method in detail and some of the reasons that it is generally believed to work. The understanding of the method has evolved somewhat since its introduction and so no effort will be made to present the *definitive* version of current understanding, rather some commonly held beliefs will be presented. Next, some theoretical problems with the method will be explained and a partial solution of these problems for inert ionic systems will be presented. We then test the theoretical ideas that have been developed with the simple examples of silicon and MgO, followed by a test of the method on one of the most frequently studied systems, i.e. water, or in this case "heavy" ice.

2.1 The Car-Parrinello Method

The Car-Parrinello method makes use of the following classical lagrangian :

$$\mathcal{L}_{CP} = \sum_i \mu_i \langle \dot{\psi}_i | \dot{\psi}_i \rangle + \frac{1}{2} \sum_I M_I \dot{\mathbf{R}}_I^2 - E[\{\psi_i\}, \{\mathbf{R}_I\}] \tag{2.1}$$

to generate trajectories for the ionic and electronic degrees of freedom via the coupled set of equations of motion

$$\mathrm{M}_I \ddot{R}_I^\alpha = -\frac{\partial E[\{\psi_i\}, \{\mathbf{R}_I\}]}{\partial R_I^\alpha} = F_{CP_I}^\alpha \tag{2.2}$$

$$\mu_i |\ddot{\psi}_i\rangle = -\frac{\delta E[\{\psi_i\}, \{\mathbf{R}_I\}]}{\delta \langle \psi_i |} \tag{2.3}$$

where M_I and $\mathbf{R}_I$ are the mass and position respectively of atom I, $|\psi_i\rangle$ are the Kohn-Sham orbitals which are allowed to evolve as classical degrees of freedom with inertial

parameters μ_i, and $E[\{\psi_i\},\{\mathbf{R}_I\}]$ is the Kohn-Sham energy functional[3] evaluated for the set of ionic positions $\{\mathbf{R}_I\}$ and the set of orbitals $\{\psi_i\}$. The functional derivative of the Kohn-Sham energy in equation 2.3 is implicitly restricted to variations of $\{\psi_i\}$ that preserve orthonormality.

The idea behind the method is that by putting the electrons to their ground state at a fixed set of ionic positions and then allowing the ions to move according to equation 2.2, the electronic orbitals should adiabatically follow the motion of the ions, performing small oscillations about the electronic ground state. The electronic orbitals will have a "fictitious" kinetic energy associated with their motion and the fictitious mass parameter μ_i. If μ_i is small enough then the motion of the orbitals will be very fast relative to the motion of the ions. It is generally thought that this motion consists of oscillations about the ground state and so by choosing a small enough value for μ_i one can ensure that the frequency spectra of the electronic orbitals and the ions are well separated from one another if there exists an energy gap between the occupied and unoccupied Kohn-Sham orbitals. This is because, within a harmonic approximation, the lowest frequency of oscillation of the orbitals about the ground state may be written as[12]

$$\omega_0 = \left(\frac{2(\epsilon_j - \epsilon_i)}{\mu_i} \right)^{1/2} \tag{2.4}$$

where ϵ_i and ϵ_j are the eigenvalues of the highest occupied and the lowest unoccupied orbitals respectively. In classical mechanics, systems which are well separated from one another in frequency can be shown to remain energetically isolated from one another (see ref.[12] and[14] and references therein). Therefore, it has been thought that by using a small enough value for μ_i, one could isolate the electrons energetically from the ions. In this way one could ensure that thermalization does not occur between electrons and ions and so the electronic orbitals remain at a low temperature, which means that they remain close to the electronic ground state.

This explanation of the method was originally proposed by Pastore et al. [12] and is the standard way in which the method is explained (see, for example, the recent review by Marx and Hütter [13]). Although parts of this explanation are true , it ignores the fact that, aswell as the high-frequency oscillations, the orbitals have a slow component to their motion. If the ions are moving, the motion of the orbitals contains a component due to the unavoidable response of the electronic orbitals to the ionic dynamics : as ions move, the ground state changes. By definition this latter motion occurs on ionic timescales and with ionic frequencies and so it may not be decoupled from the ionic motion. In fact, it will be shown in this chapter that due to this aspect of the electronic motion the electrons do not oscillate about the ground state but about an equilibrium which is displaced from it. This means that there are systematic errors in the forces on the ions and in the total stress on the system.

2.2 Car-Parrinello Dynamics Compared to Born-Oppenheimer Dynamics

We wish to compare CP dynamics to the *exact* BO dynamics. In other words, the dynamics of the ions when the electronic orbitals remain at their ground state. For this purpose, we decompose the CP orbitals as

$$|\psi_i\rangle = |\psi_i^{(0)}\rangle + |\delta\psi_i\rangle \tag{2.5}$$

where $|\psi_i^{(0)}\rangle$ are the ground state (BO) orbitals which are uniquely defined for given ionic coordinates as those that minimize $E[\{\psi_i\},\{\mathbf{R}_I\}]$. This allows us to consider separately the evolution of the instantaneous electronic ground state and the deviations of the CP orbitals from that ground state.

At this point we note that in the past some testing of the CP method[15, 16] has relied on demonstrating that the total electronic energy calculated with the CP method is very close to that calculated when the electronic orbitals take their ground state values. This is not a good criterion to use to validate the method. For molecular dynamics simulations, the important quantites are the *forces* on the ions. For a given deviation of the CP orbitals from the ground state $|\delta\psi_i\rangle$ the error in the force relative to the size of the force is generally much bigger than the error in the energy relative to the size of the energy. This can easily be seen by writing both of these quantities as Taylor expansions about their ground state values

$$\frac{\Delta E}{E} = \sum_i \frac{1}{E}\left(\frac{\delta E}{\delta|\psi_i\rangle}\bigg|_{\{\psi_i^{(0)}\}}|\delta\psi_i\rangle + \langle\delta\psi_i|\frac{\delta E}{\delta\langle\psi_i|}\bigg|_{\{\psi_i^{(0)}\}}\right) + order(\delta\psi_i^2) \tag{2.6}$$

$$\frac{\Delta F_I^\alpha}{F_I^\alpha} = \sum_i \frac{1}{F_I^\alpha}\left(\frac{\delta F_I^\alpha}{\delta|\psi_i\rangle}\bigg|_{\{\psi_i^{(0)}\}}|\delta\psi_i\rangle + \langle\delta\psi_i|\frac{\delta F_I^\alpha}{\delta\langle\psi_i|}\bigg|_{\{\psi_i^{(0)}\}}\right) + order(\delta\psi_i^2) \tag{2.7}$$

The first term on the right hand side of equation 2.6 disappears because the derivative is evaluated at the ground state. However the first term on the right hand side of equation 2.7 does not disappear. So, for a given deviation of the electronic orbitals from the ground state the error in the force depends to first order on the $\{\delta\psi_i\}$ but the error in the energy only depends to second order on $\{\delta\psi_i\}$. This means that any error in the orbitals has a much larger effect on the forces than it does on the energies. How much greater the relative error in the forces is than the relative error in the energies depends on the system, but, as will be discussed in section 2.4.3, it can be a few orders of magnitude. When testing the method it is therefore important to see how well the *forces* reproduce the Born-Oppenheimer forces.

We now write

$$|\dot{\psi}_i^{(0)}\rangle = \sum_I \dot{R}_I^\alpha \frac{\partial|\psi_i^{(0)}\rangle}{\partial R_I^\alpha} \tag{2.8}$$

and

$$|\ddot{\psi}_i^{(0)}\rangle = \sum_I \ddot{R}_I^\alpha \frac{\partial|\psi_i^{(0)}\rangle}{\partial R_I^\alpha} + \sum_{I,J} \dot{R}_I^\alpha \dot{R}_J^\beta \frac{\partial^2|\psi_i^{(0)}\rangle}{\partial R_J^\beta \partial R_I^\alpha} \tag{2.9}$$

A preliminary interesting observation now follows. If the electronic orbitals are at their ground state values, i.e. $|\delta\psi_i\rangle = |0\rangle$, then the right hand side of equation 2.3 vanishes since $\{\psi_i\} = \{\psi_i^{(0)}\}$. However, the left hand side does not by virtue of equation 2.9. So the CP orbitals cannot take their ground state values unless μ vanishes too. As a consequence of this, the ionic dynamics is affected by a bias dependent on μ and, as we will see, to the strength of the electron-ion interaction .

We now wish to explore the consequences that such a departure from the ground state has on the instantaneous CP forces F_{CP}. We therefore calculate how CP forces deviate from the BO forces F_{BO} at a given point in phase space along the CP trajectory. We may write, for the α-th cartesian component of the force on atom I:

$$\begin{aligned} -F^{\alpha}_{CP_I} &= \frac{\partial E[\{\mathbf{R}_I\};\{\psi_i\}]}{\partial R^{\alpha}_I} \\ &= \frac{dE[\{\mathbf{R}_I\};\{\psi_i\}]}{dR^{\alpha}_I} - \sum_i \left(\frac{\delta E[\{\mathbf{R}_I\};\{\psi_i\}]}{\delta|\psi_i\rangle} \frac{\partial|\psi_i\rangle}{\partial R^{\alpha}_I} \right. \\ &+ \left. \frac{\partial\langle\psi_i|}{\partial R^{\alpha}_I} \frac{\delta E[\{\mathbf{R}_I\};\{\psi_i\}]}{\delta\langle\psi_i|} \right) \end{aligned} \tag{2.10}$$

Substitution of equation 2.3 yields

$$-F^{\alpha}_{CP_I} = \frac{dE[\{\mathbf{R}_I\};\{\psi_i\}]}{dR^{\alpha}_I} - \sum_i \mu_i \left(\langle\ddot{\psi}_i| \frac{\partial|\psi_i\rangle}{\partial R^{\alpha}_I} + \frac{\partial\langle\psi_i|}{\partial R^{\alpha}_I} |\ddot{\psi}_i\rangle \right) \tag{2.11}$$

Using the expansion

$$\begin{aligned} \frac{dE[\{\mathbf{R}_I\};\{\psi_i\}]}{dR^{\alpha}_I} &= \frac{d}{dR^{\alpha}_I} \left\{ E[\{\mathbf{R}_I\};\{\psi_i\}] \Big|_{\{\psi_i^{(0)}\}} \right. \\ + \sum_i \left(\frac{\delta E[\{\mathbf{R}_I\};\{\psi_i\}]}{\delta|\psi_i\rangle}\Big|_{\{\psi_i^{(0)}\}} |\delta\psi_i\rangle \right. &+ \left. \left. \langle\delta\psi_i| \frac{\delta E[\{\mathbf{R}_I\};\{\psi_i\}]}{\delta\langle\psi_i|}\Big|_{\{\psi_i^{(0)}\}} \right) + order(\delta\psi_i^2) \right\} \\ &= -F^{\alpha}_{BO_I} + 0 + order(\delta\psi_i^2) \end{aligned} \tag{2.12}$$

we can write the error in the CP force as

$$\Delta F^{\alpha}_I = F^{\alpha}_{CP_I} - F^{\alpha}_{BO_I} = \sum_i \mu_i \left(\langle\ddot{\psi}_i| \frac{\partial|\psi_i\rangle}{\partial R^{\alpha}_I} + \frac{\partial\langle\psi_i|}{\partial R^{\alpha}_I} |\ddot{\psi}_i\rangle \right) + order(\delta\psi_i^2) \tag{2.13}$$

Having established the connection, to first order in $\delta\psi_i$, between the CP and the BO forces, we assume adiabatic decoupling and look for contributions to this difference that do not vanish when averaged over time scales longer than the typical timescales of the high frequency part of the fictitious dynamics of the electrons (τ_e) but shorter than the time scales of the ionic dynamics (τ_i). Only these contributions are expected to contribute significantly to the ionic dynamics[12]. To this end we write

$$|\delta\psi_i\rangle = |\delta\psi_i^{(1)}\rangle + |\delta\psi_i^{(2)}\rangle \tag{2.14}$$

where we have split $\delta\psi_i$ into a term which has a very high frequency relative to ionic frequencies ($\delta\psi_i^{(1)}$) and a term which varies on ionic timescales ($\delta\psi_i^{(2)}$) We rewrite equation 2.3, using equation 2.5, as

$$|\ddot{\psi}_i\rangle = |\delta\ddot{\psi}_i^{(1)}\rangle + |\delta\ddot{\psi}_i^{(2)}\rangle + \sum_I \ddot{R}_I^\alpha \frac{\partial|\psi_i^{(0)}\rangle}{\partial R_I^\alpha} + \sum_{I,J} \dot{R}_I^\alpha \dot{R}_J^\beta \frac{\partial^2|\psi_i^{(0)}\rangle}{\partial R_J^\beta \partial R_I^\alpha} \tag{2.15}$$

Since we are concerned with what happens on ionic timescales, i.e. averaged over the high-frequency component of the ψ_i, we may neglect the first term on the right-hand side.

Using equation 2.13 and equation 2.15 we may write the error in the force to first order in $\delta\psi_i$ as

$$\Delta F_I^\alpha = 2\sum_i \mu_i \Re\left\{ \left(\langle\ddot{\psi}_i^{(2)}| + \sum_J \ddot{R}_J^\beta \frac{\partial\langle\psi_i^{(0)}|}{\partial R_J^\beta} + \sum_{J,K} \dot{R}_J^\beta \dot{R}_K^\gamma \frac{\partial^2\langle\psi_i^{(0)}|}{\partial R_K^\gamma \partial R_J^\beta} \right) \left(\frac{\partial|\psi_i^{(0)}\rangle}{\partial R_I^\alpha} + \frac{\partial|\psi_i^{(2)}\rangle}{\partial R_I^\alpha} \right) \right\} \tag{2.16}$$

Any deviation $\delta\psi_i$ from the ground state depends on the fictitious mass μ since $\mu \to 0 \implies \frac{\delta E}{\delta\langle\psi_i|} \to 0$ via equation 2.3. This means that if we are to consider only terms which depend purely to linear order on μ then the terms involving $\delta\psi_i^{(2)}$ in equation 2.16 may be neglected.

To summarise : If we consider the dynamics of the electronic orbitals to consist of an adiabatic response of the electronic orbitals to the ionic dynamics and an independent fast oscillating part then, under the assumption that the timescales of the fast component are much shorter than the shortest time period in the ionic system, i.e. assuming adiabatic decoupling, the average error in the Car-Parrinello forces to first order in μ and $\delta\psi_i$ is given by (using equations 2.20 and 2.9)

$$\Delta F_I^\alpha = 2\sum_i \mu_i \Re\left\{ \sum_J \ddot{R}_J^\beta \frac{\partial\langle\psi_i^{(0)}|}{\partial R_I^\alpha} \frac{\partial|\psi_i^{(0)}\rangle}{\partial R_J^\beta} + \sum_{J,K} \dot{R}_J^\beta \dot{R}_K^\gamma \frac{\partial\langle\psi_i^{(0)}|}{\partial R_I^\alpha} \frac{\partial^2|\psi_i^{(0)}\rangle}{\partial R_K^\gamma \partial R_J^\beta} \right\} \tag{2.17}$$

This correction varies on ionic time scales and therefore does not necessarily average out as the usual "fast" component does. However, its value depends on the electronic mass. This implies that a simple way to ensure that its contribution in a CP simulation is negligible consists of reducing systematically the electronic mass. Although a smaller μ implies a smaller time step for the integration of the CP equations of motion, the time step scales as $\Delta t \sim \mu^{1/2}$, which means that reducing μ by an order of magnitude brings about a computational overhead of only a factor of three. A more quantitative discussion is presented in sections IV and V.

We also notice that if the term proportional to $\dot{R}\dot{R}$ in the r.h.s. of equation 2.17 vanishes (e.g. by symmetry, see below), and the tensor in the term proportional to $\ddot{R}$ is constant, then the correction of equation 2.17 reduces to a rescaling of the atomic masses, which is known to leave thermodynamics intact. This is discussed in more detail in the next section.

2.3 The Rigid Ion Approximation.

In order to gain insight into the scale of this problem with the CP forces we consider the simple example of rigid ions. We assume that each electron is localised around an ion and that there is no distortion of a particular ion's charge distribution as it moves in the field of the other ions. We can refer each wavefunction ψ_i to a particular ion as follows

$$\psi_i(\mathbf{r}) = \phi_{I\eta}(\mathbf{r} - \mathbf{R}_I) \tag{2.18}$$

Where the electronic states are labelled by an ion index, I, and the index η labelling the electronic state of the ion . The rigidity of the ionic charge distribution means that

$$\frac{\partial \phi_{I\eta}(\mathbf{r} - \mathbf{R}_I)}{\partial \mathbf{R}_I} = -\frac{\partial \phi_{I\eta}(\mathbf{r} - \mathbf{R}_I)}{\partial \mathbf{r}} \qquad \text{and} \qquad \frac{\partial \phi_{I\eta}(\mathbf{r} - \mathbf{R}_I)}{\partial \mathbf{R}_J} = 0 \qquad \forall J \neq I \tag{2.19}$$

Equation 2.17 becomes

$$\begin{aligned} \Delta F_I^\alpha &= 2\sum_\eta \mu_\eta \Re\Big\{ \ddot{R}_I^\beta \int \frac{\partial \phi^*_{I\eta}(\mathbf{r} - \mathbf{R}_I)}{\partial r^\alpha} \frac{\partial \phi_{I\eta}(\mathbf{r} - \mathbf{R}_I)}{\partial r^\beta} d\mathbf{r} \\ &+ \dot{R}_I^\beta \dot{R}_I^\gamma \int \frac{\partial \phi^*_{I\eta}(\mathbf{r} - \mathbf{R}_I)}{\partial r^\alpha} \frac{\partial^2 \phi_{I\eta}(\mathbf{r} - \mathbf{R}_I)}{\partial r^\gamma \partial r^\beta} d\mathbf{r} \Big\} \end{aligned} \tag{2.20}$$

The second term in equation 2.20 vanishes due to symmetry, at least assuming an atomic charge density with spherical symmetry. The first term may be written in terms of $E_k^{I\eta}$ the quantum electronic kinetic energy of an electron in state η of atom I as

$$2\sum_\eta \mu_\eta \Re\Big\{ \ddot{R}_I^\beta \int \frac{\partial \phi^*_{I\eta}(\mathbf{r} - \mathbf{R}_I)}{\partial r^\alpha} \frac{\partial \phi_{I\eta}(\mathbf{r} - \mathbf{R}_I)}{\partial r^\beta} d\mathbf{r} \Big\} = -\frac{2m_e}{3\hbar^2} \ddot{R}_I^\alpha \sum_\eta \mu_\eta E_k^{I\eta} \tag{2.21}$$

where m_e is the (real) mass of an electron. Since the ions are rigid the quantum kinetic energy associated with each one is a constant and equation 2.20 becomes

$$\Delta F_I^\alpha = -\Delta M_I \ddot{R}_I^\alpha \tag{2.22}$$

with

$$\Delta M_I = \frac{2m_e}{3\hbar^2} \sum_\eta \mu_\eta E_k^{I\eta} \tag{2.23}$$

In this case the ionic positions and velocities are updated during a Car-Parrinello simulation according to

$$(M_I + \Delta M_I)\ddot{R}_I^\alpha = F^\alpha_{BO_I} \tag{2.24}$$

In other words, for systems where the rigid ion approximation is valid, the CP approximation amounts simply to a rescaling of the ionic masses. Since the classical partition function depends only on the interaction potential, the thermodynamics of the system as calculated with a CP dynamics is identical to the thermodynamics of the BO system. The definition of temperature will however be affected, because if the actual ionic dynamics in

CP is given by equation 2.24, then the real temperature at which the system equilibrates, at least in the case of a microcanonical dynamics for the ions, is given by

$$k_B T = \frac{1}{3N} \sum_{I,\alpha} (M_I + \Delta M_I) \langle (v_I^\alpha)^2 \rangle \tag{2.25}$$

where $\langle \cdots \rangle$ signifies the average over time and N is the number of atoms. This differs from the standard definition by the addition of a term proportional to ΔM_I. The additional term in equation 2.25 can be readily traced to the additional inertia caused by the rigid dragging of the electronic orbitals. In fact, using equations 2.8 and 2.19, we can show that this term coincides, within the rigid ion model, with the fictitious electronic kinetic energy, when the contribution from the dynamics of the $\delta\psi_i$ is negligible i.e.

$$T_{el} = T_{\Delta M} \tag{2.26}$$

where

$$T_{el} = \sum_i \mu_i \langle \dot{\psi}_i | \dot{\psi}_i \rangle \tag{2.27}$$

and

$$T_{\Delta M} = \frac{1}{2} \sum_{I,\alpha} \Delta M_I \langle (v_I^\alpha)^2 \rangle \tag{2.28}$$

In other words if the electronic orbitals move rigidly with the ions the actual inertia of the ions in a CP simulation can be obtained by adding to the "bare" ionic inertia the inertia carried by the electronic orbitals. This result has been pointed out previously [17, 18] and ionic masses are commonly renormalized when dynamical quantities are being investigated.

Figure 2.29 illustrates how, within the simplified rigid-ion model, the ionic inertia depends on the kinetic energy of the electrons. For a given ionic velocity, the wavefunction at a point in space has to change more quickly when it is highly localised (and therefore with a high quantum kinetic energy) than when it is extended. To accelerate an ion one also needs to increase the rate of change of the wavefunction localised on it. Since the wavefunction carries an inertia (μ) the effective inertia of the ion is greater than the bare ionic mass. In more general (non-rigid-ion) situations, the collective movement of the ions is affected by the requirement that the "heavy" electronic wavefunctions are rearranged as the system evolves.

We now explore the consequences that such a modification of the ionic inertia has on typical observables extracted from CP simulations. First, as already mentioned, the correct definition of temperature in a microcanonical CP simulation is given by equation 2.25. Similarly, in a simulation where temperature is controlled, e.g. through a Nosé thermostat[19], the quantity to be monitored corresponds to the instantaneous value of the temperature defined in equation 2.25. Dynamical observables will also be affected by the additional inertia, as already noted in the case of phonons extracted from CP-MD in carbon systems [20, 21]. In the case of homogeneous systems (a single atomic species in which all the atoms are in similar local chemical environments) all dynamical quantities

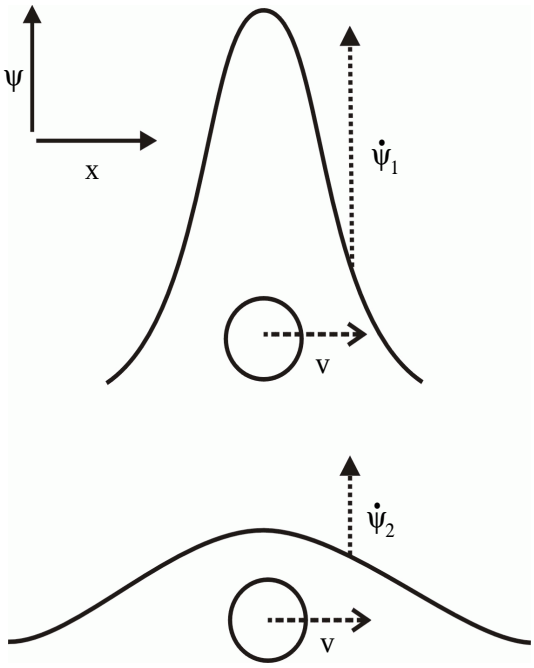

Figure 2.1: The mechanism by which the effective ionic inertia is related to the quantum kinetic energy of the localised electronic wavefunctions within the rigid-ion approximation: For two ions of the same species which are moving with the same velocity **v**, the one carrying the more localised electronic wavefunction (top) has a higher effective mass. The more localised electronic wavefunction $\psi_1(x)$ has, on average, a greater slope $d\psi(x)/dx$ (and hence kinetic energy) than the more extended wavefunction (bottom) $\psi_2(x)$. Since for a given ionic velocity **v** a greater slope implies a greater rate of change with respect to time ($\dot{\psi}_1 > \dot{\psi}_2$) , the localised wavefunction changes more per unit time than the extended wavefunction. In order to increase the ion's velocity one also needs to increase the rate of change of the massive wavefunction localised on it. The total inertia associated with this required change of the rate of change of the wavefunction is related to the quantum kinetic energy via equation 2.23 and this quantity must be added to the bare ionic mass in order to obtain its effective mass.

can be simply rescaled using the mass correction of equation 2.24. However, for heterogeneous systems the correction is not always trivial, as different mass corrections apply to different atomic species due to different atomic kinetic energies. In practice, we found that a convenient and more general way to express the mass correction of ion I is given by

$$\Delta M_I = f_I \frac{2m_e E_k^{total}}{3N\hbar^2} \tag{2.29}$$

where f_I is a dimensionless constant which takes into account the relative contribution of species I to the total quantum kinetic energy E_k^{total}. The value of f_I is generally found variationally as that which minimizes the error in the forces.

Corrections should always be applied to the temperature and the pressure as calculated using the bare ionic masses. These corrections must be calculated for each chemically

distinct species individually. For temperature, the correction for species S is

$$\Delta T_s = \frac{\Delta M_s}{M_s} T_s \tag{2.30}$$

and the correction to the partial thermal pressure of species S is

$$\Delta P_s^{\mathrm{t}} = \frac{\Delta M_s}{M_s} P_s^{\mathrm{t}} \tag{2.31}$$

Where M_s is the bare ionic mass of species S and P_s^{t} is the *thermal* contribution to its partial pressure. There is also a correction which must be applied to the internal pressure due to the fact that the electronic orbitals are not at their ground state. This correction to the internal stress is not trivial to derive since the potential energy of the system depends, via the coupling between ions and orbitals, not only on the ionic positions, but on all higher order derivatives of the ionic positions with respect to time. However, within the rigid-ion approximation, if we only consider derivatives with respect to ionic positions, using the virial theorem we may write the internal pressure as

$$P^{\mathrm{i}} = \frac{1}{\Omega} \sum_I \mathbf{F}_I \cdot \mathbf{R}_I \tag{2.32}$$

and so the rigid ion correction becomes

$$\Delta P^{\mathrm{i}} = \frac{1}{\Omega} \sum_I \frac{\Delta M}{M} \mathbf{F}_I \cdot \mathbf{R}_I \tag{2.33}$$

In practice, for a system under periodic boundary conditions, it is not possible to evaluate this quantity. However, for a system with a single species, this becomes

$$\Delta P^{\mathrm{i}} = \frac{\Delta M}{M} P^{\mathrm{i}} \tag{2.34}$$

In practice, in more general situations, in order to get an idea of the true stress of the system, one should perform a large enough number of electronic minimizations to the ground state and calculations of the stress at the ground state to get a good average of the true internal pressure.

In the next section we demonstrate, with the use of several simple examples, the validity of the theory developed in this section and the previous one. We show how masses, and therefore dynamical quantities, may be corrected using the formulae presented above. In section 2.5 we look at the more difficult case of water as an example of a system whose dynamics and thermodynamics one cannot correct so easily.

2.4 Testing the Theory

2.4.1 Introduction

In order to test the theory put forward in the previous sections and to gain more insight into its implications, we have performed CP simulations on pressurised magnesium oxide

Table 2.1: Technical Details of the Simulations

#	System	Temperature	μ_0	E_p	E_{cut}	Δt	$\sum_i \mu_i \langle \dot{\psi}_i \vert \dot{\psi}_i \rangle$	L
		Kelvin	a.u.	Ryd.	Ryd.	a.u.	a.u.$\times 10^4$	a.u.
1	Si	330	270	1.0	12.0	5.0	4.36	20.42
2	Si	330	270	1.0	12.0	5.0	4.36	20.42
3	Si(liquid)	2000	270	1.0	12.0	10.0	4.35	19.8
4	MgO	2800	400	2.7	90.0	8.0	66.3	14.5
5	Si	330	200	1.0	12.0	5.0	3.23	20.42
6	Si	330	800	1.0	12.0	10.0	12.92	20.42
7	MgO (M_O rescaled)	2800	100	2.7	90.0	4.0	16.55	14.5
8	MgO (M_O rescaled)	2800	400	2.7	90.0	8.0	66.4	14.5
9	MgO	2800	200	2.7	90.0	5.65	33.1	14.5
10	MgO	2800	100	2.7	90.0	4.0	16.55	14.5

and on silicon. Among the insulators (we restrict our analysis to insulators as adiabatic decoupling is less obvious in metallic systems and this would complicate considerably our analysis), MgO and Silicon are extremal cases: MgO is a highly ionic system with large quantum kinetic energy associated with the strongly localised charge distribution; Silicon on the other hand is a covalent system where electron states are much more delocalised. Within our pseudopotential description of MgO [22], the 1s,2s and 2p states are frozen into the core of Mg whereas only the 1s states are frozen into the core of O. Since there is very nearly complete transfer of the two 3s electrons from Mg to O (inspection of charge density contour plots reveal no evidence of any valence charge anywhere except surrounding O sites) the electron quantum kinetic energy may to a first approximation be attributed to electronic states localised on oxygen ions. This makes MgO an ideal system to study within the rigid ion model since only the oxygen mass will be rescaled. As mentioned in the previous section, additional problems arise if one deals with more than one electron-carrying species as the quantum kinetic energy must be divided between these species. The large quantum kinetic energy of MgO means that the error in the CP forces should be large relative to many materials. The simulations of MgO were performed at a high pressure ($\sim$ 900 kbar) as this enhanced its ionicity.

Silicon, on the other hand, is a covalent/metallic system with relatively low quantum kinetic energy. As such it should be one of the systems most favourable to the Car-Parrinello approximation but least favourable to description in terms of rigid ions.

2.4.2 Technical Details

In this section we present the result of ten different simulations. The technical details are summarised in table 2.1.

All simulations were performed with a cubic simulation cell of side L (see table 2.1) under periodic boundary conditions and with 64 atoms in the unit cell. We used a plane wave basis set with an energy cut off for the wavefunctions of E_{cut}. The Brillouin zone was sampled using only the $\Gamma-$point. In each simulation we have used the mass precondition-

ing scheme of Tassone *et al.*[23] and the parameters μ_0 and E_p in table 2.1 are defined as in Ref.[5]. With the use of a preconditioning scheme, whereby the electronic mass is scaled with the kinetic energy of the plane wave, the time step can be increased by a factor of 2-3 with respect to the non-preconditioned case[23] . The use of a preconditioning scheme worsens considerably the agreement of the CP forces with the BO ones. In particular, we have checked that using the parameters μ_0 and E_p that optimize the time step causes an increase by about a factor of three in the correction term of equation 2.17. However, in order to bring this error to its non-preconditioned value, a value of μ_0 three times smaller would be required, with a consequent reduction of the time step of only $\sqrt{3}$. Considering that the preconditioning scheme allows a 2-3 increase of the time step, a reduction of $\sqrt{3}$ still makes the preconditioning scheme marginally superior.

Liquid silicon is metallic and so, as suggested by Blöchl and Parrinello [15], two Nosé thermostats were used to counteract the effects of energy transfer between the ions and the $|\delta\psi_i\rangle$ due to overlap of their frequency spectra.The values of the parameters used were $Q_e = 21.3$ a.u./atom,$E_{kin,0} = 1.65 \times 10^{-4}$ a.u./atom and $Q_R = 244400$ a.u.. These were chosen for compatibility with those of Ref.[10] by taking into account the slight increase in temperature and scaling accordingly.

In all of these simulations, with the exception of simulation 2, the system was first allowed to evolve for at least 1 ps and this trajectory was discarded. For simulation 2, this initial equilibration time was 0.5 ps. All results reported are taken from the continuations of these equilibration trajectories.

In all simulations, the total quantum kinetic energy of the system, and hence the average mass correction (see equation 2.29), varied during the simulation by less than 0.3%. It was therefore taken as a constant in further analysis.

The total energy of all the degrees of freedom (including the thermostats in simulation 3) was conserved in all simulations *at least* to within one part in 10^5.

2.4.3 Results

In order to check the predictions of the theory developed in Sections II and III, we have taken segments of CP trajectories and calculated the true BO forces along these segments by putting the electronic orbitals to their ground state with a steepest descent method. We look at the instantaneous error in the α^{th} cartesian component of the CP force on atom I relative to the root-mean-squared (r.m.s) BO force component, i.e :

$$\delta F_I^\alpha(t) \;=\; \frac{\Delta F_I^\alpha(t)}{\sqrt{\frac{\sum_c \sum_{J,\beta} (F_{BO_J}^\beta)^2}{3NN_c}}} \tag{2.35}$$

and the instantaneous relative error minus the relative error predicted by the rigid-ion model :

$$[\delta F_I^\alpha(t)]_{corr} = \frac{\Delta F_I^\alpha(t) + \Delta M_I \ddot{R}_I^\alpha}{\sqrt{\frac{\sum_c \sum_{J,\beta} (F_{BO_J}^\beta)^2}{3NN_c}}} \tag{2.36}$$

where N_c is the number of ionic configurations at which the error in the CP forces was calculated and $\sum_c$ is the sum over all such configurations. The value of ΔM_I in equation 2.36 is determined using the rigid-ion-model expression equation 2.29, and E_k^{total} was given its average value during the simulation. The scaling parameters which were found to give best results for silicon and oxygen were $f_{Si} = 1.0$ and $f_O = 1.92$ respectively.

We also look at $\langle \delta F_I^\alpha \rangle$ and $\langle \delta F_I^\alpha \rangle_{corr}$ the r.m.s values of $[\delta F_I^\alpha]$ and $[\delta F_I^\alpha]_{corr}$ over all the ions, cartesian components and configurations tested.

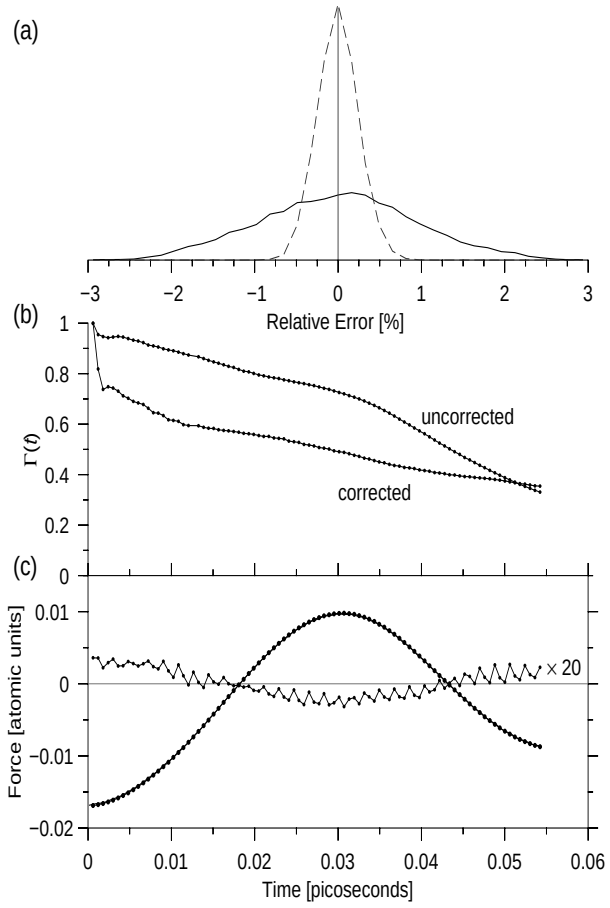

Figure 2.2: Simulation 1. (a) Distribution among all atoms I and all cartesian components α of the percentage errors in the CP forces relative to the BO forces at the same ionic positions, $100 \times \delta F_I^\alpha(t)$ (full line) and these errors when the forces have been partially corrected according to a rigid-ion model, $100 \times [\delta F_I^\alpha(t)]_{corr}$ (dashed line). (b) $\Gamma(t)$ as defined by equation 2.37 for the full error in the forces and those as partially corrected according to the rigid-ion model (c) $F^\alpha_{BO_I}$,$F^\alpha_{CP_I}$ and $(F^\alpha_{CP_I} - F^\alpha_{BO_I})$ (multiplied by a factor of 20 for visibility) for a typical force component. Dots indicate the points at which the BO force was calculated (every 5 time steps).

Since the CP forces are affected by a "fast" component whose effect on the ionic dynamics is believed to average out on the time scale of the ionic motion, we introduce

the quantity $\Gamma(\tau)$, defined as

$$\Gamma(\tau) = \int_0^\tau \frac{1}{3N} \sum_{I,\alpha} \left| \frac{\int_{t_0}^{t_0+\tau} \Delta F_I^\alpha(t) dt}{\int_{t_0}^{t_0+\tau} |\Delta F_I^\alpha(t)| dt} \right| d\tau \tag{2.37}$$

If we begin our comparison between CP and BO forces at some instant t_0 along the trajectory then inspection of $\Gamma(\tau)$ gives a feeling for how large the fast component is. If the errors in all the forces of the system oscillate rapidly with an average of zero then $\Gamma(\tau)$ decreases very quickly from the value of one at $\tau = 0$ to zero at $\tau \sim \tau_e$. For systematic errors $\Gamma(\tau)$ should decrease gradually from one to zero on a timescale of the order of the period of τ_i. In realistic cases $\Gamma(\tau)$ drops from one and levels off to a smaller value for $\tau \sim \tau_e$, and then decreases gradually to zero for τ exceeding τ_i. The value of $\Gamma(\tau)$ on the plateau between τ_e and τ_i provides a measure of how much the errors calculated in equations 2.35 and 2.36 are attributable to a systematic (i.e. "slow") departure from the BO surface.

We begin by looking at the forces in Silicon in both the solid at 330 K and the liquid at 2000 K (simulations 1,2 and 3). Simulation 1 was preceded by a short run where the temperature was set to about 1000 K. Electrons were then relaxed in their ground state and the ionic velocities set to zero. This allows the electrons to smoothly accelerate with the ions. A microcanonical simulation followed where the ionic temperature reached, after a short equilibration, the value of 330 K. This procedure was followed in all the simulations reported here, except where discussed. In solid Si at 330 K (Fig. 2.2) we find that the standard deviation of the error in the Car-Parrinello forces is 0.94%. However, most of this error can be attributed to a rigid dragging of the Si atomic orbitals. The standard deviation of the error is in fact reduced to 0.24% after the rigid-ion correction of equation 2.24 is subtracted. The $\sim 30\%$ drop of $\Gamma(t)$ (corrected) shown in Fig. 2.2b indicates that $\sim 30\%$ of the residual 0.24% error can be attributed to "fast" oscillations, so that the overall average error introduced by the CP approximation, once corrected for the rigid dragging and under the assumption that the fast component is not relevant, is less than 0.2%.

As has been pointed out previously by Remler and Madden [24], it is important to begin the dynamics with electrons and ions moving in a consistent way as we have done here in all simulations except the one we now discuss (simulation 2) and in the case of liquid Si (simulation 3). We found that the error in the forces increases substantially if the simulation is not started from zero ionic velocities, a procedure that would otherwise have the advantage of shortening considerably the time needed to reach thermal equilibrium. Simulation 2 started from the end of simulation 1, but electrons have been put in the ground state before restarting (ionic velocities and positions were instead kept unchanged). Forces were tested after 0.5ps from the electron quenching.

The standard deviation of the error in forces is now 5.7% and the error in the forces as corrected according to the rigid ion approximation at 5.68%, is not significantly improved. However clearly from inspection of $\Gamma(t)$ in Fig. 2.3b and the sample force component in Fig. 2.3c most of this error can be attributed to the high frequency oscillations of the electronic orbitals. If we assume that these oscillations do not influence the ionic dynamics,

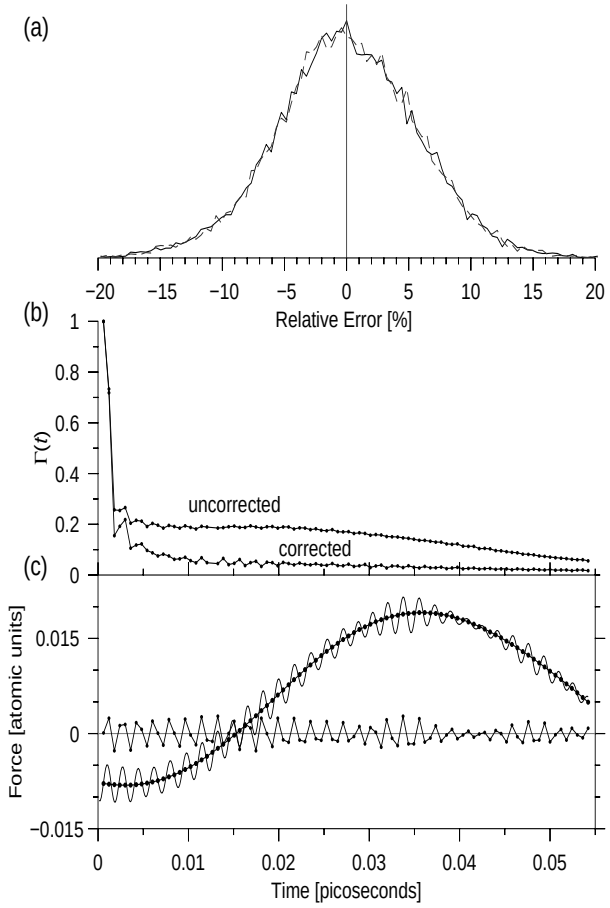

Figure 2.3: Simulation 2, Crystalline Si at 330K when the electrons receive a 'kick' at the beginning of the simulation. See caption of Fig. 1 for explanation. $(F^{\alpha}_{CP_I} - F^{\alpha}_{BO_I})$ has not been scaled for visibility.

the error reduces to about 1.2% for the uncorrected forces and to less than 0.5% for the corrected forces. The amplitudes of these oscillations are nevertheless significant and may affect the thermodynamics in a way that is not easy to predict. These oscillations clearly originate from the initial jerk experienced by the the electrons in their ground state and survive for a long time due to the adiabatic decoupling. In the liquid (figure 2.4)

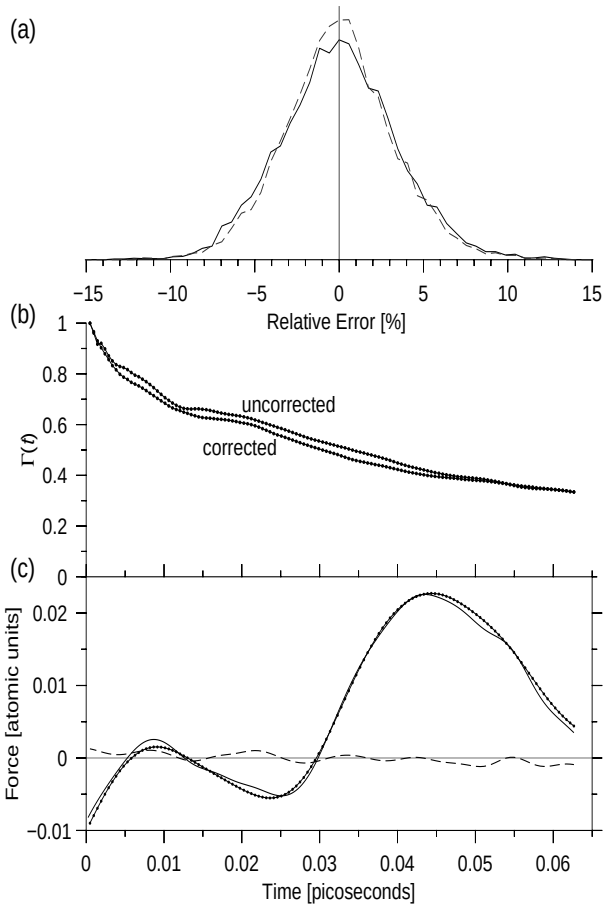

Figure 2.4: Simulation 3, Liquid Si at 2000 K. See caption of Fig. 1 for explanation. $(F^{\alpha}_{CP_I} - F^{\alpha}_{BO_I})$ has not been scaled for visibility.

the situation is considerably worse than in the crystal. The standard deviation of the error in the forces is 3.4% which improves only to 3.1% with the rigid-ion correction. There do not seem to be high frequency, high amplitude oscillations here despite the simulation being started with finite ionic velocities. However, there are oscillations of a lower frequency (although still quite high relative to ionic timescales) which are probably due to the presence of the Nosé thermostat. It may be that the Nosé thermostat has the effect of damping out the kinds of oscillations seen in Fig. 2.3 but the presence of these other oscillations is hardly an improvement. This highlights the need for careful choice of parameters for the Nosé thermostat, particularly the value of $E_{kin,0}$. The issue of thermostatting the electronic orbitals will be discussed later in this section.

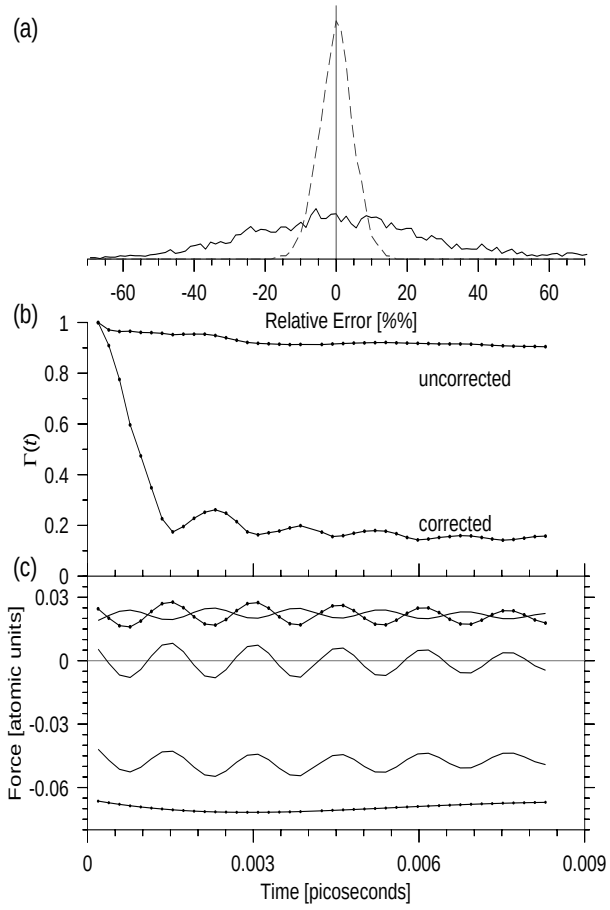

Figure 2.5: Simulation 4. Forces on the oxygen ions in crystalline MgO at 2800 K. (a) and (b) are as in Fig. 1(c) From top to bottom : the error in the CP forces ($F^{\alpha}_{CP_I} - F^{\alpha}_{BO_I}$), the error in the CP forces as predicted by the rigid-ion model $-\Delta M_O \ddot{R}^{\alpha}_I$(dotted line), the difference between the true error in the CP forces and the predicted error ($F^{\alpha}_{CP_I} - F^{\alpha}_{BO_I} + \Delta M_O \ddot{R}^{\alpha}_I$), the CP force $F^{\alpha}_{CP_I}$ and the BO force at the same ionic positions $F^{\alpha}_{BO_I}$ for a typical force component. Dots indicate the points at which the BO force was calculated (every time step).

We now look at the forces in crystalline MgO with $\mu_0 = 400$a.u (figure 2.5). The relatively high quantum kinetic energy associated with states attached to the O ions means that, according to equation 2.21, the errors in the forces are considerably larger for the O ions than we have seen for Si. The errors in the CP forces have in fact a standard deviation as large as 32% . However, when this is corrected as in equation 2.24 by attributing all the quantum kinetic energy to states rigidly following the O ions the standard deviation of the error reduces to 4.8%. Furthermore, the corrected value of $\Gamma(t)$ indicates that about 80% of the error on the O forces cancels out after account is taken for the high frequency oscillations, suggesting that a more appropriate estimate of the error is $\sim 0.4\%$. The amplitude of the fast oscillations is a cause for concern however and since the simulation was begun at zero ionic velocity it is not clear how it may be reduced further.

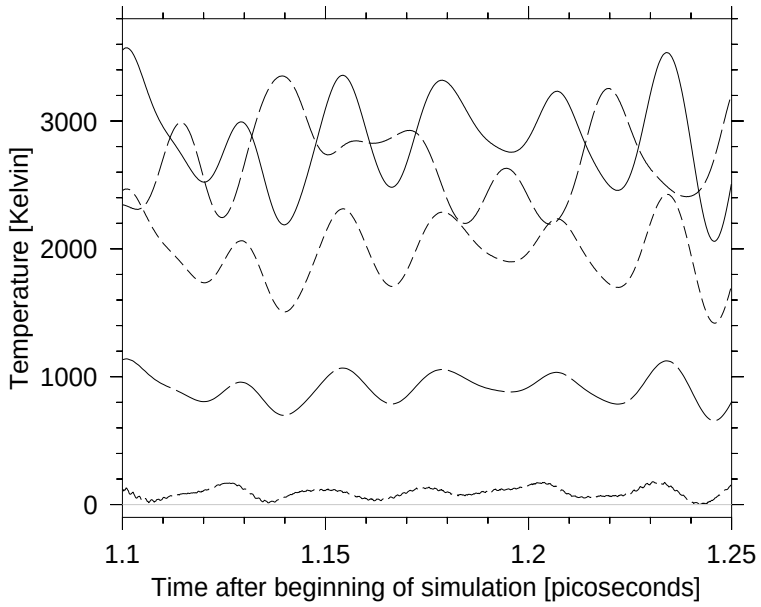

Figure 2.6: Simulation 4. Dashed lines from top to bottom are : Mg temperature, O temperature, T_{el} ,and $10 \times (T_{el} - T_{\Delta M_O})$. The full line is the Oxygen temperature when it is calculated with a mass which is increased by A_O.

Temperature

We focus here only on MgO, as the effects of the electronic dragging are enhanced. According to the results of Section III, we should expect a difference between the naive definition of temperature and the definition corrected by the electronic dragging, equation 2.25. In the case of MgO, as noted in the previous section, this correction affects only the oxygen atoms, as only a minor amount of electronic charge is carried by the Mg^{2+} ion. In Fig.2.6 we show the behavior of the instantaneous values of the naive and corrected temperatures. The corrected temperature exceeds the naive definition by about 500 K. More interestingly, we report in Fig.2.6 also the contributions to the temperature of the

two atomic species. It is clear that the naive definition would imply that the two species are not at thermal equilibrium. On the other hand, use of the corrected definition for the oxygen temperature brings the temperature of the two species in much better agreement, supporting the conclusion, based on the rigid ion model, that thermodynamics can be restored by a simple rescaling of the oxygen mass. The mass rescaling, as calculated with equation 2.20 amounts to $\Delta M_O \sim 7.5$ atomic mass units ($M_O = 16$ atomic mass units). We also report in Fig.2.6 the instantaneous value of the fictitious electronic kinetic energy, the l.h.s. of equation 2.26, and the difference between this quantity and the r.h.s. of equation 2.26, which represents the contribution due to the rigid dragging of the electronic orbitals. The difference is very small, implying that residual contributions due, for example, to the fast electronic oscillations are negligible in MgO compared to the slow dragging of the orbitals.

Thermostatting the Electronic Orbitals

In simulating liquid silicon, which is metallic, we have used a standard technique for maintaining a low fictitious kinetic energy of the electrons. This is to use two separate thermostats in the simulation : one for the electronic orbitals and one for the ions. This technique was first introduced by Blöchl and Parrinello[15] and has very recently been updated by Blöchl [16]. In reference [15] the recommended temperature of the electronic thermostat, $E_{kin,0}$, has been determined on the basis of the rigid ion model to be twice the value of $T_{\Delta M}$ (as defined by equation 2.28). The reasoning behind this is that the electrons should be free to follow the ions and also have room to perform the high frequency oscillations. In our simulation of liquid silicon we have used a value of $E_{kin,0}$ compatible with reference [25] however we note that this is considerably smaller than the value recommended in reference [15]. We have also done simulations using higher values of $E_{kin,0}$ and in all cases the errors in the forces have been greater. It is likely therefore that by decreasing further $E_{kin,0}$ we might improve further the forces however this has not been attempted here.

It is important to note that for some systems, the choice of $E_{kin,0}$ is crucial and cannot be based on the simple formula of reference [15]. This can be seen by inspection of figure 2.7 which is a magnification of the lowermost curve in figure 2.6. This is a plot of $(T_{el} - T_{\Delta M_O})$ during the MgO simulation. One can clearly distinguish the high-frequency oscillations of electronic orbitals from the ionic-timescale oscillations due to deviations from the rigid-ion description. The amplitudes of the high frequency oscillations is, roughly, ~ 1 K. This is 3 orders of magnitude smaller than T_{el} and yet it results in oscillations in the force which have an amplitude of $\sim 7\%$. This suggests that choosing the recommended value for this system would lead to very large errors in the forces, and that in order to maintain the errors within a few percent requires a prediction of $E_{kin,0}$ which is correct to within $\sim 0.1\%$. It is unlikely whether such precision is possible and anyway for MgO the variations in $E_{kin,0}$ along the molecular dynamics trajectory was found to be $\sim 0.3\%$.

The updated form of the electronic thermostat recently proposed by Blöchl is different in that it never actually heats the electrons, but cools them down when they exceed the

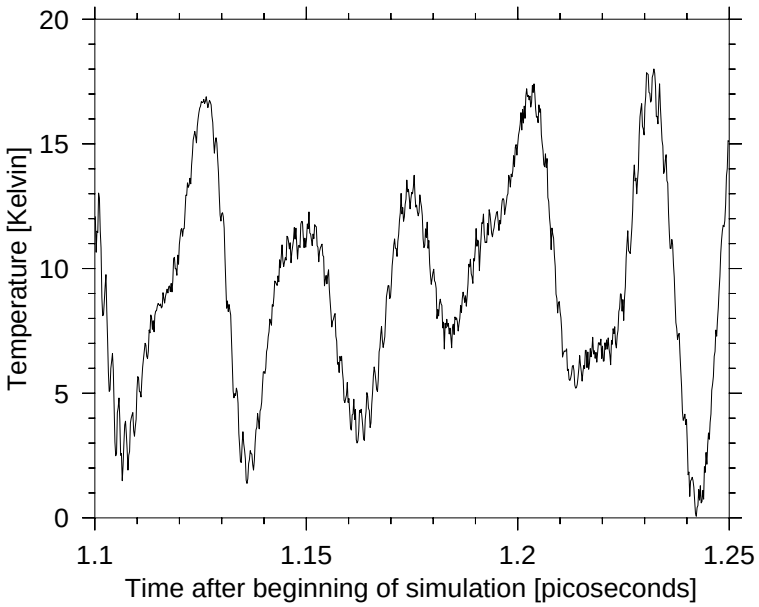

Figure 2.7: Simulation 4 - $(T_{el} - T_{\Delta M_O})$. Within the rigid-ion approximation, this is the contribution to the electronic kinetic energy from the high-frequency oscillations. Even though this is very small, the oscillations in the forces are very large as shown in figure 2.5. Small deviations from the ground state can lead to large errors in the forces.

specified value. Similar problems should be expected for this system however, since for a system in which T_{el} is increasing, its value will frequently be close to the specified value, or at least of the same order of magnitude.

Phonon Spectra

We have calculated the phonon densities of states of crystalline Si and MgO by fourier transforming the velocity autocorrelation function. In all cases, the first picosecond of the simulation was discarded and results obtained by averaging over at least one subsequent picosecond. For silicon the velocity autocorrelation function was calculated on a time domain of length 1.2ps and for MgO on a time domain of length 0.5ps.

In silicon (Fig. 2.8) the difference is reasonably small. According to the rigid ion model the frequencies should be corrected using

$$\omega_{corrected} = \omega_{CP}\sqrt{1 + \Delta M/M} \tag{2.38}$$

where ω_{CP} is the frequency as extracted directly from the CP simulation. We find that for silicon this overestimates by about a factor of two the amount of the correction. This small discrepancy may be due to the length of simulation used for calculating the frequency spectra or due to a breakdown of the rigid-ion description when $\mu_0 = 800 a.u.$. It may also be that neglecting the effect of the fast oscillations is not be completely appropriate when the dragging contribution is small.

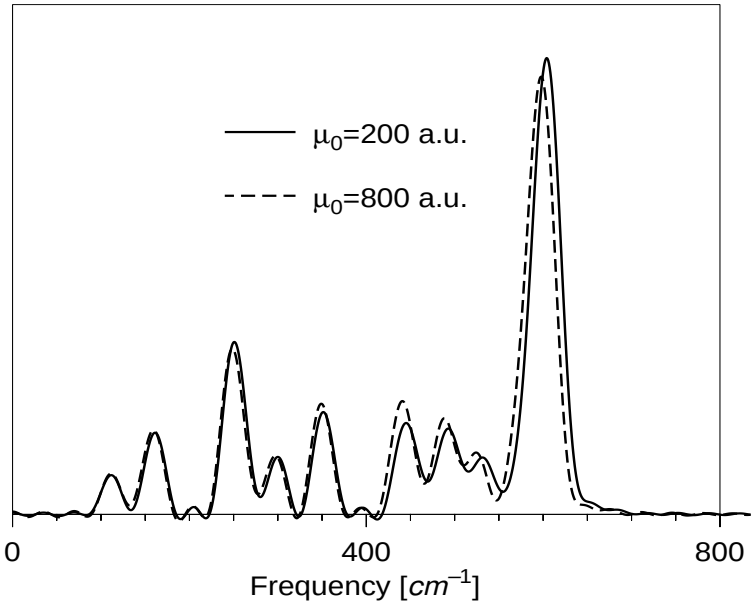

Figure 2.8: Phonon density of states of crystalline Silicon for $\mu_0 = 200$ a.u. (simulation 5) and for $\mu_0 = 800$ a.u (simulation 6).

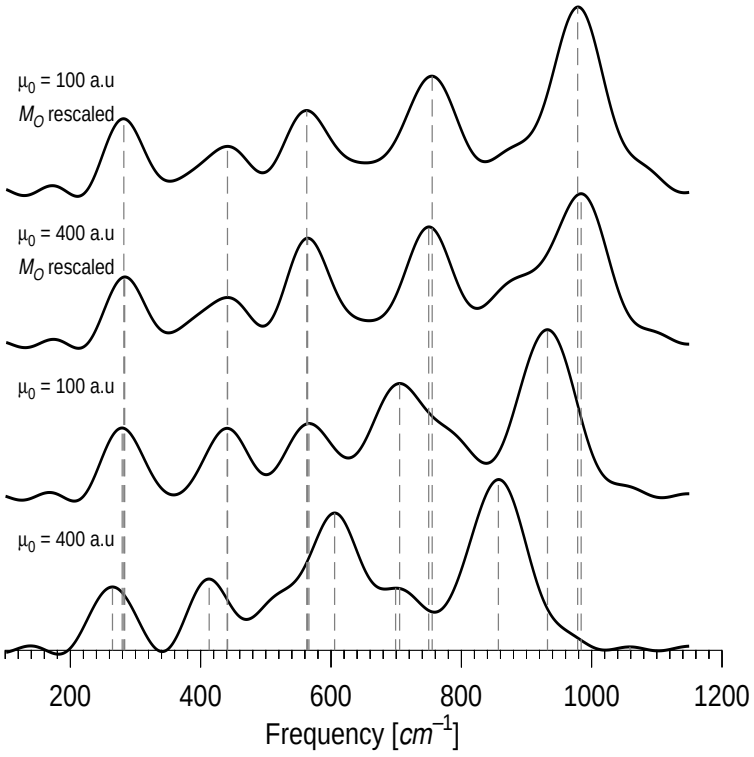

Figure 2.9: Phonon density of states of crystalline MgO for $\mu_0 = 100$ a.u. and for $\mu_0 = 400$ a.u. with rescaled (simulations 7 and 8) and unrescaled (simulations 10 and 4) oxygen masses.

In MgO, as expected the difference is much larger. We calculate the phonon spectra for $\mu_0 = 400$a.u. and for $\mu_0 = 100$a.u and find large differences between them (see Fig. 2.9) highlighting again how the dynamics depends on the value of μ. The fact that two species are involved complicates matters as the mass correction is different for the two species (it actually vanishes for Mg). Therefore we should not expect simply a rigid shift of the frequencies. However, if the rigid-ion approximation is valid, one may conceive to rescale the oxygen mass *a priori* in equation 2.2 as $\tilde{M}_O = M_O - \Delta M_O$, so that the actual CP dynamics expressed in terms of the BO forces, equation 2.24, becomes identical to the BO dynamics if the rigid ion approximation holds. We have done this for MgO, again for $\mu_0 = 400$a.u. and $\mu_0 = 100$a.u and we see that the results are much improved. There are only small differences in the positions of the peaks and the overall shapes of the curves are very similar. We notice that with $\mu_0 = 100$a.u. (and no mass correction) frequencies are within 8% the correct ones. This implies that in order to obtain a phonon spectrum of MgO with a 4% accuracy in the peak positions (4% is the typical uncertainty of a pseudopotential DFT approach[26]) the value of μ_0 should be about 50 a.u., which implies a $\Delta t \sim 2.8$ a.u., or about 1.5×10^4 time steps per picosecond.

Dependence of error on μ

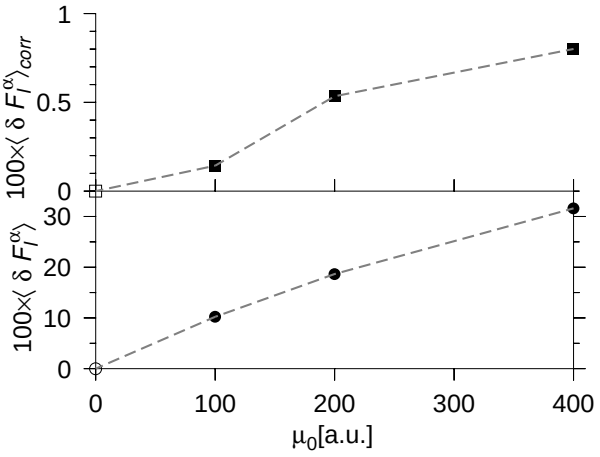

Figure 2.10: Scaling of the standard deviation of the errors in the forces on the oxygen ions with μ_0 (Simulations 4,9 and 10). $\langle \delta F_I^\alpha \rangle_{corr}$ has been reduced to eliminate cancelling high frequency oscillations by inspection of $\Gamma(t)$.

We now try to address the question of how the error in the CP forces depends on the fictitious electron mass. We do not know what the true μ-dependence of the error in equation 2.16 is. We have made the assumption in equation 2.17 that it is, to a first approximation, linear if one assumes that the oscillations in $|\delta\psi_i^{(1)}\rangle$ have a small amplitude. Fig. 2.10 shows $\langle \delta F_I^\alpha \rangle$ and $\langle \delta F_I^\alpha \rangle_{corr}$ for the oxygen ion for three different values of μ_0 where $\langle \delta F_I^\alpha \rangle_{corr}$ has been scaled to eliminate the contribution of errors from high frequency oscillations by inspection of $\Gamma(t)$.

The uncorrected error is dominated by the effect of the displacement of the equilibrium positions of the orbitals from the ground state, this scales approximately linearly with μ_0, thereby vindicating our neglect of terms in equation 2.17 of higher than linear order in μ. The small error which remains after the rigid ion correction has been applied could have contributions from many different sources including deviations from the rigid ion description and contributions from higher order error terms. It is also of the order of the fluctuations in E_k^{total} during the simulation.

2.5 Water

So far in this chapter it has been shown that systematic errors are present in Car-Parrinello simulations, the magnitude of which are proportional to the fictitious mass parameter. The examples of Si and MgO examined were used mainly to verify that our derivation of equations 2.17, 2.22 and 2.23 were correct and to show that for strongly ionic systems such as MgO, the error in the dynamics can be corrected and that it does not seriously alter the thermodynamics once properties such as the temperature and the pressure have been corrected.

We now turn our attention to water. Water in all its phases has been one of the most studied systems with the Car-Parrinello method [27, 28, 29, 30, 31, 32] and it looks likely to continue to be so in the future due its obvious importance in nature and particularly due to the fact that it forms the basis for all of biology. The ability of the Car-Parrinello method to describe water well is therefore of great importance as much of the current understanding of its microscopic properties has come from such simulations.

Water is a more difficult case to simulate with CPMD than either silicon or MgO and is therefore a better test of the method. Unlike silicon it has a considerable quantum kinetic energy and unlike MgO there is some subtlety to its bonding in the sense that it cannot be considered a completely ionic system. There is a degree of covalency to the intramolecular bonding and intermolecular interactions are dominated by hydrogen bonds. Here we look at ice, or more specifically, at "heavy" ice, D_2O because it is easier to simulate and it is generally what has been simulated in the past. Protons are very light and this can cause problems of energy transfer between ionic and electronic degrees of freedom. The lower symmetry and higher temperature in water and the lower mass of the proton relative to the deuteron means that errors should be, if anything, greater than those observed here.

2.5.1 Details of the Simulation

We have used norm-conserving pseudopotentials to describe the oxygen[22] and hydrogen[33, 34] atoms respectively. We have used a plane-wave cutoff of 70 Ryd. and a gradient-corrected exchange-correlation functional (BLYP)[35]. Only the Γ-point was used to sample the Brillouin zone. Simulations were performed on a $24 \times 24 \times 12$ a.u. simulation cell containing 32 D_2O molecules.

By variationally minimizing the error in the Car-Parrinello forces relative to the ground

state forces with respect to the ionic masses in a preliminary simulation of liquid water, we have obtained the rigid-ion mass corrections (in a.u.) for oxygen and deuterium of 6.766μ and 0.213μ respectively. We have later verified that these mass corrections are optimal for ice also. We have rescaled the ionic masses *a priori* by subtracting these corrections from them.

We have begun our simulations by doing a long simulation of ice at low temperature ($\sim$ 100 K) using an *ab initio* parametrized polarizable effective potential of the same form as that described for silica in chapter 5. This does not provide a very realistic description of water but it was deemed preferable to randomizing the positions. In order to minimize the errors due to high frequency oscillations of the orbitals, as discussed in section 2.4.3, we then began the simulation with the electrons at their ground state and the ions at zero velocity. We used a fictitious mass of $\mu = 900$ a.u. No mass-preconditioning scheme was used. After half a picosecond, when the ions were at a temperature of ~ 120 K, a Nosé thermostat[19] was attached to the ions and the temperature was increased to approximately 250 K during half a picosecond of simulation. The system was then equilibrated without a thermostat for approximately 3.5 picoseconds. The temperatures of the oxygen and hydrogen subsystems were calculated independently using the corrections given by equation 2.30 and according to this definition of temperature the subsystems remained at different temperatures, indicating that the system was not well thermalized. This can be seen in figure 2.5.1. It is worth noting that somebody unaware of the issue of mass rescaling would, in this case, see a thermalized system. The simulation was now continued, using the ionic and orbital velocities from the previous MD run, in two separate MD runs : one using a value $\mu = 100$ a.u. and the other remaining with $\mu = 900$ a.u (see figure 2.5.1). Changing the value of μ during a simulation perturbs the orbital dynamics only very slightly and has no significant lasting effect on the forces such as are seen when more severe shocks take place (see section 2.4.3). For a system where the rigid-ion approximation is valid, the fact that we have rescaled *a priori* the masses means that the simulations at the different values of μ should be identical.

It was found that after more than a further 2.5 ps the simulation with $\mu = 900$ a.u. still showed no sign of thermalization. The deuterons remained at a low temperature relative to the oxygen ions. In the simulation with $\mu = 100$ a.u., however, the system very quickly showed signs of thermalization and the subsystems were at the same temperature after $1.5 - 2$ ps. Since we would like to compare the phonon spectra for the two different values of μ and we would like to do this for reasonably well equilibrated systems, at the same temperature, it was decided to continue *both* simulations from the end of this initial 2.4 ps run with $\mu = 100$ a.u. Both for $\mu = 100$ a.u. and $\mu = 900$ a.u., a further 5.5 ps of simulation were carried out during which time the oxygen and deuterium subsystems remained at the same temperatures in both simulations. We may speculate at this point that the difficulty which the $\mu = 900$ a.u. simulation has in thermalizing is due to the presence of inertia between the oxygen and deuterium ions which impedes the motion of the deuterons. The difference in temperature has to be due to the deuterons moving too slowly relative to the oxygen ions. The bonding between them has a degree of covalency and this covalent bond carries an inertia which one should not expect to be well accounted for in the rigid-ion approximation. Therefore, the fact that when the covalent bond is

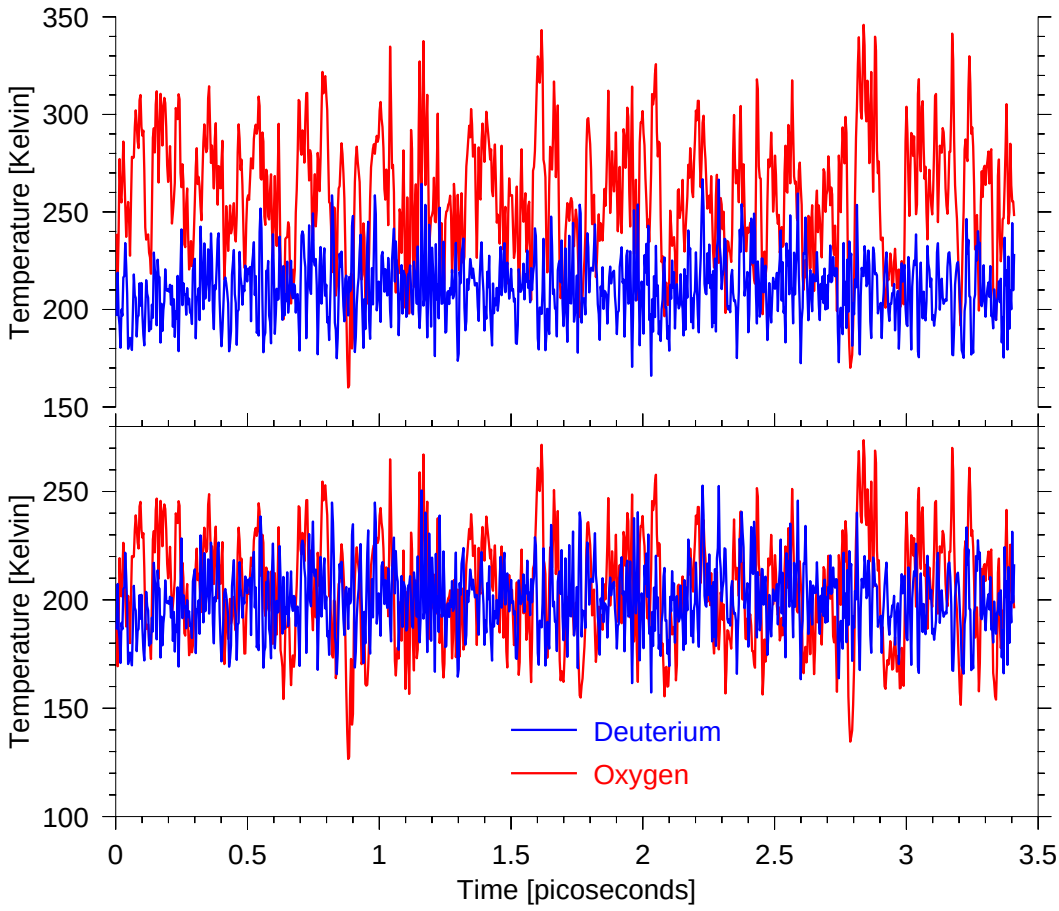

Figure 2.11: Temperature of the oxygen and deuterium subsystems as a function of time according to the correct definition of temperature in which the extra mass due to the electronic orbitals is accounted for (top) and according to the naîve definition (bottom) in which the temperature is not corrected.

less "heavy" the deuterons can move faster suggests that this may be an effect due to the orbital's fictitious inertia.

Forces

After 1 ps of the $\mu = 900$ MD run, the forces were compared with the ground state forces. The force on an individual oxygen or deuterium ion is dominated by the intra-molecular force, the force due to the other two ions in the D_2O molecule. Since the molecule remains relatively rigid, it is more sensible to examine the more subtle inter-molecular forces which are of primary concern to those studying the structure of water. In order to do this we look at the sum of the forces on a molecule. In figure 2.5.1 we plot some sample forces on D_2O molecules. It is clearly seen that there are very large differences between the CP forces and the ground-state forces but that much of this difference can be corrected with the rigid-ion correction. However, the error that remains still looks quite large and may

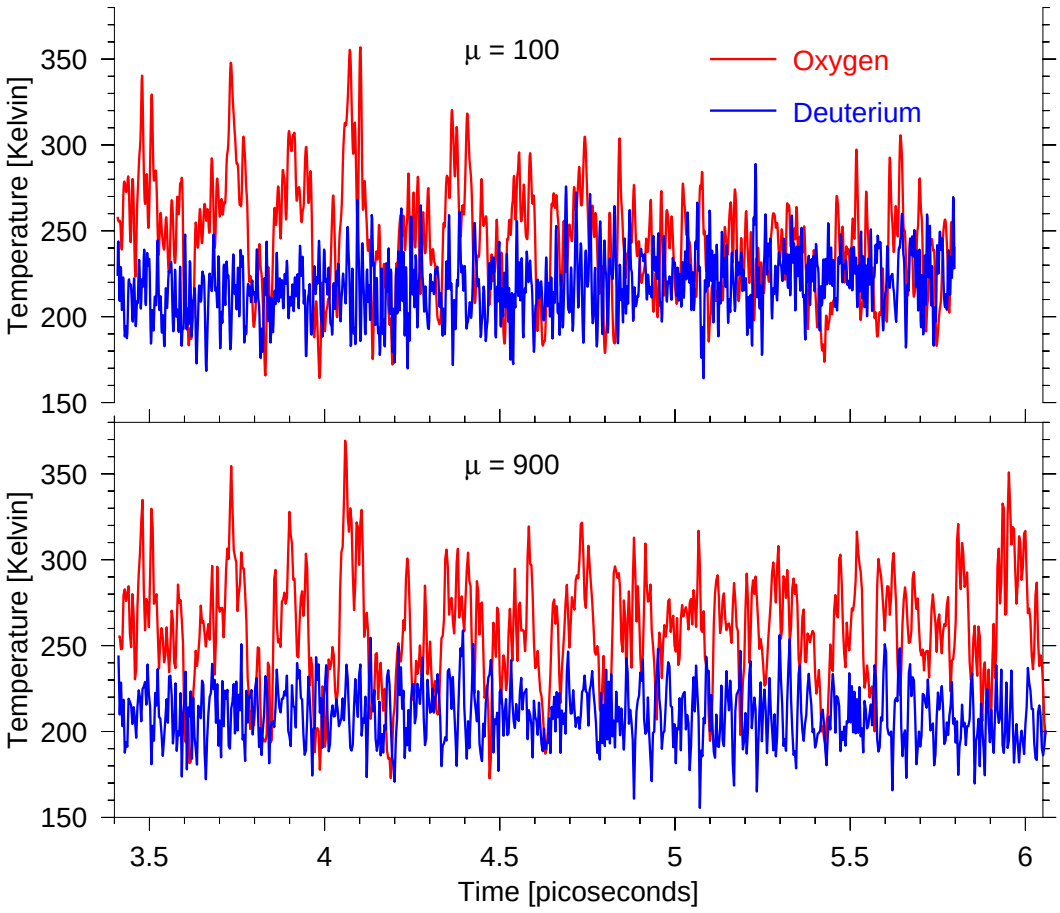

Figure 2.12: Corrected temperatures of the oxygen and deuterium subsystems as a function of time for $\mu = 100$ a.u. (top) and $\mu = 900$ a.u. (bottom).

be a cause for concern. The error before correction amounts to $\sim 45\%$ of the root-mean-square ground-state force component. After correction, this number reduces to 12.5%.

Although forces are very important in molecular dynamics, they are not generally the quantity which are extracted from simulations and it is not obvious how, in general, errors in forces map onto errors in thermodynamic quantities. In order to get a feel for the scale of these errors we look at the forces along the same trajectory for the local density approximation (LDA) [36, 37] and the Perdew-Burke-Ernzerhof(PBE) exchange-correlation functionals. There has been much discussion in the literature about what exchange-correlation functional one should use for water[29]. It is generally accepted that the LDA performs very poorly for water and most people use generalized gradient approximations which seem to give better results. Different gradient corrected functionals have been shown to give quite different radial distribution functions for liquid water [29]. Figure 2.5.1 shows a comparison of the forces from BLYP, LDA and PBE functionals. We found that the average difference between PBE and BLYP forces was $\sim 7.8\%$ and the difference between LDA and BLYP forces was $\sim 45\%$. It is also worth noting that, in

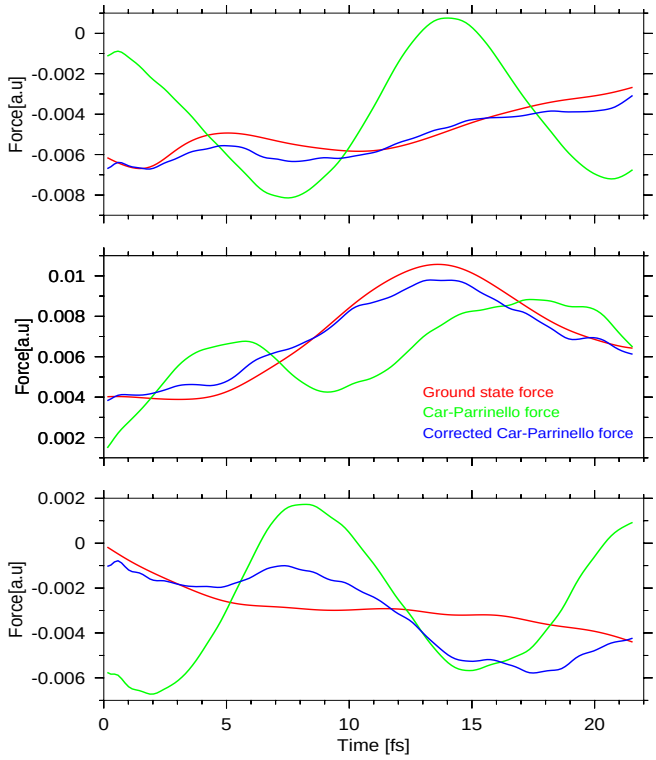

Figure 2.13: Some sample forces on D_2O molecules. The Car-Parrinello force is compared to the ground state force and the Car-Parrinello force once corrected using the rigid-ion correction.

general, although there are clear differences in the magnitude of the forces from LDA and BLYP, for example, the time-derivative is generally quite similar for all the functionals tested. This is not the case for the Car-Parrinello force, where the derivative of the force differs quite strongly from the ground state force.

Finally, we have looked at the forces after very brief simulations in which velocity rescaling was employed. Velocity scaling is commonly used for CP simulations and has been used in the past to equilibrate liquid water[30]. However, it gives an equivalent shock to the electronic degrees of freedom as beginning a simulation with ions at finite velocities does. In this test, the velocity rescaling followed the initial 0.5 ps simulation at 120 K and the velocities were rescaled to bring the temperature to 220 K. Velocities were adjusted only 4 times in total and then the system was equilibrated for 1 ps. We found, once again, that there were large-amplitude oscillations in the forces with frequencies typical of the electronic orbitals. These oscillations also appeared much less harmonic than the oscillations which were seen in the cases of Si and MgO in section 2.4.3. The magnitude of these oscillations highlights the fact that it is dangerous to perturb the electronic system by changing abruptly the ionic velocities, particularly considering the small ionic temperature change involved in this test.

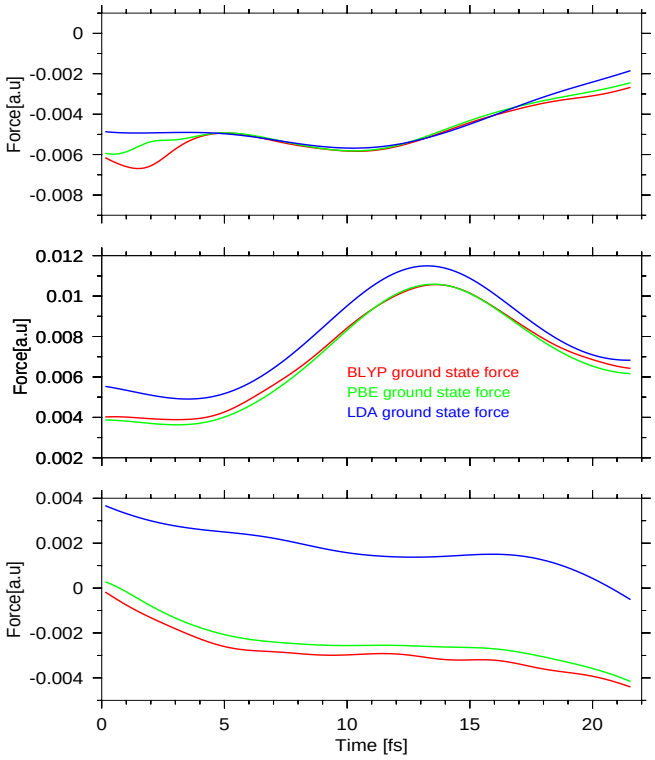

Figure 2.14: Some sample forces on D_2O molecules. The ground state forces along the same trajectory as plotted in figure 2.5.1 using the three different exchange-correlation functionals BLYP[35], LDA[37] and PBE[74]

Phonon Frequencies

For the two different values of μ we have calculated the phonon densities of states by fourier transforming a velocity autocorrelation function which was calculated on a time domain of length 1.45 ps by averaging over the final 5.5 ps of simulation. As with the case of MgO, if one does not rescale ionic masses, the differences in the phonon spectra are extremely large. However here we are only concerned with errors which cannot be corrected in this way. The results are shown in figure 2.5.1. Once again, these spectra should be identical if the rigid-ion approximation is valid. The main features of the two phonon spectra are similar, indicating that the rigid-ion approximation works very well for the vibrational properties of ice. The $\mu = 900$ curve shows a slight increase ($\sim 1.5\%$) in the frequency of the O-D bending mode and a corresponding decrease in the frequencies of the O-D stretching modes. We do not have enough statistics to examine in detail the translational and rotational modes of the molecule, but the main differences seem to be in the intensities of the peaks with little, affect on the frequencies.

So, despite what seem like large errors in the forces, the vibrational properties of the crystal are not greatly effected. The errors are similar in scale to the differences using different gradient-corrected exchange-correlation functionals[31].

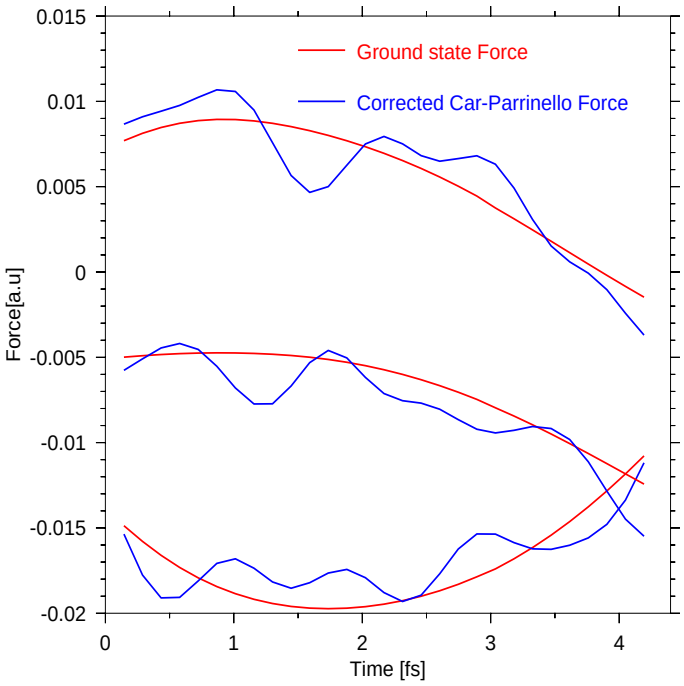

Figure 2.15: Some sample forces on O ions following scaling of ionic velocities. The Car-Parrinello forces with the rigid-ion correction are compared to the ground-state forces.

2.6 Discussion

We have shown in section 2.2 how, for any finite value of the fictitious mass μ, the Car-Parrinello method differs in principle from Born-Oppenheimer dynamics, even in the limit of the electronic orbitals having a minimum kinetic energy. What this amounts to saying is that in a Car-Parrinello simulation, electronic orbitals do not oscillate about their ground state but about a different equilibrium. There is therefore a lower bound on the error in the Car-Parrinello forces which is dependent on the fictitious mass μ. Under the assumption that high frequency electronic oscillations (i.e. the dynamics of the $|\delta\psi_i\rangle$) are small and independent of ionic motion, we have shown that Car-Parrinello simulations amount to solving the equation of motion for the ions

$$M_I \ddot{R}_I^\alpha = F_{BO_I}^\alpha + 2\sum_i \mu_i \Re\left\{ \sum_J \ddot{R}_J^\beta \frac{\partial\langle\psi_i^{(0)}|}{\partial R_I^\alpha}\frac{\partial|\psi_i^{(0)}\rangle}{\partial R_J^\beta} + \sum_{J,K} \dot{R}_J^\beta \dot{R}_K^\gamma \frac{\partial\langle\psi_i^{(0)}|}{\partial R_I^\alpha}\frac{\partial^2|\psi_i^{(0)}\rangle}{\partial R_K^\gamma \partial R_J^\beta}\right\} \quad (2.39)$$

if one may neglect terms in μ of higher than linear order.

For systems with a low quantum kinetic energy or small coupling between electrons and ions, such as the example of silicon which we have discussed in section 2.4.3, the resulting errors in the forces are extremely small and so neither the dynamics nor the thermodynamics should be strongly affected. For strongly ionic systems such as MgO, there are very large errors which are however mostly attributable to a rescaling of the mass of the oxygen ion thereby preserving the thermodynamics. When corrected for

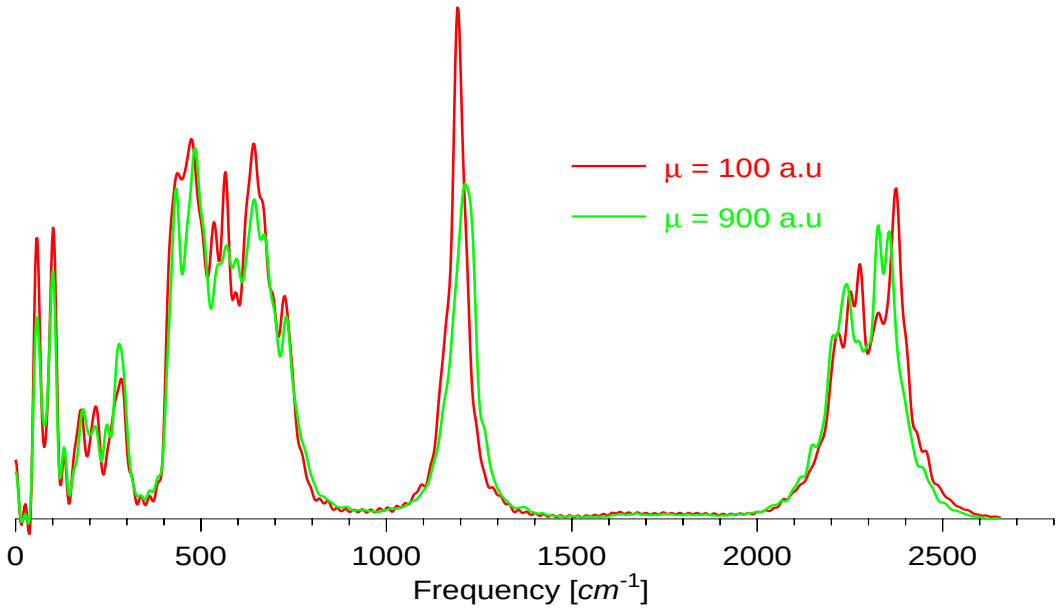

Figure 2.16: The phonon densities of states of heavy ice for $\mu = 100$ a.u. and $\mu = 900$ a.u.. Ionic masses have been rescaled according to the rigid-ion approximation.

this effect the errors are slightly higher than those in crystalline Si but still quite small. If we "measure" the departure of the CP dynamics from the BO dynamics in terms of $\Delta M/M$, with ΔM defined as in equation 2.24, then it appears that the elements where the departure is expected to be larger are located in the upper right of the periodic table, because they combine a low atomic mass with a large binding energy of the valence electrons (and thus a large quantum kinetic energy). Transition metals may also be strongly affected, because of the large number and strong localisation of the d-electrons. However, the higher the localisation of the orbitals, the higher the chances that the description of the electronic dynamics in terms of rigid orbitals is correct. The large departure observed in the case of MgO suggests that a proper assessment of how much the CP forces differ from the BO ones is mandatory in most systems. This can be achieved by either calculating the BO forces for selected ionic configurations, or by performing simulations for different (smaller) values of μ, and checking how the results scale with decreasing μ. If the departure is large then it is likely that in many cases the CP forces can be brought into good agreement with the BO ones by simply rescaling the ionic masses. We have seen in section 2.5 that at low temperatures even systems which should not be well described by the rigid-ion approximation, such as ice, the vibrational spectrum can be quite well corrected using the rigid ion approximation. Under conditions of lower symmetry or higher temperature this may no longer be the case.

Additional complications may arise when the dynamics lead to fundamental changes in the electronic structure. The first and second derivatives of the electronic orbitals with respect to the positions of the ions, which appear in equation 2.16, may become relevant in regions of phase space where the electrons play a significant role. For example, if charge

transfer between ions occurs, or if a substantial rearrangement of the electronic orbitals takes place, as in a chemical reaction, then the simple method of rescaling the ionic masses will no longer work. We have also neglected in our analysis higher order dependences of the Car-Parrinello forces on the fictitious mass and it may be that in certain systems and for large masses these terms of equation 2.16 become relevant. An important test which should always be performed is to check results of CP simulations for a dependence on μ.

If one is to judge the quality of a CP simulation by the errors in the forces as we have largely done here, then a question which needs to be addressed is to what extent these errors manifest themselves as errors in the properties of interest in the simulation. It is likely that random high frequency oscillations in the forces such as those due to the dynamics of the $\delta\psi_i$ have no discernible effect on the thermodynamics of the system if such oscillations are small. The magnitude of the oscillations seen here in the case of MgO and ice may be a cause for concern however. The apparent anharmonicity of these oscillations in the case of water may also lead to problems.

All of the effects discussed in this chapter are dependent on the choice of the fictitious mass parameter, μ, and by reducing this parameter all thermodynamic and dynamic properties of a simulation may be brought arbitrarily close to those in a Born-Oppenheimer system. A reduction of μ has the drawback that the time step required to integrate the equation of motion for the electronic orbitals is reduced thereby decreasing the computational efficiency of the method. However, the time step scales as $\Delta t \sim \mu^{1/2}$. This means that reducing μ by an order of magnitude increases the simulation time by only a factor of three. By checking how the property of interest in a simulation scales with μ one can control the level of approximation with which it is calculated.

In the past it has been thought[12] that once the fictitious kinetic energy of the orbitals stayed small and reasonably constant in a simulation, the dynamics were essentially independent of the electronic mass. For this reason, its value is frequently not reported in articles along with other relevant technical details. We show here that the mass is an important parameter which has a significance which is at least comparable to, for example, the choice of exchange-correlation functional.

There is a clear need, in light of our theoretical findings, to test the ability of Car-Parrinello simulations to model chemical reactions, phase transitions and systems of low symmetry. These are the kinds of systems which are most frequently simulated with CPMD and they are also the systems in which a serious dependence of *thermodynamic* properties on the fictitious mass would be most likely to occur.

Chapter 3

Simple Models of Ionic Systems

3.1 Introduction

The problem of simulating ionic materials has a long history[38]. One of the oldest, and still the most widely used interaction potential for such systems treats the ions as though they are small rigid particles which are undistorted by their environment. This is the Born-Mayer pair potential[39],

$$U_{IJ}(R_{IJ}) = \frac{q_I q_J}{R_{IJ}} + B_{IJ} e^{-\alpha_{IJ} R_{IJ}} - \frac{C_{IJ}}{R_{IJ}^6} - \frac{D_{IJ}}{R_{IJ}^8} \tag{3.1}$$

where U_{IJ} is the interaction energy of particles I and J which are a distance R_{IJ} apart. q_I and q_J are charges on the ions and the first term on the right hand side is the electrostatic energy of the point-like charges and is generally evaluated using the method of Ewald summation[40]; the second term reflects the fact that an isolated electron distribution tails off exponentially and so the repulsion between ions at short range due to the Pauli exclusion principle can be approximated by a constant (B_{IJ}) times an exponential overlap of ionic charge distributions ; the final two terms model the ion dispersion interactions which are always attractive and which represent the correlated motions of electrons on different ions which can be represented as a sum of dipole - induced dipole (R_{IJ}^6 term), dipole - induced quadrupole (R_{IJ}^8 term) and higher order terms which are generally neglected. q_I,α_{IJ},B_{IJ},C_{IJ} and D_{IJ} are all parameters of the model which may be determined either by physical reasoning, empirical considerations or by fitting to data obtained from *ab initio* calculations.

This potential form has the advantage that it has a pairwise form and it is quick and easy to evaluate, so that large system sizes and long times may be simulated with relative ease. However, it has been recognised for some time [41, 42] that this form does not contain some of the physics relevant for many real ionic systems. Many systems contain anions which have an appreciable size relative to interionic distances and which are not rigid, in the sense that they become aspherically distorted and can change their size in the condensed phase depending on their environment. A distorted ion is one with multipole moments, the most important of which is the lowest order or dipole moment. The induction, via electrostatic interactions, or short range Pauli exclusion-type interactions

of dipole moments on ions can have a significant effect on the electrostatics of a system. In particular, the oxide ion is known to be highly distortable and polarizable and many attempts have been made to model this in the past.

3.1.1 The Shell Model

The Shell-Model[38, 43, 44, 45] is the oldest and most common method of incorporating environmental effects. In this scheme a shell of charges is attached to the nucleus via a harmonic (or indeed anharmonic) spring (see figure 3.1). In this way, the ion may become polarized via a displacement of the shell of charge from being centered on the nucleus. The induction of dipoles via short-range forces may be implemented by having these forces act between shells (which can be thought of as representing the electrons) rather than between nuclei. An extension of this model to allow for an isotropic *breathing* motion of the shell has been introduced by Schröder [46]. A disadvantage of the shell model is that it introduces extra degrees of freedom into the system and therefore can slow down simulations. However it has been used with some success for many years, primarily to include the important polarization effects which have the marked effect in ionic crystals of reducing frequency differences between the transverse optical and longitudinal optical phonon modes.

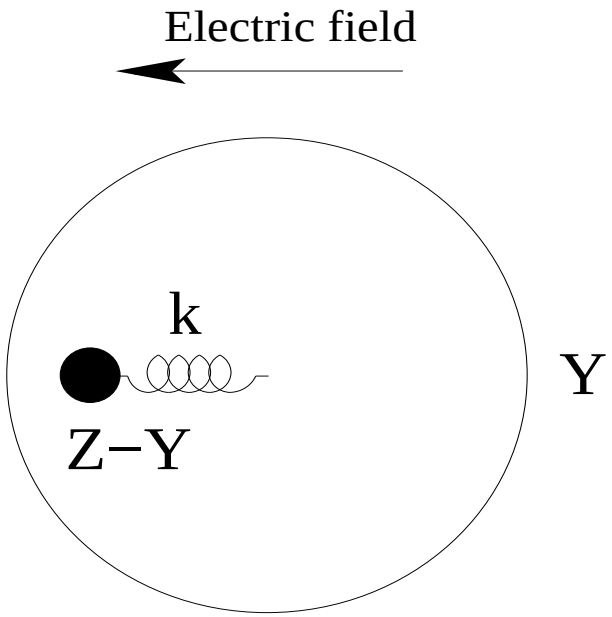

Figure 3.1: An illustration of the shell model of ionic polarizability. A massless shell of charge Y is connected by a spring of spring-constamt k to the massive ionic core which carries a charge $Z - Y$ where Z is the net ionic charge.

The use of the Shell Model in the past has been to some extent due to the fact that in its simplest and standard form it depends on only two parameters, the spring constant and the shell charge. Until recently, all parameters needed to be determined empirically

or from physical arguments and a simple relation exists between these parameters and the dipole polarizability of the ion which may be determined experimentally. However, frequently if one chose the parameter which best reproduced experimental quantities such as densities or bulk moduli, it did not correspond well to its known physical interpretation. Shell model parameters are also generally non-transferable between different chemically related materials, or even between different phases of the same material. It has been suggested [47] that the Shell Model representation of the effects of polarization and expansion/compression of the anion is overly restrictive in that it couples all these effects in too simple a way so that they may be described by as few parameters as possible. Although all these effects are clearly connected, their relationship is unlikely to be as simple as it is represented in the Shell Model.

In a series of papers over several years many people, most prominently, Wilson, Madden and coworkers have developed a new way of representing the many body effects in ionic systems[47, 48, 49, 50, 51, 52, 53]. The current state of this research will be explained in this chapter followed by a description of the approach that we have taken to the same problem which differs in many important ways from previous approaches.

3.2 Many-body Interactions in Simple Ionic Systems

It has been shown[52] that an effective way of treating the interactions in simple ionic systems is to divide them into the following independent sets of contributions :

1. Electrostatic effects. These include
   - Interactions between the ionic point charges.
   - Screening of these interactions by induced multipoles and local variations in the degree of ionicity[53].
   - Induction of multipoles through distortions of ionic charge distributions by short-range interactions with neighbouring ions and the impact of these multipoles on the electrostatic field.
2. Short-Range repulsive interactions between ions. These are basically exponential in form but may be affected by
   - Spherical "breathing" or "compression" of the ions.
   - Aspherical shape deformations of the ions.
3. Dispersion interactions which may also be damped at short range when ionic charge densities overlap[54].

Clearly there is a degree of arbitrariness in this division and there is a clear overlap between some of these effects. For example, the dipoles induced by short-range interactions are physically the same thing as the aspherical distortions which are caused by and impact on the short-range repulsive interactions. Nevertheless, as a practical scheme this division has proved useful and Rowley *et. al.* have shown that in magnesium oxide,

the phonon dispersion curves can be well reproduced by independently adding in these effects[52]. More recently, Aguado *et. al.* have reparametrized the original model of Rowley *et al.* using density functional theory calculations to produce a much improved set of phonon dispersions[55].

We now discuss the model that they have used in detail.

3.3 Electrostatic Effects

To supplement the interactions of point charges and following previous work[48, 50] Rowley *et al.* allowed the induction of a dipoles and a quadrupoles on each oxygen ion in MgO. They assumed that the degree of ionicity was fixed such that the Mg atom lost exactly two electrons to the O atom and they allowed for no local changes in ionicity. This latter assumption is supported by our density functional theory calculations of MgO (see chapter 2) where we observe no significant deviation from full ionicity. They have also allowed for the induction of multipoles via short-range interactions.

3.3.1 Electrostatic Polarization

The induction of multipoles complicates the calculation of the electrostatic forces considerably since not only does one have to calculate charge-dipole, dipole-dipole, charge-quadrupole, dipole-quadrupole and quadrupole-quadrupole interactions for each pair of ions, the correct values of the dipoles and quadrupoles on each ion must first be calculated. This is not a trivial problem since the multipoles on an ion are proportional to the derivatives of the electrostatic potential at the position of the ion. However, the electrostatic potential is itself dependent on the multipoles. For example, for the case of dipoles we may write[56]

$$\mathbf{p}_I = \alpha_I \mathbf{E}_I \tag{3.2}$$

$$\mathbf{E}_I = \mathbf{E}_I^0 + \sum_{IJ} \mathbf{T}_{IJ} \cdot \mathbf{p}_J \tag{3.3}$$

where the dipole $\mathbf{p}_I$ on ion I is proportional to the electric field $\mathbf{E}_I$ at the position of ion I. The constant of proportionality is the scalar polarizability. $\mathbf{E}_I^0$ is the "fixed" part of the electric field due to charges, permanent dipoles and any other applied field.The electric field in turn depends on all the dipoles via $\mathbf{T}_{IJ}$ the dipole-dipole interaction tensor. To solve this pair of equations amounts to solving a set of $3N \times 3N$ linear equations and even to do this iteratively would be far too computationally expensive for most applications.

One solution, proposed originally by Sprik and Klein [48] and used in all the works by Wilson, Madden and coworkers[50] is to treat the dipoles in an extended lagrangian scheme analogous to the Car-Parrinello molecular dynamics scheme for the electronic structure problem[4]. In other words, a lagrangian is written in which the dipole moments on the ions are expressed as extra degrees of freedom of the system with a *fictitious* mass associated with them.

$$\mathcal{L} = \frac{1}{2} \sum_I \mathrm{M}_I \dot{\mathbf{R}}_I^2 + \sum_I \mu_I \dot{\mathbf{p}}_I^2 - U[\{\mathbf{p}_I\}; \{\mathbf{R}_I\}] \tag{3.4}$$

M_I and μ_I are the masses of atom I and the dipole on atom I respectively. Beginning with the dipoles at their minimum energy values, the ionic system is evolved and just as in the electronic case the dipoles are expected to remain close to their minimum energy values (i.e : the values for which $\frac{\partial U}{\partial p_I} = 0 \quad \forall\, I$) if their fictitious kinetic energy is small. It is thought that this may be achieved either by choosing a small enough fictitious mass so that due to adiabatic decoupling there is only a small transfer of energy between dipoles and ions or in many cases by applying a thermostat to both the electronic and ionic subsystems in the same way as was proposed by Blöchl and Parrinello for the electronic case[15].

In practice, the dipoles are normally represented by two or more charges at fixed distances from the ion center but with variable magnitudes and orientation. This is because it is easier to evaluate the Ewald sum for charges than it is for dipoles. The inclusion of quadrupolar interactions is achieved in a similar manner but with six degrees of freedom in addition to the three dipolar degrees of freedom[57].

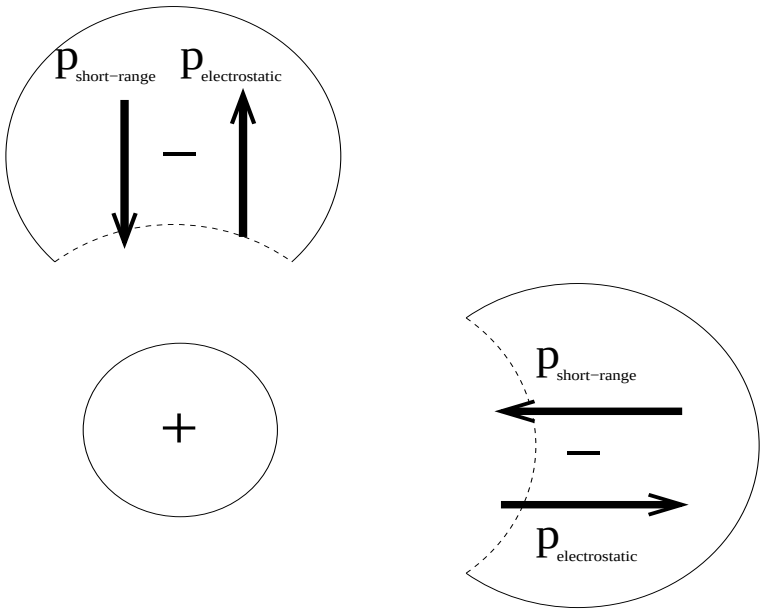

Figure 3.2: An illustration of how short-range repulsive interactions between ions can induce effective multipoles. In this picture, the small cation "dents" the charge distribution of the much larger cation and the resulting aspherical distribution has a dipole moment which is opposite to that induced electrostatically by the cation.

3.3.2 Polarization by Short-Range Interactions

Wilson and Madden found that the simple electrostatic polarization model had significant shortcomings. The ions tended to become over-polarized and particularly in the melt, small anion-cation distances resulted in very large induction forces which overcame the short-range Pauli exclusion repulsion. In the real system at such distances, the cation

distorts the anion and the resulting dipole is of opposite sign to the electrostatic dipole which would be induced if the cation and anion were isolated. This is illustrated in figure 3.2. Wilson and Madden found a convenient way of representing this short-range induced dipole. They wrote the dipole induced on each ion as

$$\mathbf{p}_I = \alpha_I \mathbf{E}_I + \sum_{J \neq I} \alpha_I g_{IJ}(R_{IJ}) \frac{q_j \mathbf{R}_{IJ}}{R_{ij}^3} \tag{3.5}$$

where

$$g_{IJ}(R_{IJ}) = c_{IJ} e^{b_{IJ} R_{IJ}} \sum_{k=0}^{n_k} \frac{(b_{IJ} R_{IJ})^k}{k!} \tag{3.6}$$

and c_{IJ} and b_{IJ} are negative and positive constants respectively, and for dipoles n_k took the value 4. A similar scheme was used for quadrupoles [57]. The function $g_{IJ}(R_{IJ})$ was first introduced by Tang and Toennies as a damping function for dispersion effects (see section 3.5) and its use in this context was justified by Wilson and Madden based on its ability to fit numerically the results of electronic structure calculations[58] on distorted crystalline environments.

3.4 Short-Range Repulsive Interactions

The use of the standard exponential repulsion term found in the Born-Mayer potential rests on the assumptions that ions are spherical and of fixed size and that the repulsion between them due to the Pauli exclusion principle is proportional to the overlap between the ions whose charge distribution tails off exponentially. Although this may be an adequate approximation in crystals of high symmetry at low temperatures and a given pressure , at higher temperatures or at a different pressure or when a change of phase occurs, it is likely that anions will readjust their size and shape to fill the available space. In order to cope with this, and in an attempt to improve the ability of ionic models to reproduce experimental equations of state and the relative energetics of different crystal structures, Wilson *et al.* have developed a compressible ion model[47]. Another strong motivation was the fact that the Cauchy relation between the elastic constants ($C_{44} = C_{11}$)[59] is known to be violated in both MgO and CaO in the NaCl structure. For MgO, the ratio C_{44}/C_{12},extrapolated to 0K at zero pressure reaches 1.68 for MgO [60] and 1.44 for CaO[61]. This relation holds for centrosymmetric crystals under zero stress if the interactions may be modelled in a simple pairwise way.

Wilson *et al.* wrote the potential energy due to short-range repulsive interactions between anion and cation as

$$V_{+-}^{\mathrm{SR}}(\{R_I\};\{\delta\sigma_I\}) = V_{\mathrm{self}}(\{\delta\sigma_I\}) + V_{\mathrm{ov}}(\{R_I\};\{\delta\sigma_I\}) \tag{3.7}$$

where V_{self} is the sum of the changes in the internal energies of the ions and V_{ov} is the total potential energy due to interaction between the ions, and $\delta\sigma_I$ is the change in the radius of the ion from its average value σ_I^0. From electronic structure calculations of the

perfect cubic crystal it was found that $V_{\rm self}$ could be written as

$$V_{\rm self}(\{R_I\};\{\delta\sigma_I\}) = \sum_{I\epsilon -} D_I \cosh(\beta\delta\sigma_I) \tag{3.8}$$

and the standard exponential form was adopted for the interaction energy :

$$V_{\rm ov}(\{R_I\};\{\delta\sigma_I\}) = \sum_{I\epsilon -, J\epsilon +} B_{IJ} e^{-\alpha_{IJ}(R_{IJ}-(\sigma_I^0+\delta\sigma_I))} \tag{3.9}$$

At each timestep, during a simulation, the $\{\delta\sigma_I\}$ were required to take values that minimized $V^{\rm SR}$ and this was achieved, once again by using a Car-Parrinello-type extended lagrangian approach with the $\{\delta\sigma_I\}$ as the variables with which a fictitious dynamics was associated.

Although this has been successful in reproducing some low temperature properties of MgO and CaO such as the crystal energies as a function of volume, the prediction of phonon frequencies with this model was found to be quite poor. This is because the distortion of the anions are in general not spherically symmetric if the crystal is disordered. To account for aspherical distortions of the anion, Rowley *et al.*[52] have extended the previous compressible-ion model. They allowed for the effect of purely spherical distortions on the anion-anion interactions and the extended the compressible ion model to allow for aspherical distortions to affect the anion-cation intetraction.

The self energy $V_{\rm self}$ is extended to include distortions of the anions of dipolar and quadrupolar symmetry

$$V_{\rm self}(\{\delta\sigma_{I\epsilon -}\};\{\boldsymbol{\nu}_I\};\{\boldsymbol{\kappa}_I\}) = \sum_I [D_I \cosh(\beta\delta\sigma_I) + (e^{\xi^2|\boldsymbol{\nu}_I|^2} - 1) + (e^{\eta^2|\boldsymbol{\kappa}_I|^2} - 1)] \tag{3.10}$$

where $\boldsymbol{\nu}_I$ is a set of three variables describing the dipolar distortion of the oxide ion and $\boldsymbol{\kappa}_I$ is a set of five independent variables describing the quadrupolar shape distortions. They only considered distortions to affect the anion-cation interactions so that

$$\begin{aligned} V_{\rm ov}(\{R_I\};\{\delta\sigma_I\};\{\boldsymbol{\nu}_I\};\{\boldsymbol{\kappa}_I\}) &= \sum_{I\epsilon -, J\epsilon +} B_{+-} e^{-\alpha_{+-}\rho_{IJ}} \\ &+ \sum_{I\epsilon -, J\epsilon -} B_{--} e^{-\alpha_{--}(R_{IJ}-\delta\sigma_I-\delta\sigma_J)} \\ &+ \sum_{I\epsilon +, J\epsilon +} B_{++} e^{-\alpha_{++}R_{IJ}} \end{aligned} \tag{3.11}$$

where

$$\rho_{IJ} = R_{IJ} - \delta\sigma_I - S^{\alpha}_{(1)}\nu^{\alpha}_I - S^{\alpha\beta}_{(2)}\kappa^{\alpha\beta}_I \tag{3.12}$$

$$S^{\alpha}_{(1)} = R^{\alpha}_{IJ}/R_{IJ} \tag{3.13}$$

$$S^{\alpha\beta}_{(2)} = 3R^{\alpha}_{IJ}R^{\beta}_{IJ}/(R_{IJ})^2 - \delta^{\alpha\beta} \tag{3.14}$$

$$\tag{3.15}$$

and summation of repeated *greek* indices is implied.

Once again, in this scheme, $V^{\mathrm{SR}} = V^{\mathrm{self}} + V^{\mathrm{ov}}$ is minimized with respect to set of all $\delta\sigma_I$,ν_I^α, and $\kappa_I^{\alpha\beta}$ and these nine variables per anion are evolved as classical degrees of freedom using a Car-Parrinello-like lagrangian.

With this aspherical-ion model and including dispersion effects (to be discussed in the next section) and polarization effects, Rowley *et al.* managed to find parameters which gave good phonon dispersion curves for MgO. Very recently Aguado *et al.* have used an almost identical model, but with many of the parameters found from DFT calculations, to produce phonon dispersion curves and thermal expansion curves of a very high quality[55]. Since thermal expansion depends on the second derivatives of the potential energy with respect to the ionic positions, this is a good test of this model's representation of the potential energy surface of the crystal.

3.5 Dispersion Forces

Dispersion forces arise from correlated electronic fluctuations between separated ions. These take the form of multipole-induced multipole forces the lowest order and most important of which is the dipole-induced dipole interaction. A dipole produced by random electronic fluctuations in one ion can induce an opposing dipole in a neighbouring ion. This may result in their polarities fluctuating in synchronisation and these opposite dipoles attract one another with a $1/R^6$ dependence. Dipole-induced quadrupole interactions have a $1/R^8$ dependence and successively higher order terms decay more rapidly. However, when ions become closer and overlap these forces become damped. Electrons lose some of their freedom to fluctuate in this way as they become part of the same charge distribution and the correlations in their motion acquire a much more complicated form.

Tang and Toennies [54] have found a simple functional form for the rate at which this damping occurs. This is given by equation 3.6. In the simulations of Aguado *et al.* and Rowley *et al.* they have included the two dispersion terms of lowest order with short-range Tang-Toennies damping functions $g^{(6)}$ and $g^{(8)}$:

$$V_{\mathrm{disp}} = -\sum_{IJ} [g_{IJ}^{(6)}(R_{IJ})\frac{C_{IJ}^{(6)}}{R_{IJ}^6} + g_{IJ}^{(8)}(R_{IJ})\frac{C_{IJ}^{(8)}}{R_{IJ}^8}] \tag{3.16}$$

3.6 Discussion of Existing Approaches

So far in this chapter, some of the existing approaches for modelling ionic systems and specifically simple oxides have been outlined. There are very clear indications such as the experimental violation of the Cauchy relation (see section 3.4) or the inability of pairwise potentials to fit the DFT forces (to be discussed in chapter 5) that many-body forces are important to accurately describe the interactions in such systems. Pair potentials have failed to model the phonon dispersions or the thermal expansion in MgO , although it is difficult to tell where this is a fault of the potential form and where it is a fault of the parametrization which in the past has been almost entirely empirical.

Much emphasis has been given here to the system of many-body interactions developed by Wilson, Madden and coworkers. The reason for this is that they have shown clearly that, at least for the crystalline simple oxides the potential form that they use provides a good description of the ions' potential energy surface. However, although it is clear that the full model that they use is sufficient to describe the physics of MgO, it is not clear whether all the interactions that they have included are necessary or, as they discuss in the paper by Rowley *et al.*[52], whether or not the full model is overcomplete. Although they try to address these issues, the parametrization scheme that they use is empirical and each contribution is parametrized independently. As can be clearly seen from the results of chapter 6 and their subsequent paper [55] they did not take full advantage of their functional form which can only be done by fitting all parameters simultaneously.

A serious problem with their method lies in the fact that they use the Car-Parrinello extended lagrangian approach for all of their many-body interactions. This means that to each anion is associated eighteen additional degrees of freedom. These additional degrees of freedom are associated with the five groups of variables which describe electrostatic dipoles and quadrupoles, and ionic distortions of monopolar, dipolar and quadrupolar symmetry. In order to make this work one needs to make sure that each set of dynamical variables remains energetically isolated from every other one. Or, at least, that all of them remain adiabatically decoupled from the ions insofar as this is possible. The time step is determined by the fastest degree of freedom and in the paper by Aguado *et al.* the time step that they report using for crystalline MgO at 300K is approximately 1/20 of a femtosecond. This is at least a factor of thirty smaller than the timestep that could normally be used for this system and is presumably the timestep required for accuracy within this approach.

Another possible problem with this method is that there may be effects, particularly in less symmetric phases than the NaCl structure, analogous to those that have been discussed in chapter 2 for the electronic problem. It can be shown (as was done for the electronic orbitals in section 2.2) that if the ions are moving, it is not possible for the extra dynamical variables to take their minimum energy values on average. In fact, the average error in the αth force component on ion I, to first order in the deviations of the fictitious degrees of freedom from their instantaneous average values and the fictitious mass, may be written as

$$\begin{aligned} \Delta F_I^\alpha &= \sum_i \mu_i \Bigg\{ \sum_J \ddot{R}_J^\beta \frac{\partial \eta_i}{\partial R_I^\alpha} \frac{\partial \eta_i}{\partial R_J^\beta} \\ &+ \sum_{J,K} \dot{R}_J^\beta \dot{R}_K^\gamma \frac{\partial \eta_i}{\partial R_I^\alpha} \frac{\partial^2 \eta_i}{\partial R_K^\gamma \partial R_J^\beta} \Bigg\} \end{aligned} \tag{3.17}$$

where $\sum_i$ is the sum over all the fictitious degrees of freedom η_i. Once again, the magnitude of this error depends on the extent to which the dynamical variables vary with ionic positions and it scales linearly with the fictitious mass μ_i. It is not known how important this problem is in general. For the case of the NaCl crystal structure at 300K, tests of the extended lagrangian approach to the dipole polarizable and the simple compressible ion model have been published[50, 47] and the values of the fictitious degrees of freedom are

to be in very good agreement with their minimum energy values. However, it is likely that any problem that may exist would be less serious under these conditions of high symmetry and low temperature than, for example, in a liquid or during a phase transition.

In the aspherical ion model, the anion is only allowed to distort with either dipolar or quadrupolar symmetry. It would be desirable to be able to include anion distortions of arbitrary shape as they may become relevant in low symmetry phases.

3.7 Our Approach to Modelling Ionic systems

It was decided that for the reasons of computational speed and accuracy outlined in the previous section it was best to try to avoid the use of any Car-Parrinello-like extended lagrangian approach to modelling the many-body forces in ionic systems. Another compelling reason is that in the parametrization process (see chapter 4) one does not have the benefit of a previous time step from which to extrapolate or evolve the degrees of freedom. Since parametrization is a computationally expensive process, it is important to find a way which is reasonably fast even when calculating the force for the first time. It is unlikely that putting the eighteen degrees of freedom per anion to their potential energy minimum via steepest descent or any other method would be sufficiently fast for parametrization purposes and, in fact, in the paper by Aguado *et al.* where they parametrize their model by fitting the forces to those from DFT calculations they only parametrize the non-electrostatic parts of their model in this way. Since the electrostatics are the most important part, but also the most time-consuming part of any simulation of an ionic system one may speculate that the reason they did not fit the ionic charges and polarizabilities was due to the computational expense involved.

Since dipolar polarization is the most important electronic screening mechanism in most simple ionic systems, we have decided to model this in our approach. However, we have not included quadrupolar polarization which in the paper of Rowley *et al.* was shown to have only a small effect on the phonon spectrum of MgO and which would increase significantly both the computational expense of the model and the man-hours required to implement the model. We have neglected the effect of charge transfer between ions, as did Wilson,Madden and coworkers, on the basis that for the systems we are interested in studying, no evidence was initially found to suggest that this was an important effect.

We also would like to model the effect that size and shape distortions of the anion has on the short-range interactions.

Since we would like to avoid the use of an extended lagrangian approach, we have had to find different approaches to modelling polarization and anion-distortion. In section 3.7.1 we outline the approach that we have taken to the polarization problem and in sections 3.7.2 and 3.7.3 we describe a new many-body potential for ionic systems which attempts to model anion distortions in an analytic way.

3.7.1 Polarization

As previously discussed in section 3.3.1, the difficulty in treating dipole polarization is that one must solve the $3N \times 3N$ linear system represented by equations 3.2 and 3.3. The charge-dipole and the dipole-dipole interaction terms decay as $1/R^3$ and $1/R^5$ respectively. Unfortunately, this decay is not sufficiently rapid for one to be able to truncate the interactions between particles at a reasonably small interionic distance, and so, as with the charge-charge interactions, all the dipole terms must be calculated using an Ewald summation technique [40, 63, 64]. The procedure that we have taken to this problem and that has been taken in the past [64, 65, 66] is to solve the system of equations in a self-consistent way. In other words, starting with an initial guess for the dipole moments on each ion we calculate the electric field at the site of each ion due to the combination of dipoles and charges. The new set of dipole moments is then easily calculated by multiplying the electric field on each ion by its polarizability. When the root-mean-square value of the difference between the components of the electric field from successive steps in the self-consistency procedure is within a specified tolerance, the system is deemed to be at convergence. It was found that during an MD simulation, a quantity which tended to vary much more slowly than the dipole moment on each ion was the contribution of all the dipoles in the system to the electric field at each ion's position. Therefore, the initial guess of the dipoles which was used in the self-consistent minimization was calculated from a guess of this quantity which was extrapolated from three previous timesteps. We also include the short-range contributions to the induced dipole moments using the functional form proposed by Madden and Wilson [50] and discussed in section 3.3.2.

The algorithm that we use for calculating all electrostatic contributions to the total energy, forces and stress at time step n is as follows :

1. Using the method of Ewald summation [40], the contribution from the *charges* on the ions to the total energy (U_{qq}), forces ($F^{\alpha}_{qq_I}$) and stress ($S^{\alpha\beta}_{qq}$) is calculated.

2. The short-range induced dipole moment on each ion is calculated as :

$$\mathbf{p}_I^{\mathrm{sr}} = \sum_{J \neq I} \alpha_I g_{IJ}(R_{IJ}) \frac{q_j \mathbf{R}_{IJ}}{R_{ij}^3} \tag{3.18}$$

   where $g_{IJ}(R_{IJ})$ is given by equation 3.6.

3. The initial guess of the dipole contribution to the electric field on each ion I is calculated to be[1]

$$\mathbf{E}_{\mathbf{p}I}^{\ \mathrm{guess}} = 3\mathbf{E}_{\mathbf{p}I}^{\ (n-1)} - 3\mathbf{E}_{\mathbf{p}I}^{\ (n-2)} + \mathbf{E}_{\mathbf{p}I}^{\ (n-3)} \tag{3.19}$$

   where $\mathbf{E}_I^{(n-1)}$ is the electric field at ion I calculated at the previous MD time step. For the first three time steps, of an MD simulation, or during parametrization, the value $\mathbf{E}_I^{\mathrm{guess}} = \mathbf{0}$ is chosen.

[1] It was found that the period of the oscillations in the dipole moment was generally large enough that the algorithm would almost certainly be made more efficient by extrapolating from more than three previous time steps, but this has not yet been implemented in the MD program.

4. The self consistent polarization cycle begins and proceeds as follows where m is the number of the iteration step :

   (a) If $m = 1$ then the total electric field on ion I is

   $$\mathbf{E_T} = \mathbf{E}_{\mathbf{p}_I}^{\text{guess}} + \frac{\mathbf{F}_{\mathbf{q}_I}}{q_I} \tag{3.20}$$

   otherwise

   $$\mathbf{E_T} = \beta \mathbf{E}_{\mathbf{p}_I}^{(m-1)} + (1-\beta)\mathbf{E}_{\mathbf{p}_I}^{(m)} + \frac{\mathbf{F}_{\mathbf{q}_I}}{q_I} \tag{3.21}$$

   where β is a parameter which is optimised at the beginning for fast convergence. β typically takes values of between 0.6 and 0.8.

   (b) The dipole moment on each ion is calculated as

   $$\mathbf{p}_I = \alpha_I \mathbf{E}_{\mathbf{T}I} + \mathbf{p}_I^{\text{sr}} \tag{3.22}$$

   (c) Using the current set of dipole moments $\{\mathbf{p}_I\}$, $\mathbf{E}_{\mathbf{p}_I}^{(m)}$ is calculated for each ion using Ewald summation[64].

   (d) The quantity

   $$\Gamma^{(m)} = \sqrt{\sum_I \frac{\alpha_I^2}{N} |\mathbf{E}_{\mathbf{p}_I}^{(m)} - \mathbf{E}_{\mathbf{p}_I}^{(m-1)}|^2} \tag{3.23}$$

   is calculated where N is the number of polarizable ions.

   (e) If $|\Gamma^{(m)} - \Gamma^{(m-1)}| < \delta$, where δ is a predefined convergence criterion then go to step 5, otherwise return to step (i).

   The most economical value of δ that can be used can vary from system to system and depends on the degree of energy conservation required but a value of 10^{-6} was found to conserve energy to a very high precision in all the systems studied. During the parametrization process, one does not need such a low tolerance for convergence and so a value of $\delta = 5 \times 10^{-4}$ was used. With this value, forces and stress were converged to within $\sim 0.3\%$.

5. Using the converged values of $\mathbf{E}_{\mathbf{p}_I}^{(n)}$, the dipole moments are recalculated as

   $$\mathbf{p}_I = \alpha_I (\mathbf{E}_{\mathbf{p}_I}^{(n)} + \frac{\mathbf{F}_{\mathbf{q}_I}}{q_I}) + \mathbf{p}_I^{\text{sr}} \tag{3.24}$$

   and these are used to calculate the energy (U_{dq},U_{pp}), forces ($F^{\alpha}_{qp_I}$,$F^{\alpha}_{pp_I}$) and stress ($S^{\alpha\beta}_{qp}$,$S^{\alpha\beta}_{pp}$) due to charge-dipole and dipole-dipole interactions using Ewald summation[64].

6. The contribution of the short-range induction of dipole moments to the energy (U_{sr}) , forces ($F^{\alpha}_{\text{sr}_I}$) and stress ($S^{\alpha\beta}_{\text{sr}}$) is calculated[50, 52].

7. All contributions to the energy forces and stress are added together. For example, for the energy :

   $$U = U_{qq} + U_{dq} + U_{dd} + U_{\text{sr}} \tag{3.25}$$

Unfortunately, this self-consistent minimization procedure is not guaranteed to converge. For example, if an anion and a cation come very close together the dipole on the anion can become unphysically large. This can have a drastic effect on the surrounding electric field and the dipole field diverges. We have found that when such a configuration occurs convergence, fails regardless of the initial guess $\mathbf{E}_{\mathbf{p}_I}^{\text{guess}}$. Luckily, experience has shown that the more physical the electrostatic and short-range dipole-induction parameters we have, the less likely this dipole "explosion" is to occur, but we have not managed to eliminate it completely. This is a big problem as when this happens, the MD simulation is effectively over. It is not possible to recover as, even if one continues with unconverged dipoles (e.g: those calculated simply from the charge contribution to the electric field), the kinetic energy of the system increases dramatically and conservation of energy is lost. This is only a problem for liquid systems and is much more likely to occur at very high temperatures and pressures significantly different from the pressure at which the model was parametrized. Its occurrence, if frequent, may indicate the need for a new parametrization of the potential.

Similar problems have been reported for the Car-Parrinello approach [50].

3.7.2 A Distortable Ion Model

In this section a general framework will be developed for the inclusion of environmental effects on the size and shape of an ion and the subsequent effect of such distortions on the short-range interionic forces. In the next section we will show how this general framework has been implemented in practice.

We will be primarily concerned with the anion-cation interaction. Of much lesser concern, initially at least, is the anion-anion interaction energy which has been found to provide only $\sim 3\%$ of the energetics of the perfect crystal[52, 47]. Although, the same cannot be said with any degree of certainty of more disordered phases, or systems of different stoichiometry such as SiO_2, it is nonetheless the most obvious place to start when constructing a potential.

We assume that a distortable ion (such as O^{2-}) has its shape and size "influenced" by all sufficiently close neighbouring ions. Much as in the scheme of Wilson, Madden and coworkers[47, 52], an ion is described as a nucleus surrounded by a single membrane (representing the electrons) the radius of which is allowed to vary with the two polar angles (although in their case, the radius only varied in certain symmetric ways). The influence an ion J exerts on ion I can be loosely thought of as a restraining force on the ion's tendency to expand and this restraint has a dependence on the polar angles (θ, ϕ) in the spherical coordinate system centered on I. We also assume that the influence exerted at coordinates (θ, ϕ) is zero if the angle between the outward unit vector at those coordinates $\ell(\theta, \phi)$ and the vector $\mathbf{R}_{JI} = \mathbf{R}_J - \mathbf{R}_I$ is greater than $90°$.

We write the total influence on I at (θ, ϕ) due to all the other ions as

$$\rho_I^{(1)}(\theta, \phi) = \sum_{J \neq I} f_{IJ}(R_{IJ}) \ell(\theta, \phi) \cdot \mathbf{x}_{JI} \Theta(\ell(\theta, \phi) \cdot \mathbf{x}_{JI}) \tag{3.26}$$

where $\mathbf{x}_{JI} = \frac{\mathbf{R}_{JI}}{R_{JI}}$ and

$$\Theta(\ell(\theta,\phi)\cdot\mathbf{x}_{JI}) = \begin{cases} 1 \text{ if } \ell(\theta,\phi)\cdot\mathbf{x}_{JI} > 0 \\ 0 \text{ if } \ell(\theta,\phi)\cdot\mathbf{x}_{JI} < 0 \end{cases} \tag{3.27}$$

The subscripts on the scalar function f_{IJ} are to indicate that a different function is used for every distinct pair of ionic species.

Apart from a multiplicative constant, the spherical average of $\rho_I^{(1)}(\theta,\phi)$ is

$$\rho_I^{(0)} = \sum_{J\neq I} f_{IJ}(R_{IJ}) \tag{3.28}$$

We write the angular dependent radius , $\sigma_I(\theta,\phi)$ of an ion as

$$\sigma_I(\theta,\phi) = \sigma_I^{(0)}(\rho^{(0)}) + \sigma_I^{(1)}(\rho^{(0)}, \rho_I^{(1)}(\theta,\phi)) \tag{3.29}$$

In other words, the radius at (θ,ϕ) is written as a sum of an average value due to the influence of all the ions and deviations from that average. The distance between the membranes of ions I and J along their line of centers is

$$L_{IJ} = R_{IJ} - \sigma_I(\theta_{JI},\phi_{JI}) - \sigma_J(\theta_{IJ},\phi_{IJ}) \tag{3.30}$$

where θ_{JI} and ϕ_{JI} are defined such that $\ell(\theta_{JI},\phi_{JI}) = \mathbf{x}_{JI}$ and it will be convenient to use the notation

$$\begin{aligned} \rho_{IJ}^{(1)} &= \rho_I^{(1)}(\theta_{JI},\phi_{JI}) && (3.31)\\ \sigma_{IJ}^{(1)} &= \sigma_I^{(1)}(\rho^{(0)}, \rho_I^{(1)}(\theta_{JI},\phi_{JI})) && (3.32)\\ \sigma_{IJ} &= \sigma_I(\theta_{JI},\phi_{JI}) && (3.33)\\ A_{IJK} &= \Theta(\mathbf{x}_{IJ}\cdot\mathbf{x}_{IK}) && (3.34) \end{aligned}$$

We now define the total energy of the system as a sum of pairwise interactions between membranes.

$$U = \sum_{I,J>I} U_{IJ}(L_{IJ}) g_{IJ}(R_{IJ}) \tag{3.35}$$

where $g_{IJ}(R)$ takes the value 1 for $R < R_a$, 0 for $R > R_b$ and decays smoothly from 1 to 0 between R_a and R_b. This allows us to truncate the interaction at intermediate distances.

The αth force component on ion K is then written as

$$\begin{aligned} F_K^\alpha = &- \sum_{I,J>I} g_{IJ}\frac{\partial U_{IJ}}{\partial L_{IJ}}\left(x_{IJ}^\alpha(\delta_{IK}-\delta_{JK}) - \frac{\partial\sigma_{IJ}}{\partial R_K^\alpha} - \frac{\partial\sigma_{JI}}{\partial R_K^\alpha}\right) \\ &- \sum_{I,J>I} U_{IJ}\frac{\partial g_{IJ}}{\partial R_{IJ}} x_{IJ}^\alpha(\delta_{IK}-\delta_{JK}) \end{aligned} \tag{3.36}$$

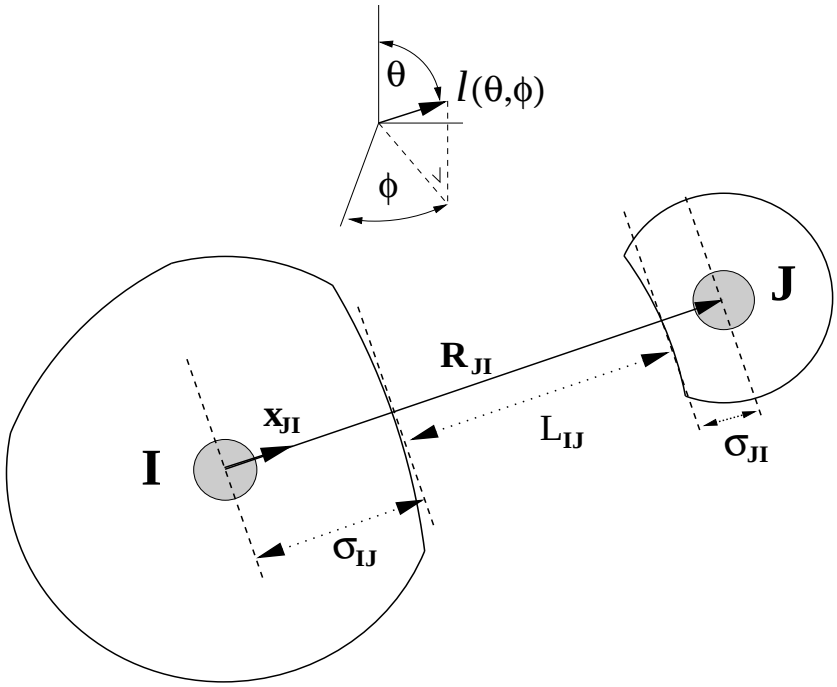

Figure 3.3: The distortable ion model. See text of section 3.7.2.

and

$$\frac{\partial \sigma_{IJ}}{\partial R_K^\alpha} = \left(\frac{\partial \sigma_I^{(0)}}{\partial \rho_I^{(0)}} + \frac{\partial \sigma_{IJ}^{(1)}}{\partial \rho_I^{(0)}} \right) \frac{\partial \rho_I^{(0)}}{\partial R_K^\alpha} + \frac{\partial \sigma_{IJ}^{(1)}}{\partial \rho_{IJ}^{(1)}} \frac{\partial \rho_{IJ}^{(1)}}{\partial R_K^\alpha} \tag{3.37}$$

$$\frac{\partial \rho_I^{(0)}}{\partial R_K^\alpha} = \sum_{L(I)} \frac{\partial f_{IL}}{\partial R_{IL}} x_{IL}^\alpha (\delta_{IK} - \delta_{LK}) \tag{3.38}$$

$$\begin{aligned} \frac{\partial \rho_{IJ}^{(1)}}{\partial R_K^\alpha} &= \sum_{L(I)} \frac{1}{R_{LI}} (\delta_{LK} - \delta_{IK}) (\delta^{\alpha\beta} - x_{LI}^\beta x_{LI}^\alpha) x_{JI}^\beta f_{LI} A_{IJL} \\ &+ \sum_{L(I)} \frac{1}{R_{JI}} (\delta_{JK} - \delta_{IK}) (\delta^{\alpha\beta} - x_{JI}^\beta x_{JI}^\alpha) x_{LI}^\beta f_{LI} A_{IJL} \\ &+ \sum_{L(I)} x_{LI}^\beta x_{JI}^\beta \frac{\partial f_{LI}}{R_{LI}} x_{LI}^\alpha (\delta_{LK} - \delta_{IK}) A_{IJL} \end{aligned} \tag{3.39}$$

The notation $\sum_{L(I)}$ has been introduced to indicate that the summation is over all ions L which are neighbours of I. This is necessary for practical implementation due to the truncation of interactions and to avoid summing over all the particles. Expanding

equation 3.36 we get

$$
\begin{aligned}
F_K^\alpha &= -\sum_{J(K)} U_{KJ}\frac{\partial g_{KJ}}{R_{KJ}}x_{KJ}^\alpha \\
&- \sum_{J(K)} \frac{\partial U_{KJ}}{\partial L_{KJ}} g_{KJ} x_{KJ}^\alpha \\
&+ \sum_{I(K)} \frac{\partial f_{KI}}{\partial R_{KI}} x_{KI}^\alpha \sum_{J(I)} \frac{\partial U_{IJ}}{\partial L_{IJ}} g_{IJ}\left(\frac{\sigma_I^{(0)}}{\partial \rho_I^{(0)}} + \frac{\sigma_{IJ}^{(1)}}{\partial \rho_I^{(0)}}\right) \\
&+ \left(\sum_{J(K)} \frac{\partial U_{KJ}}{\partial L_{KJ}} g_{KJ}\left(\frac{\sigma_K^{(0)}}{\partial \rho_K^{(0)}} + \frac{\sigma_{KJ}^{(1)}}{\partial \rho_K^{(0)}}\right)\right)\left(\sum_{I(K)} \frac{\partial f_{KI}}{\partial R_{KI}} x_{KI}^\alpha\right) \\
&- \sum_{I(K)} \frac{f_{KI}}{R_{KI}} \sum_{J(I)^{(1)}} \frac{\partial U_{IJ}}{\partial L_{IJ}} g_{IJ} \frac{\partial \sigma_{IJ}^{(1)}}{\partial \rho_{IJ}^{(1)}} x_{IJ}^\alpha A_{IJK} \\
&+ \sum_{I(K)} \frac{x_{KI}^\alpha}{R_{KI}} f_{KI} \sum_{J(I)} \frac{\partial U_{IJ}}{\partial L_{IJ}} g_{IJ} \frac{\partial \sigma_{IJ}^{(1)}}{\partial \rho_{IJ}^{(1)}} x_{KI}^\beta x_{IJ}^\beta A_{IJK} \\
&+ \sum_{I(K)} \frac{\partial U_{KI}}{\partial L_{KI}} g_{KI} \frac{\partial \sigma_{KI}^{(1)}}{\partial \rho_{KI}^{(1)}} x_{KI}^\alpha \sum_{J(K)} \frac{f_{JK}}{R_{JK}} A_{KIJ} \\
&- \sum_{I(K)} \frac{\partial U_{KI}}{\partial L_{KI}} g_{KI} \frac{\partial \sigma_{KI}^{(1)}}{\partial \rho_{KI}^{(1)}} \sum_{J(K)} \frac{f_{JK}}{R_{JK}} x_{KJ}^\beta x_{KI}^\beta x_{KJ}^\alpha A_{KIJ} \\
&- \sum_{I(K)} \frac{\partial U_{KI}}{\partial L_{KI}} \frac{g_{KI}}{R_{KI}} \frac{\partial \sigma_{IK}^{(1)}}{\partial \rho_{IK}^{(1)}} \sum_{J(I)} x_{IJ}^\alpha f_{IJ} A_{IKJ} \\
&+ \sum_{I(K)} \frac{\partial U_{KI}}{\partial L_{KI}} g_{KI} \frac{\partial \sigma_{IK}^{(1)}}{\partial \rho_{IK}^{(1)}} \frac{x_{KI}^\alpha}{R_{KI}} \sum_{J(I)} x_{KI}^\beta x_{IJ}^\beta f_{IJ} A_{IKJ} \\
&+ \sum_{I(K)} \frac{\partial U_{KI}}{\partial L_{KI}} \frac{g_{KI}}{R_{KI}} \frac{\partial \sigma_{KI}^{(1)}}{\partial \rho_{KI}^{(1)}} \sum_{J(K)} x_{KJ}^\alpha f_{KJ} A_{KIJ} \\
&- \sum_{I(K)} \frac{\partial U_{KI}}{\partial L_{KI}} \frac{g_{KI}}{R_{KI}} \frac{\partial \sigma_{KI}^{(1)}}{\partial \rho_{KI}^{(1)}} x_{KI}^\alpha \sum_{J(K)} x_{KI}^\beta x_{KJ}^\beta f_{KJ} A_{KIJ} \\
&- \sum_{I(K)} \frac{\partial f_{KI}}{\partial R_{KI}} x_{KI}^\alpha \sum_{J(I)} \frac{\partial \sigma_{IJ}^{(1)}}{\partial \rho_{IJ}^{(1)}} \frac{\partial U_{IJ}}{\partial L_{IJ}} g_{IJ} x_{KI}^\beta x_{IJ}^\beta A_{IJK} \\
&+ \sum_{I(K)} \frac{\partial U_{KI}}{\partial L_{KI}} g_{KI} \frac{\partial \sigma_{KI}^{(1)}}{\partial \rho_{KI}^{(1)}} \sum_{J(K)} x_{KJ}^\beta x_{KI}^\beta x_{KJ}^\alpha \frac{\partial f_{KJ}}{\partial R_{KJ}} A_{KIJ}
\end{aligned}
\tag{3.40}
$$

In the derivation we have made the further assumptions that $f_{IJ} = f_{JI}$, $U_{IJ} = U_{JI}$ and $g_{IJ} = g_{JI}$. This monstrous-looking equation actually has a very small computational

overhead relative to that for the dipole polarization, provided that R_b is chosen to be reasonably small, and it scales with the number of distortable ions.

3.7.3 Applying the Model

In order to apply this model we clearly need to find suitable expressions for the functions f_{IJ},$\sigma_I^{(0)}$, and $\sigma_{IJ}^{(1)}$. We begin by making the same assumption that was made in the extended Lagrangian approach that the most important interaction is the anion-cation interaction although this will be extended at a later stage to include the anion-anion interaction in a limited way. For the moment we are concerned with systems with two species such as MgO and we assume that the cation is small and rigid. For MgO it is likely that this is a very good assumption, given its degree of ionicity.

In order to draw a correspondence with the compressible ion model of Wilson *et al.*[47] (see section 3.4) we write the total energy of the system due to short-range repulsion as

$$\begin{aligned} V^{\mathrm{SR}} &= \sum_{I\epsilon -} V_I^{\mathrm{self}}(\sigma_I^{(0)}) + \sum_{I\epsilon -, J\epsilon +} B_{+-} e^{-\alpha_{-+}(R_{IJ} - \sigma_I^{(0)})} \\ &+ \sum_{I, J\epsilon -, J>I} B_{--} e^{-\alpha_{--} R_{IJ}} + \sum_{I, J\epsilon +, J>I} B_{++} e^{-\alpha_{++} R_{IJ}} \end{aligned} \tag{3.41}$$

The values of the anion radii at any time should be such that this repulsive energy is minimized. In other words

$$\frac{\partial V^{\mathrm{SR}}}{\partial \sigma_I^{(0)}} = 0 \quad , \quad \forall I \tag{3.42}$$

$$\Longrightarrow \frac{\partial V_I^{\mathrm{self}}}{\partial \sigma_I^{(0)}} + \alpha_{-+} e^{\alpha_{-+}\sigma_I^{(0)}} \sum_{J\epsilon +} B_{+-} e^{-\alpha_{-+} R_{IJ}} = 0 \tag{3.43}$$

To simplify the notation we write $B' = \alpha_{-+} B_{+-}$ and $\zeta(\sigma_I^{(0)}) = \frac{\partial V^{\mathrm{self}}}{\partial \sigma_I^{(0)}}$.

$$\zeta(\sigma_I^{(0)}) e^{-\alpha_{-+}\sigma_I^{(0)}} = -\sum_{J\epsilon +} B' e^{-\alpha_{-+} R_{IJ}} \tag{3.44}$$

At this point we note that there has been much discussion about the form of the self-energy of compressible ions. Although in the original paper by Wilson *et al.* the form used was that of a hyperbolic cosine of the amount of compression $\delta\sigma$, in another work Matsui has used a harmonic expression for this energy [67] and in an even more recent paper [68] Marks *et al.* have argued that for the oxide ion one should treat the $2p^6$ shell and the s^2 shells separately with harmonic and exponential compression energies respectively.

However, the justification for all of these forms has been on the basis of quantum chemical calculations of the perfect crystal. There is no reason to believe that this is a good basis for determining what the energy function should be in a distorted crystal or a melt and there does not seem to be strong physical reasoning behind any of the forms used. In fact, an examination of the calculated values of the self-energy in, for

example, reference [47] shows that for values of R_{IJ} that one might expect to find at low temperatures and pressures, the calculated self-energy could be reasonably well fit even with a straight line.

For these reasons, as a preliminary test we have chosen an exponential form as this simplifies considerably the mathematics. $\zeta(\sigma_I^{(0)})$ will also have an exponential form so we may write

$$A_I e^{-\beta_I \sigma_I^{(0)}} e^{-\alpha_{-+}\sigma_I^{(0)}} = -\sum_{J\epsilon+} B' e^{-\alpha_{-+}R_{IJ}} \tag{3.45}$$

By merging constant terms to simplify the notation, this equation can be rewritten in the form

$$\sigma_I^{(0)}(\rho_I^{(0)}) = C_1 + C_2 \ln(\rho_I^{(0)}) \tag{3.46}$$

where we say that

$$\rho_I^{(0)} = \sum_J C_3 e^{-C_4 R_{IJ}} \tag{3.47}$$

and C_1,C_2..etc are constants. By analogy with equation 3.28 we can say that

$$f_{IJ} = C_3 e^{-C_4 R_{IJ}} \tag{3.48}$$

One is not confined to such simple forms for the self-energy but for many forms one cannot write equation 3.44 in terms of $\sigma_I^{(0)}$ and one is forced to find $\sigma_I^{(0)}$ by an iterative procedure. This only has a very slight impact on the efficiency of calculating the potential. Another form which we have tried, and for which this procedure is used is

$$V_I^{\text{self}}(\sigma_I^{(0)}) = \frac{\epsilon_1}{\epsilon_2 + \sigma_I^{(0)}} + \frac{\epsilon_3}{(\epsilon_4 + \sigma_I^{(0)})^2} \tag{3.49}$$

where ϵ_1,ϵ_2..etc are constants. This form was chosen according to the (admittedly, highly simplistic) physical reasoning that the internal factors which determine an ion's radius are the electrostatic energy which varies like the inverse of a distance and the kinetic energy of the electrons which varies like the inverse of a distance squared.

The above analysis has shown that the distortable-ion model presented is mathematically equivalent to the compressible-ion model of Wilson *et al.* if $\sigma_{IJ}^{(1)} = 0$ in the limit that the fictitious mass of the extended-lagrangian approach goes to zero.

It is not possible to map our approach onto the aspherical-ion model. However, we take a different approach to aspherical distortions. Given the functions f_{IJ} and $\sigma_I^{(0)}$ as a starting point we may postulate a form for $\sigma_{IJ}^{(1)}$. We assume that distorting an ion in an aspherical way is energetically the same as distorting it spherically. In other words, we say that there is no energy penalty for deviating from sphericity. We therefore write

$$\sigma_{IJ}^{(1)} = C_5 \ln\left(\frac{\rho_{IJ}^{(1)}}{\rho_I^{(0)}}\right) \tag{3.50}$$

Since we will be parametrizing this force by fitting to *ab initio* data, the minimization routine has the freedom either to make the constant C_5 very small or zero if this is not a

reasonable functional form, or if aspherical distortions are really energetically equivalent to spherical ones, it can make $C_2 = C_5$ in which case, the distortions of purely spherical symmetry disappear and

$$\sigma_{IJ} = C_1 + C_5 \ln(\rho_{IJ}^{(1)}) \tag{3.51}$$

Although all the above derivation has assumed that this potential is only to be used for modelling cation-anion interactions, the generality and freedom afforded us by our parametrization procedure (see chapter 4) means that we lose nothing by trying to apply it to the anion-anion interaction also. We have done this by fitting parameters for the anion-anion interaction and we have found that it does improve the ability of the model to fit the *ab initio* forces. A more sensible, but also more expensive way of tackling the anion-anion interaction would be to introduce a self-consistent procedure to minimize the angular dependent radii simultaneously.

We also note that, as has been pointed out by Marks *et al.*, different electronic shells have different compression characteristics. This could be modelled within the present scheme by having two or more such distortable ion potentials acting in parallel.

Chapter 4

Parametrizing Effective Potentials

4.1 Introduction

Ever since the first molecular dynamics simulations were performed one of the crucial issues has been the method of parametrization of the effective force-field used. Not only does one need to represent, in terms of a reasonably simple functional form, the relevant physics at play, this functional form needs to take parameters which are realistic for the system under consideration.

In the past parameters have been chosen based on physical arguments, or empirically so that the potential reproduced known properties of the material, or a combination of the two. This resulted in potentials which were qualitative at best. The general procedure was to use physical or chemical arguments for as many parameters as possible and to fit the remaining parameters so that experimental quantities such as the density, bulk modulus or dielectric constant were reproduced. The problem with this is that the number of parameters that can be determined from physical arguments is generally very small and in order to parametrize empirically the number of physical quantities used should be large relative to the number of parameters required in order that they be determined uniquely. Otherwise a set of parameters determined to reproduce, say, structural properties might give awful results for dynamical properties. Since the number of experimentally determined physical quantities that are available is generally quite small, and since they are frequently properties which are not completely trivial to calculate with the potential, the number of parameters that one can find in this way is usually very small. This, in turn, causes the problem that one needs to use a functional form for the potential which is simple enough to contain only a few parameters. Functional forms which are too simple cannot generally describe the forces between the ions in an accurate way. For most systems this requires complicated functions which capture phenomenologically the behaviour of the electrons. Such potentials for ionic systems are discussed in detail in chapter 3.

Another problem with potentials which have been used in the past is that they were frequently parametrized using data relevant to a given set of thermodynamic conditions (e.g. pressure and temperature) or a given phase. One of the main advantages of MD simulations is that they may be used for exploring *new* situations which are difficult or

inaccessible for experiment. This means that potentials were frequently used in conditions different from those under which they were parametrized. Any change in physical conditions such as temperature, pressure, or phase results in changes in the underlying electronic structure of the system. If such changes are large enough, the degree to which a given potential can reproduce the interatomic interactions can be seriously diminished.

A solution to all of these problems is to parametrize a potential using information extracted from first-principles calculations [69]. From such calculations one can extract a wealth of information such as the force on each atom, the stress on the system and the energy differences between different configurations. Since a reasonably high degree of accuracy may be achieved from density functional theory calculations and since DFT calculations are economical enough to allow one to treat large numbers of atoms ($\sim$ 100) which are representative of bulk systems when simulated under periodic boundary conditions, they are the obvious choice for performing the first-principles calculation. One can, in principle, perform *ab initio* calculations for any atomic configurations at any density and so the force-field may be parametrized for the particular physical conditions that one is interested in simulating.

The other major advantage is that an arbitrarily large amount of information may be extracted and this allows one to use force-fields which are much more complicated and therefore have many more parameters than traditional force-fields. However, in order to do this it is necessary to use a careful, well-defined parametrization procedure so that problems do not occur due to there being too little *ab initio* data. The basic requirement that must be fulfilled is that a potential which is parametrized for use under a given set of conditions should be able to describe *all* sufficiently large systems under these conditions with the same degree of accuracy.

In this chapter the parametrization procedure, which was originally developed by Ercolessi and Adams [69] and later developed further by Laio *et al.* [70], will be described along with the details of the ab initio calculations that we have used for the oxides, SiO_2 and MgO.

4.2 Parametrizing from *Ab-Initio* Data

4.2.1 The Force-Matching Method

In a molecular dynamics simulation the important quantities are the forces on each atom, and if one is performing simulations at constant pressure, the stress on the simulation cell. For this reason, and because forces are plentiful in number in an *ab initio* calculation, Ercolessi and Adams have introduced the idea of fitting parameters to reproduce *ab initio* forces as well as possible. Laio *et al.* [70] were interested in simulating systems under high pressure and so have extended this slightly by trying to fit also the calculated stress. In the following we also include in the function to be optimized, the energy differences between different configurations. Given a form for the interatomic force-field, which depends on a set of parameters $\{\eta\}$, we minimize the function :

$$\Gamma(\{\eta\}) = w_f \Delta F + w_s \Delta S + w_e \Delta E \tag{4.1}$$

with respect to the parameters $\{\eta\}$ where

$$\begin{aligned}
\Delta F &= \frac{\sqrt{\sum_{k=1}^{n_c}\sum_{I=1}^{N}\sum_{\alpha}|F^{\alpha}_{cl,I}(\{\eta\})-F^{\alpha}_{ai,I}|^2}}{\sqrt{\sum_{k=1}^{n_c}\sum_{I=1}^{N}\sum_{\alpha}(F^{\alpha}_{ai,I})^2}} \\
\Delta S &= \frac{\sqrt{\sum_{k=1}^{n_c}\sum_{\alpha,\beta}|S^{\alpha\beta}_{cl}(\{\eta\})-S^{\alpha\beta}_{ai}|^2}}{3B\sqrt{n_c}} \\
\Delta E &= \frac{\sqrt{\sum_{k,l}^{n_c}((U^{cl}_k-U^{cl}_l)-(U^{ai}_k-U^{ai}_l))^2}}{\sqrt{\sum_{k,l}^{n_c}(U^{ai}_k-U^{ai}_l)^2}}
\end{aligned}$$

Here $F^{\alpha}_{cl,I}$ is the $\alpha-$th component of the force on atom I as calculated with the effective potential, $F^{\alpha}_{ai,I}$ is the force component as calculated *ab initio*, $S^{\alpha\beta}_{cl}$ is the stress tensor component as calculated with the effective potential and $S^{\alpha\beta}_{ai}$ is the stress tensor component as calculated *ab initio*, B is the bulk modulus, U^{cl}_k and U^{ai}_k are the potential energy of configuration k as calculated with the force-field and *ab initio* respectively, n_c are the number of atomic configurations for which *ab initio* calculations have been performed. The quantities w_f,w_s and w_e were chosen to reflect the amount of available data for each quantity, i.e : $w_f > w_s > w_e$. It was found that the final fit was quite insensitive to the values chosen as long as w_e was relatively small due to the fact that only one energy may be extracted per configuration.

In order to be sure that the minimization procedure was meaningful n_c was required to be reasonable large. Its value depended on the system studied, the potential form used and the number of atoms in the unit cell. For SiO_2 we generally used a value of $n_c = 5$. For MgO, a functional form with more parameters was used and there were fewer atoms in the unit cell and so it was found that a value of $n_c = 10$ was required. In each case at least another 5 configurations were retained during each fitting procedure in order to test that the final functional form fit these configurations as well as it did those that were used in the minimization of $\Gamma(\{\eta\})$.

Minimization of $\Gamma(\{\eta\})$ with respect to $\{\eta\}$ was performed using a combination of "simulated annealing"[71] and "Powell minimization"[72]. A basin in the surface defined by $\Gamma(\{\eta\})$ in $\eta-$space was initially found using simulated annealing and, once found, further minimization was performed using the method of Powell. Minimization in general, and particularly simulated annealing, is a very computationally expensive process. However simulated annealing is very useful for two reasons : 1. It is very stable; Powell minimization can break down if numerical errors (such as overflow errors) occur due to unphysical values of the parameters; 2. In principle it can always bring one to the global minimum; In practice however this depends on how much computer time one is willing to allocate it. These properties of the simulated annealing method makes it particularly useful when fitting a potential for the first time. One does not need to start with reasonable or physical values of the parameters in order for it to converge and this means that one may parametrize exotic potentials for which the parameters have no obvious physical interpretation.

The freedom which one is afforded using the combination of *ab initio* data and simulated annealing is crucial. It simply would not be possible to parametrize a force field such as the distorted-ion model introduced in section 3.7.2 without either one of these assets.

4.2.2 The Optimal Potential Method

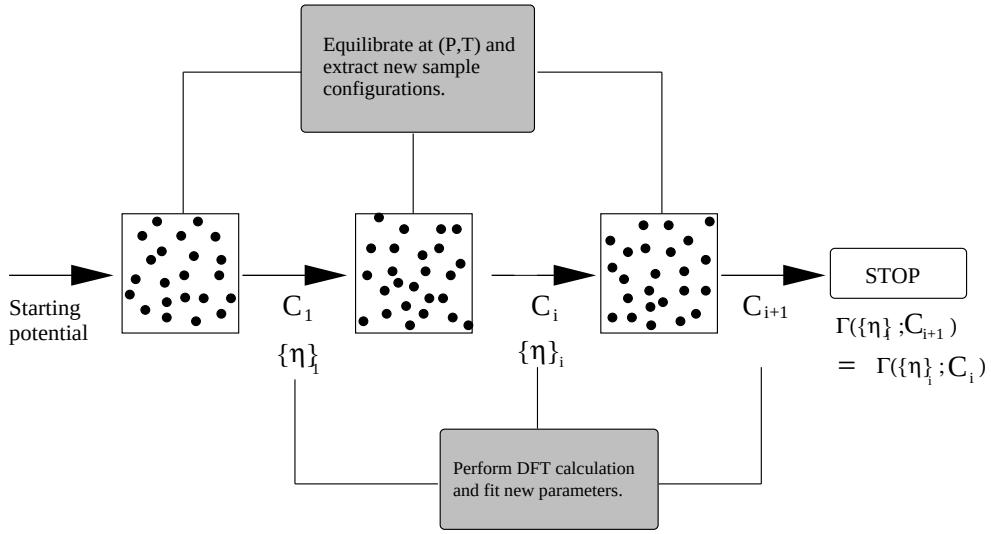

Figure 4.1: Iterative procedure for constructing the optimal potential at (P, T).

It is important when fitting to the *ab initio* configurations that one fits to configurations which are representative of the real system. This is particularly important for liquids. The liquid should have a structure which is close to that of the real liquid. However, if one doesn't have a good potential to begin with, one can't construct by means of an MD simulation a good liquid. One solution is to generate configurations using *ab initio* molecular dynamics. Our attempts to simulate liquid MgO with Car-Parrinello MD proved too difficult however due to large errors of the form described in chapter 2 for levels of the fictitious mass which allowed a reasonable equilibration time, i.e. $\mu_0 > 100$ a.u. For this reason we have used an adapted form of an iterative procedure for generating the potential which was first used by Laio *et al.*[70] (see figure 4.1). Beginning with the best potential available, the system of interest is thermalized with an MD simulation (typically of ~ 20 ps) at the thermodynamic conditions (P, T) for which one would like to create the potential. Once equilibrated, a number of well separated (typically by ~ 1 ps) atomic configurations are generated. On these configurations, density functional theory calculations (see section 4.3) of total energy, forces and stress are performed and these are used to perform the parametrization. We will denote the *ab initio* data extracted during step i of the iterative procedure collectively as $\mathbf{C_i}$ Using the parameters obtained during the minimization at this step, a new equilibration is peformed (as a continuation of the previous one) and new atomic configurations extracted. Once again, *ab initio* calcula-

tions are performed and a new set of parameters obtained. This cycle is stopped once the current parameter set fits the current ($\mathbf{C_i}$) and the previous ($\mathbf{C_{i-1}}$) *ab initio* data to the same degree, i.e. $\Gamma(\{\eta\}_i; \mathbf{C_i}) = \Gamma(\{\eta\}_i; \mathbf{C_{i-1}})$.

4.3 *Ab-Initio Calculations*

As mentioned previously, the *ab initio* calculations which we perform are all done within density functional theory[2, 3]. In 1964 Hohenberg and Kohn [2] proved that all properties of an electronic system are uniquely defined by its ground state probability density. Subsequently, Kohn and Sham [3] turned this theorem into a practical scheme by recasting the many-body Schrödinger equation into a set of single particle Schrödinger equations in which each particle sees an effective potential which is a functional of the probability density. Walter Kohn shared the Nobel Prize for chemistry in 1998 for his part in the development of this theory.

Unfortunately, the Kohn-Sham effective potential is not known in general and so one cannot solve the equations exactly. Instead, various approximations to the unknown part of the potential (which is called the *exchange-correlation potential*) are used. Although the exchange- correlation potential $\hat{V}_{\rm xc}$ is fully non-local, the approximations to it are local or semilocal. The most commonly used approximate functional is called the "local density approximation" (LDA). This is a local operator in which the exchange-correlation potential at a point is chosen to be the same as that felt by an electron in a uniform electron gas of the same density. The result for the uniform electron gas was calculated numerically by Ceperley and Alder [36] and parametrized by Perdew and Zunger[37] among others. This approximation has been incredibly successful considering its simplicity, and for many systems it can produce results (such as structural parameters, phonon frequencies and elastic moduli) which are in good agreement with experiment. The general consensus nowadays is that another class of functionals, so called "generalized gradient approximations" (GGA), which depend not only on the density at a point but also on its spatial derivative are superior in most situations, but particularly for studying molecules. This empirical observation is supported by the fact that, of the conditions which the true functional is known to obey, more of them are satisfied (by construction) by some of the more recent GGAs [73, 74] than the LDA.

All our calculations are performed within the planewave pseudopotential method[75, 76]. In this method, electronic states of an atom which are changed negligibly by the presence of other atoms due to the fact that they are very low in energy and are close to the nucleus, are considered frozen. Electrons which do respond to the presence of other atoms are then treated as though they see an effective non-local potential, called a pseudopotential, due to the nucleus surrounded by these unreactive electrons. The eigenfunctions of the Kohn-Sham hamiltonian of the system of pseudopotentials and electrons are represented in a basis of plane waves. The planewave method relies on the use of periodic boundary conditions whereby the basic simulation cell is repeated periodically in all directions. Periodic boundary conditions are particularly suitable for studying bulk materials as the infinitely repeated periodic images can imitate the effect of an infinitely

large system, provided that the elementary unit cell is sufficiently large.

In principle, density-functional theory with the plane-wave pseudopotential method is an *ab initio* method in the sense that all one needs is the atomic number of the constituent elements of a system in order to calculate the properties of the system. In practice however there is a very strong empirical element to it. The details of the calculation are not uniquely defined. Various choices which one may make during a calculation, such as the method of creating the pseudopotential and the choice of exchange-correlation functional, can have a strong impact on the properties calculated. For this reason, as it is most frequently used, it is a semi-empirical method, albeit a very good one. For a solid, it is generally applied with reference to such experimental data as volume, bulk modulus, or lattice parameters and if suitable agreement is not found, the underlying details of the calculation are revised. The hope is, that by using a scheme which gives good agreement with these experimental properties, one improves the chances of this scheme working well for other properties. This is never guaranteed but it is the best approach available within this method. For example, different choices of the Mg pseudopotential, which were, by our estimation, all equally reasonable, led to equilibrium volumes of MgO which varied by up to 10%. The scheme that we have chosen was shown[6] to give good results and was thoroughly tested. However, it was not formally more justifiable than any other. It may be that this is an extreme case, however there is always some significant variation and particularly in elastic properties such as the bulk modulus.

4.3.1 Computational Details

In the creation of the effective force-fields we have performed *ab initio* calculations for two different materials, MgO and SiO_2.

For SiO_2, the scheme that we used was chosen for convenience (the pseudopotentials already existed and the exchange-correlation functional was already implemented in the plane wave program) rather than based on empirical considerations. Its empirical justification lies in the ability of the resulting effective force-field to reproduce experimental properties of crystalline and liquid silica. This is discussed in detail in chapter 5. The pseudopotentials used for silica and oxygen were both of the form introduced by Trouillier and Martins [22]. Although in the calculations of silica we have used a rather old gradient-dependent exchange-correlation functional [77], in the atomic calculations which were used to create the pseudopotentials we have used different functionals for both oxygen and silicon. For silicon the functional used was the LDA[36, 37] and for oxygen we used a different gradient-dependent functional [35]. The practice of using different functionals in the atomic and bulk calculations is generally frowned upon, however from a formal mathematical or physical point of view we are not aware of any reason why it is not as justified as any other scheme. Nevertheless, mixing functionals in this way can lead to confusion and it needlessly complicates the details of a calculation and so is not advisable in general. In addition to this, our use of the planewave pseudopotential method is purely as a means of parametrization and if there is a formal difficulty with mixing functionals as we have done, it is highly unlikely that errors incurred in this way are greater than other errors associated with our effective force-fields.

For MgO, we have used identical pseudopotentials to those that have previously been used successfully to calculate its vibrational properties for a large range of pressures and temperatures[6]. We require our simulations to produce good quality forces and this is a much more rigorous test of its ability than it would have been feasible for us to perform. The exchange-correlation functional used in this case was the LDA.

An important parameter in any planewave calculation is the highest energy planewave used in the expansion of the wavefunctions. For SiO_2 the value used was 130 Ryd. and for Mgo the value used was 120 Ryd. These values are very large relative to most calculations, however we required a relatively precise determination of the stress and this converges very slowly with respect to this parameter.

A unit cell containing 24 SiO_2 units was used in the simulation of silica and a cell containing 32 MgO units was used in the simulation of MgO. These sizes were deemed large enough to be a good representation of the bulk and , in any case, it would not have been computationally feasible to use cells which were significantly larger.

The brillouin zone was sampled with only the Γ-point in each case.

Chapter 5

Silica

5.1 Introduction : Why study silica ?

Silicon dioxide or silica is one of the most widely and intensively studied of all materials. There are many reasons for this. First of all, it is one of the most common materials in nature, silicates making up more than 90% of the minerals in the earth's mantle and crust. It is a vital industrial material. An obvious example is that it makes up approximately 75% of the composition of the glass that is used for everything from window panes to optical fibres. It is also used extensively as an insulator in the semiconductor electronics industry. These are only two of a vast range of uses.

Silica has an extremely rich phase diagram with a large number of allotropic forms. The best known of these are quartz, cristobalite, tridymite, coesite, stishovite and of course silica glass. All the low pressure crystal structures of silica are composed of corner-sharing SiO_4 tetrahedra and even in the glass and the liquid almost all of the Si atoms are tetrahedrally coordinated. Silica is a main constituent of most zeolites which are metastable microporous crystalline solids which are extensively mined and fabricated for their unique structural properties. Their porosity makes them useful as molecular sieves in large scale industrial chemistry. Zeolites are also used as catalysts, the reactions taking place in their large internal cavities.

Its abundance in the earth's mantle makes the response of silica to extreme conditions of temperature and pressure of great importance to those constructing geophysical models of the earth's interior. Although it generally appears with other elements such as Mg,Al,Fe,Na...etc in the form of silicates, the first step in understanding silicates is to understand silica itself. Likewise, the first step in modelling such systems with computer simulation is to successfully model silica. The behaviour of liquid silica and silicates as a function of pressure and temperature is of importance to those studying the formation and cooling of the earth.

Silica is a prototype of strong network-forming glass formers. For this reason alone there has been intense interest in studying the structural and dynamical properties of the liquid and the glass.

Molecular dynamics plays an important role in the study of silica in all its forms since, in principle, it allows one full access to the microscopic structural details. Experiment,

on the other hand, can only provide averaged quantities such as structure factors. Experiments have difficulties with extreme conditions of temperature and pressure but, at least in principle, MD is not as constrained and so it is particularly relevant for studies at high temperature and pressure where there is little experimental data.

5.2 Modelling Silica

Silica is quite a difficult oxide to model, at least compared to the simplicity of MgO. It has traditionally been considered to be a covalent system[78], and although there is almost certainly some covalency present, it has been found that it is more appropriate to model it as an ionic system[79] and, more recently, that some of the effects previously attributed to covalency[81, 82] could, in fact, be explained using a polarizable ionic model [83]. It is precisely the features of its bonding which have caused confusion in the past, i.e. the mix of ionicity and covalency, which makes it a particularly challenging system. Nevertheless, as discussed in the introduction, it is an extremely important system and so any improvement is worthwhile.

For many systems experience has shown that it is easier to model the broad features of its potential energy surface, which play a dominant role in determining structure, than it is to model the fine details, which can strongly effect dynamics. For silica its ionicity makes it reasonable to suppose that these broad features are dominated by electrostatic considerations. The small degree of covalency, on the other hand is probably more local in its effects and therefore of importance for dynamics but of lesser importance for determining structure. Here we would like to test our polarizable-ion potential and our parametrization method by trying to create a potential which reproduces the structural properties of silica.

There have been a large number of potentials proposed for silica in the past. Many of these include three-body angular dependent terms and so are intrinsically biased in favour of a tetrahedral crystal structure[80, 81, 82]. These are of little use to us as we aspire to creating a potential which is suitable for disordered aswell as crystalline phases. Demiralp *et al.* [84] have proposed a many-body potential for silica which improves on the prediction of the crystal structures with respect to pair potentials. The many-body character of this potential is a charge equilibration model[53] which allows for local changes in the degree of ionicity. Although it is very likely that the degree of ionicity changes with pressure, there is no evidence that we are aware of to suggest that this happens dynamically at a given pressure or temperature. The polarizability of the oxygen ion is well established however[85, 86] and it may be that inclusion of charge-transfer mimics to a certain extent the effects of polarization. It is likely that inclusion of charge-transfer is necessary for transferability between polymorphs with different silicon coordination, for example, for modelling the pressure induced transition from 4-fold coordinated quartz to 6-fold coordinated stishovite.

The most commonly used potentials for silica are all pair-potentials of the form

$$U_{IJ}(R_{IJ}) = \frac{q_I q_J}{R_{IJ}} + B_{IJ} e^{-\alpha_{IJ} R_{IJ}} - \frac{C_{IJ}}{R_{IJ}^6} \tag{5.1}$$

In other words, a Born-Mayer-like form but without the R^{-8} term. There have been a number of parametrizations of this potential form for silica in the past[79, 87, 88]. Most recently, van Beest, van Santen and Kramer (BKS)[88] have fit the parameters to reproduce the energetics of small hydrogen-terminated silica clusters as well as the experimental structural parameters and elastic constants of quartz. The resulting potential has been extensively applied to study a large range of dynamic and thermodynamic properties of silica in many different phases and under many different thermodynamic conditions[89].

A polarizable potential for silica has previously been proposed by Wilson *et al.*[85] and shown to be important for reproducing the infrared absorption spectrum of the amorphous solid with respect to pair potentials of the BKS form. The model that they have used is discussed in section 3.3.1 and their parametrization was mainly empirical.

As mentioned previously, we are primarily interested in improving the description of the electrostatics with respect to previous models and we therefore use a model similar to that of Wilson *et al.* but with the well-defined and controlled parametrization procedure which is outlined in chapter 4. We use the polarizable potential described in section 3.7.1 with short-range dipoles induced by the cation on the anion. The short-range repulsive interactions are modelled with a pair potential of Morse-Stretch form :

$$U_{ij} = \frac{q_i q_j}{r_{ij}} + D_{ij}[e^{\gamma_{ij}(1-\frac{r_{ij}}{r_{ij}^0})} - 2e^{\frac{\gamma_{ij}}{2}(1-\frac{r_{ij}}{r_{ij}^0})}] \tag{5.2}$$

where the interaction between an atom of type i and an atom of type j is defined by the parameters q_i,q_j,D_{ij},γ_{ij},r_{ij}^0 and the distance between them r_{ij}. This form was chosen over the Born-Mayer form as it proved to be more transferable between different phases.

As we have discussed in chapter 4, it is important to take into account the effect that temperature and pressure have on the electronic structure of any material and that it should be verified that potentials are sufficiently transferable when using them under new thermodynamic conditions or in a new phase. For silica we aspire to creating a potential which can be used over the large range of allotropes which are seen at low pressures (i.e. < 5 or 10 GPa.) and at temperatures up to those that are relevant for studying the liquid with MD. The high viscosity of silica liquid means that in order to observe substantial diffusion on a MD timescale, very high temperatures ($3000 - 4000$ K) are required. It is not obvious *a priori* that our potential form can stretch across this range of conditions. However, all the low-pressure polymorphs consist of corner-sharing tetrahedra and the liquid and glass are known to be mostly composed of networks of such tetrahedra. In other words, the short-range order doesn't change much across these phases. In order to find a system which is not biased towards a particular crystal structure we have decided to parametrize the potential by fitting to *ab initio* data on the liquid at 3000 K. This was done using the procedure outlined in chapter 4 and the results will be discussed in the next section.

We will draw comparison with experiments, Car-Parrinello simulations of liquid silica [90] and one of the most commonly used effective potentials for silica : the BKS potential [88]. Another very commonly used form is the potential of Tsuneyuki *et al.*[87] which has the same form as BKS and was parametrized in a similar manner. Therefore most of the problems with BKS which we highlight here are equally applicable to this potential.

5.3 Results

5.3.1 Fitting to *Ab-Initio* Data

In order to obtain a benchmark for the parametrization of the new potential, we first tested the ability of the BKS potential to fit the *ab initio* data. The values of $\Delta F = 0.51$,$\Delta S = 0.057$[1] and $\Delta E = 0.82$ (see section 4.2.1) that we obtain for the BKS potential in the liquid at 3000K and zero pressure point to a rather poor accuracy of this potential, at least at our working conditions for the fitting procedure. This is quite surprising if one considers that the ability of the BKS potential to reproduce some structural properties of the solid phases is good overall[91], and confirms our suggestion that the simplest force fields should be used with great caution at physical conditions that differ from those where they have been parametrized or from those where they are known to provide accurate results. It is possible to substantially reduce these errors by minimizing Γ (see equation 4.1) with respect to the parameters of the Born-Mayer potential, i.e. by constructing the "optimal" Born-Mayer potential for the liquid at 3000 K and zero pressure. However a large number of such minimizations were attempted and although it was possible to reduce ΔF and ΔS to values of about 0.3 and 0.015 respectively, the resulting potentials gave unrealistic values for the structural parameters and densities of the low pressure solid polymorphs. For example, the equilibrium density of quartz at 300 K varied for such potentials between values as low as 0.3 g cm^{-3} and as high as 4.5 g cm^{-3}. A minority of these potentials worked reasonably well for quartz but they did not necessarily work well for the other polymorphs and choosing these potentials out of the many created would represent an empirical procedure. We would like to avoid empiricism as much as possible. It is clear from the poor fit to *ab initio* data and the fact that improving this fit disimproved structural properties considerably, that the rigid ion model is too simple to allow for an accurate description of silica at low pressure and for a temperature range encompassing both solid and liquid phases. It seems that more ingredients are required in the potential model in order to improve its ability to reproduce the *ab initio* forces.

We now look at the results of our parametrization of the polarizable model. We have created and tested only one parameter set for the polarizable potential and we report the results of those tests here.

The results of the fit of the polarizable model described in the previous section were very encouraging. The values of ΔF,ΔS and ΔE for the final parameter set were 0.16,0.014 and 0.18 respectively, indicating a dramatic improvement over BKS, but also over the best (optimal) potential with the Born-Mayer form. The parameters are listed in Table 5.1. The fact that inclusion of polarization both improves the ability of the potential to fit the *ab initio* forces and allows one to forego the empiricism of selecting a potential that reproduces experiment out of more than one created, strongly suggests that polarization is a crucial ingredient in the bonding of silica.

[1] ΔS has been computed relative to a roughly estimated bulk modulus of $B = 30$GPa.

Table 5.1: Force field parameters (atomic units)

q_{O}	q_{Si}	α	b	c
-1.38257	2.76514	8.89378	2.02989	-1.50435

$D_{\mathrm{O\text{-}O}}$	$D_{\mathrm{Si\text{-}O}}$	$D_{\mathrm{Si\text{-}Si}}$
2.4748×10^{-4}	1.9033×10^{-3}	-2.08460×10^{-3}

$\gamma_{\mathrm{O\text{-}O}}$	$\gamma_{\mathrm{Si\text{-}O}}$	$\gamma_{\mathrm{Si\text{-}Si}}$
12.07092	11.15230	10.45517

$r^0_{\mathrm{O\text{-}O}}$	$r^0_{\mathrm{Si\text{-}O}}$	$r^0_{\mathrm{Si\text{-}Si}}$
7.17005	4.63710	5.75038

5.3.2 Testing the Potential

In order to check the reliability of our improved potential we compare its thermodynamic and structural properties with experiments[92] on the equation of state of liquid silica, and with available ab initio data[90, 86] on the microscopic structure of the liquid. Experimental data on liquid silica is scarce and so we have compared with the Car-Parrinello simulations of liquid silica performed by Trave *et al.* and Sarnthein *et al.*. Although the considerations of chapter 2 mean that one cannot guarantee these simulations to be of Born-Oppenheimer quality, we will compare only with structural properties and it is reasonable to expect that they are at least much more reliable than pair-potentials. Furthermore, agreement between MD results using our potential and CPMD results would indicate a probability that both are in agreement with what would be obtained from Born Oppenheimer MD. However, since only short simulation times and small system sizes are possible with CPMD, the thermodynamic averages that can be extracted are poor. This is particularly bad for liquid silica at low pressure as its viscosity is so high that diffusion is negligible on an *ab initio* MD timescale.

Equation of State

The poor *ab initio* statistics can clearly be seen in figure 5.1 where three different types of MD simulations (Car-Parrinello, BKS and our polarizable potential) are compared with experimental results. The *ab initio* data consists of simulations from two different starting points. In one set of simulations (those at lower volumes), quartz was melted at zero pressure and successively higher pressures were continuations of the simulations at previous pressures. In the other set, the initial configuration was taken from a well equilibrated liquid simulation using our polarizable potential. The viscosity of silica and silicates in general is known to decrease dramatically with pressure [93, 94] and it can be seen that the discrepancy between the two sets of results decreases at higher pressures where the liquid is better able to diffuse. However, there are clear problems with the *ab initio* simulations and this highlights the need for accurate effective potentials which are economical enough for large system sizes and long simulation times to be feasible.

The experimental data is from experiments at ~ 1620 K whereas the *ab initio* simulations were at a temperature of $\sim 3500K$ and the classical MD simulations were at ~ 3100

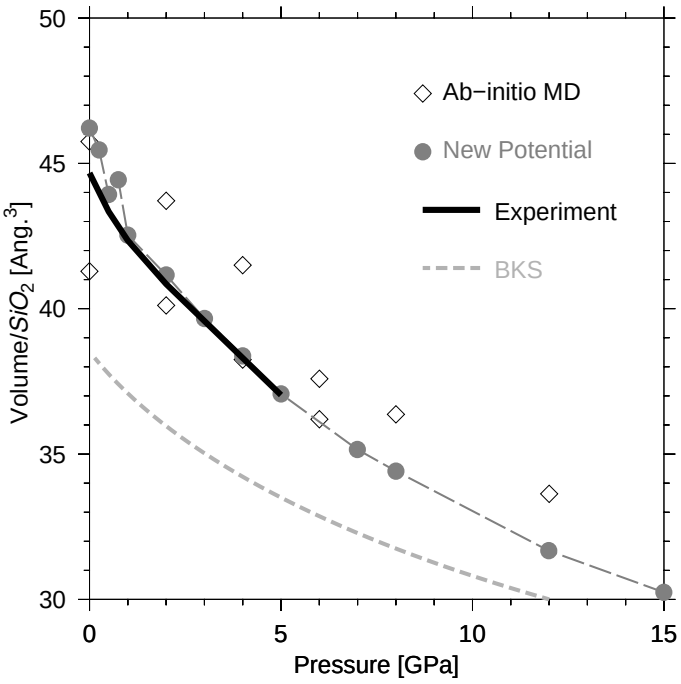

Figure 5.1: Pressure as a function of volume in liquid silica from classical MD using the new polarizable potential compared with results from the BKS potential, *ab initio* simulations[90] and experiment[92].

K. However, at zero pressure we have verified that thermal expansion of the liquid is small ($\sim 10^{-5}K^{-1}$, consistent with experimental estimates[95]) and that taking account of it would in fact bring our zero pressure results into even better agreement with experiment. Volumes were obtained as averages along constant-pressure[96] molecular dynamics runs of at least 50 ps following 20 ps of equilibration and with simulation cells containing 576 atoms. At lower pressures (< 3 GPa) where diffusion is slower, averages were obtained along runs of more than 100 ps. The overall agreement with experiment is rather good, and definitely better than any atomistic model proposed so far. The BKS model underestimates systematically the volume by $\sim 13\%$, a likely consequence of its inability to reproduce the ab initio stress. Our improved potential compares with experiment even better than the ab initio results, a likely consequence of the poor thermodynamic averaging in the *ab initio* simulations. It is also the case that *ab initio* simulations tend to either systematically overestimate (in the case of GGA) or systematically underestimate (in the case of LDA) the volume[97] and that, probably fortuitously due to the mixture of the two functionals that we have used, our potential predicts volumes that lie approximately midway between the two.

Particularly at low pressures, the large viscosity of liquid silica means that even for our relatively large system size (576 atoms) obtaining a reliable statistical average of volume requires *at least* 50 picoseconds. For the *abinitio* system (72 atoms) a considerably longer run would be required. However, in spite of our much larger simulations, there is a kink in

the equation of state at a pressure of between 0.5 and 0.75 GPa. It could be that the system is diffusing so slowly at these low pressures that longer simulation times are required in order to get an average of adequate precision. Another possibility is that there is a transition between two different liquid phases at low pressures and that the discontinuity is at (or near) the point where the transition occurs. However we have examined a large number of structural features such as pair-correlation functions and angular distributions and have not identified any first-order change of structure with pressure. This does not mean that such a change doesn't occur however. Averaged quantities such as distribution functions may be quite insensitive to such a transition. These simulations were extremely expensive, each low pressure data point being the result of approximately 24 days of single processor computer time and so it has not yet been feasible to redo or refine the simulations to see if an entirely new liquid created from fresh initial conditions would produce the same results. Moreover the average over any 50 ps segment (after the equilibration time) gave results which were very close to the average over the full 100 ps. We have verified that the system is diffusing at these pressures but the diffusion is extremely slow and so we cannot say with any degree of certainty what is the cause of this anomaly in the equation of state.

We have checked that simulations using a 72 atom simulation cell (the same size as was used for the *ab initio* simulations) , gave results in almost perfect agreement with those of a 512 atom cell. This indicates that finite size effects are negligible. This may well be due to the effective "electronic" screening of the long range electrostatic interactions between ions which is present in our model in the form of dipoles.

Structure of the Liquid

We now focus on the microscopic structure of liquid silica. Fig. 5.2 shows a comparison of the silicon-oxygen-silicon angle distributions in the liquid. It has been pointed out [85] that by counteracting the repulsion between silicon atoms, the inclusion of dipole effects can shift the oxygen centered angle distribution towards lower angles. This is clearly seen in this comparison between the results of the BKS simulations and the *ab initio* and polarizable potential simulations. The very close correspondence between the *ab initio* distribution and the polarizable potential distribution justifies both our description of the electrostatics in terms of dipoles and the inclusion of short-range induced dipoles which contribute very significantly to the dipole moment on each ion and which are therefore strongly linked to the distribution of angles. The peak at around 90 degrees in the polarizable and Car-Parrinello angle distributions is due to the presence of microscopic configurations consisting of rings containing two silicon and two oxygen atoms. These do not appear in the BKS distribution, indicating that they are energetically unfavourable with this potential.

Fig. 5.3.2 shows the proportions of N-fold coordinated silicon atoms as a function of pressure compared to the results of Car-Parrinello simulations [90] and simulations using the BKS potential [99]. Our results are in much better qualititative agreement with the CP calculations than with the classical BKS calculations despite the fact that simulations are performed at high pressures where the parameter set may become increasingly inac-

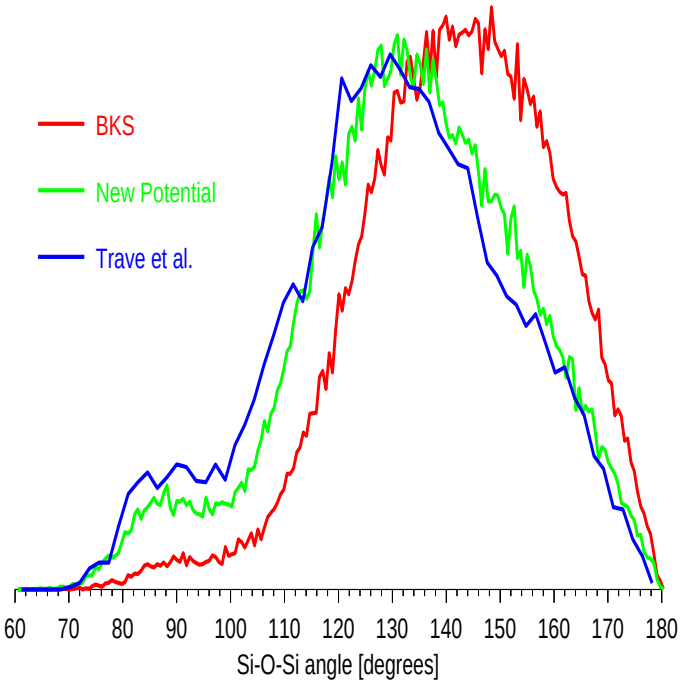

Figure 5.2: Distribution of oxygen-centered angles in liquid silica as a function of pressure from Car-Parrinello MD [98], BKS MD and MD with our polarizable potential.

Table 5.2: Quartz

	Experiment. (Ref. [100])	New Potential	BKS
a [$\AA$]	4.916	4.925	4.941
c [$\AA$]	5.405	5.386	5.449
ρ [g/cm^{-3}]	2.646	2.665	2.598
Si-O-Si	143.7	144.5	148.1

curate. This implies that the inclusion of realistic physics into the potential improves its transferability as well as its accuracy. Our results indicate that the tetrahedral structure of the liquid is more stable at higher pressures than is predicted by the BKS potential. Since diffusion is strongly linked to the presence of defects such as 3-fold and 5-fold coordinated silicon atoms, the ability of a potential to reproduce the correct distributions of such defects is important if it is to properly describe the diffusion mechanism as a function of pressure.

Crystal Structures

As a final test of the potential we examine its ability to describe the most important low pressure polymorphs of silica. The various crystal parameters for at zero pressure and 300 K for quartz, cristobalite and coesite are given in tables 5.2, 5.3 and 5.4 respectively.

Stishovite, the stable form of silica at high pressure (above $\sim$ 8 GPa) and which

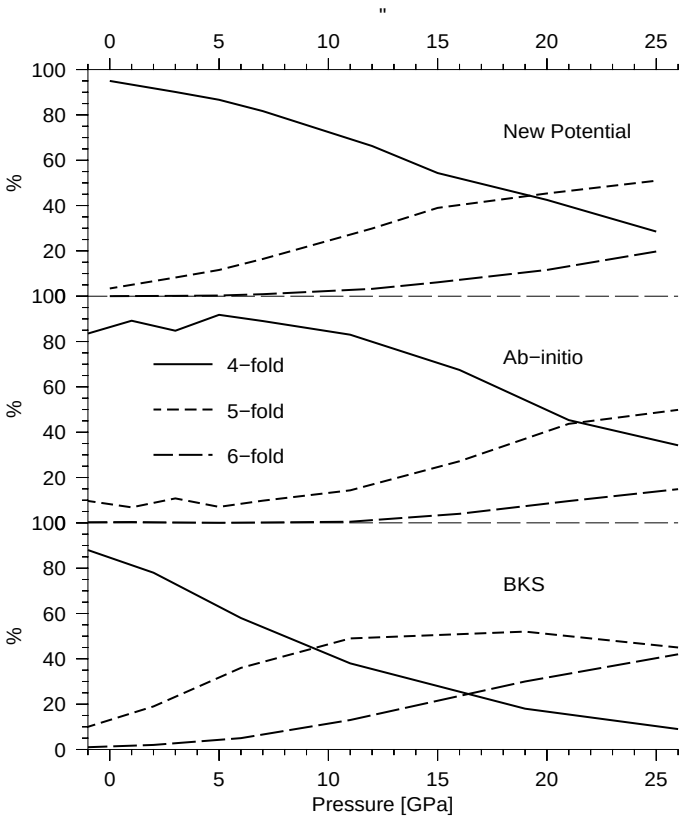

Figure 5.3: Percentage of $N-$fold coordinated silicon atoms in liquid silica as a function of pressure for the new potential compared to CP simulations[90] and the BKS potential[99].

can also be stabilized at ambient conditions was also simulated. However, in this case, although the system relaxed initially to very close to the correct density (within 2%), it always collapsed within several picoseconds to lower density structures. This would indicate that the energy barrier which keeps stishovite metastable at low pressures is hugely underestimated with this potential. It is not surprising that the potential has problems describing stishovite. Stishovite differs from all the other polymorphs considered in that the silicon ions are sixfold coordinated. This inevitably means that there are local changes in electronic structure with respect to the tetrahedral structures and therefore a loss of accuracy of our parameter set.

The tetrahedral crystal structures are all in very good agreement with experiment. In

Table 5.3: Cristobalite

	Experiment. (Ref. [101])	New Potential	BKS
a [$\mathring{A}$]	4.957	4.936	4.920
c [$\mathring{A}$]	6.890	6.847	6.602
ρ [g/cm^{-3}]	2.334	2.412	2.515
Si-O-Si	146.8	144.0	143.9

Table 5.4: Coesite

	Experiment. (Ref. [102])	New Potential	BKS
a [$\AA$]	7.136	7.165	7.138
b [$\AA$]	7.174	7.162	7.271
c [$\AA$]	12.369	12.377	12.493
β	120.34	120.31	120.76
ρ [g/cm^{-3}]	2.921	2.933	2.864
Si-O-Si	143.6	144.0	150.5

fact the agreement is so good that it surpasses the agreement with previously published fully *ab initio* calculations[97, 103]. As with the density of the liquid, this agreement is almost certainly fortuitous.

5.4 Discussion

We have demonstrated in this chapter how our inclusion of polarization effects coupled with our parametrization routine can produce a potential with extremely good structural properties. We have not yet extensively tested the dynamical properties of this potential, however we have noted that the α to β-cristobalite transition occurs at too low a temperature (by about 35%) with our potential, and diffusion of the liquid seems to be faster in general than diffusion with the BKS potential. This potential, is itself considered to have diffusion which is too fast based on extrapolations of low temperature data[104, 105]. It is not surprising if our potential does not describe dynamics well. We note that, particularly if covalency is present, the functional form would seem to be ill-equipped to describe shorter-range interactions. This can also be seen by the fact that we reproduce *ab initio* forces only to within 16% and yet our description of the structural properties of the crystalline allotropes is really excellent. This would suggest that most of this 16% can be attributed to short-range (non-electrostatic) forces which are important for a good description of dynamics.

The many-body distortable-ion model outlined in section 3.7.2 and the previous aspherical-ion model of Rowley *et al.*[52] are designed to improve dynamics in simple ionic systems where relatively minor distortions of anions occur. The distortion self-energy of the ions is not well researched (see section 3.7.3) and the idea that the force between ions depends only on the distance between electron clouds *along their line of centers* is one of many gross over-simplifications which one should not expect to work for spatially extended and highly distorted charge distributions such as have been found in electronic structure calculations of silica (see [106] and references therein). We have attempted to apply this model to silica and we see a small improvement of the fit to the forces (to about 14%). However, little time was spent in the parametrization process and we have not yet tested this potential. Future work may yield a potential with which dynamical properties may confidently be modeled.

Chapter 6

Magnesium Oxide

6.1 Introduction

Magnesium oxide is considered to be the simplest oxide for a number of reasons. It is an ionic oxide with a $1:1$ stoichiometry and it has a very simple structure - the cubic NaCl structure (see figure 6.1) - which has been shown experimentally to be stable at pressures up to *at least* 227 GPa[107]. Beryllium oxide, the only group II oxide with fewer electrons forms the less symmetric $B4$ (wurtzite) structure. MgO is known to be extremely ionic, with the Mg atom giving up two of its electrons almost entirely to the O atom and so to a good approximation, the O^{2-} and Mg^{2+} ions both have closed $n = 2$ shells of electrons.

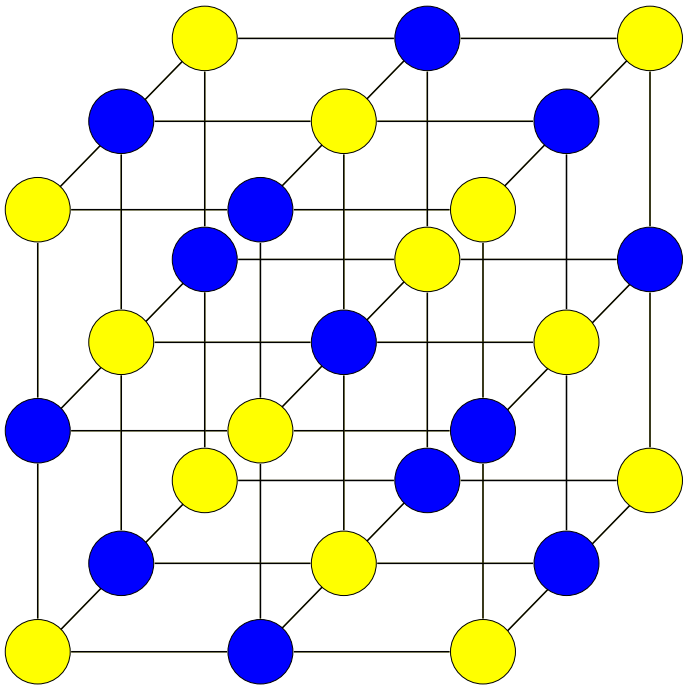

Figure 6.1: The structure of MgO.

The simplicity of MgO makes it a natural starting point in attempts to understand or model oxides which make up one of the most important groups of compounds. Important oxides include water, a necessity for all known life, and the cuprates, a class of complex copper oxides in which high-temperature superconductivity is found. Both of these examples are the subjects of intense research, but as we will see, even MgO a much more simple system, is not well understood. Although an understanding of MgO will clearly not automatically lead us to an understanding of other oxides, if we can't understand the electronic structure and the interactions between atoms in a system as simple as MgO, we cannot expect to have much success with more difficult systems.

MgO is an important component of the earth's lower mantle[108]. It is estimated that it makes up approximately 20% of the lowermost part of the mantle, the other most important compounds being $MgSiO_3$ and SiO_2 (see chapter 5). The behaviour of MgO under conditions of extreme pressure (up to $\sim$ 130 GPa) and temperature (up to $\sim$ 3000 K) is important for understanding deep Earth geophysics. Once again, its relative simplicity makes it the starting-point for experimental and theoretical techniques that are used to probe the properties of deep mantle minerals, the vast majority of which are oxides. The stability of MgO under pressure also means that it is frequently used as a pressure calibration standard for high pressure and temperature experiments.

MgO is also important industrially, primarily as a catalyst but it has a wide range of uses. It is an important component of glass, it is used as an electrical and thermal insulator and it is used as an ingredient in the production of fertilizer among other things.

For the reasons outlined, MgO has been the subject of intense theoretical and experimental study and there is an enormous literature on it's properties and behaviour under pressure and temperature. However, experimental difficulties at high pressures and temperatures and problems with theoretical methods of simulating ionic systems, some of which are discussed in chapter 3, have meant that some properties are still a matter of debate. From a theoretical point of view, a large number of empirical, semi-empirical and *ab initio* techniques have been applied to MgO. Density functional theory within the local density approximation has shown itself to be very accurate for the calculation of the static and vibrational properties of crystalline MgO [6, 26, 5] and it is probable that it is also very good for simulating the liquid. However, *ab initio* molecular dynamics has proven difficult (see chapter 2) and at any rate what can be studied with *ab initio* timescales and system sizes is very limited. Empirical and semi-empirical models have been disappointing for many properties, particularly for dynamical properties such as phonon frequencies[52, 109]. The papers by Rowley *et al.*[52] and Aguado *et al.*[55] have shown that effective potentials can model crystal dynamics but a model which is practical for simulations of reasonably large systems is still lacking.

An important outstanding problem is the behaviour of the melting temperature as a function of pressure. There have been a number of attempts to simulate the melting of MgO in the past [112, 115, 113, 111, 114] . Some of the results are shown in figure 6.2. The theoretical results show a difference of a factor of between 2.5 and 7.3 in the slope dT_{melting}/dP, at zero pressure with respect to the results of diamond-anvil-cell experiments [110]. It has been suggested by a number of people that there is a systematic error in the experiment, however the lack of agreement between the different theoretical approaches,

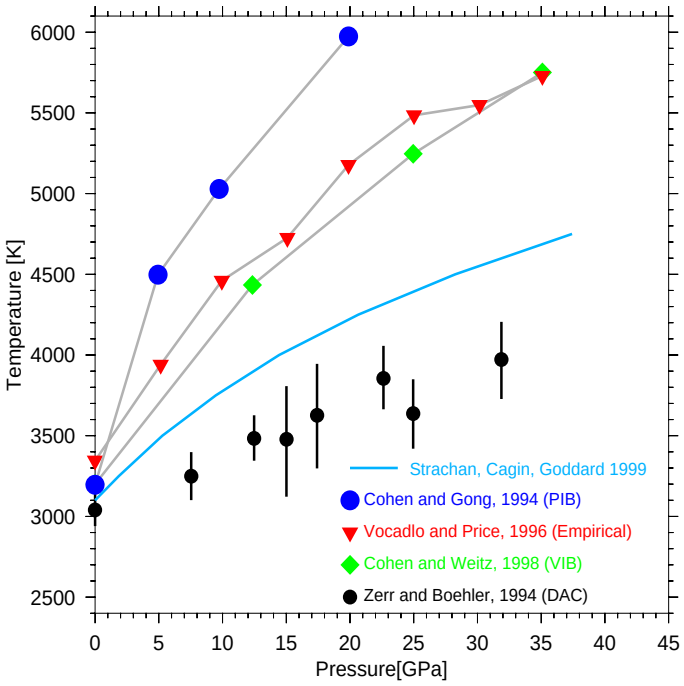

Figure 6.2: The melting temperature of MgO as a function of pressure from experiment[110] and from simulations using the variational induced breathing (VIB) model[111], the potential induced breathing model[112], and the effective potentials of Vocadlo and Price [113] and Strachan,Cagin and Goddard [114].

and the inability of these approaches to describe the phonon spectrum of MgO means that the case for repeating the experiment is not as strong as it might be. It would have very important geophysical consequences if, in fact, there was a problem with the experiment and MgO has a much steeper melting slope[116].

Between the Earth's lower mantle and its outer core of molten iron there is a boundary layer in which seismic observations have indicated a drastic drop in sound velocities[117]. An open question is whether this is due to a change in chemical composition or to melting. The magnitude of this velocity change, especially in the shear velocity, favours melting. If this is the case then there will be a constraint on the temperature at the core-mantle boundary (which is an important but not well-known quantity) from the solidus temperature of the mantle. It was found by experiments[110, 118] that the melting lines of MgO and (Mg,Fe)SiO_3-perovskite cross at about 50 GPa, so that at the pressure of the core-mantle boundary, the melting temperature of MgO is lower than that of (Mg,Fe)SiO_3-perovskite. Previously it had been thought that the eutectic composition of the mantle lay near the composition of perovskite, the major component. Zerr and Boehler's results indicate that, in fact, the eutectic composition is probably much more MgO-rich. This has then been used to deduce new constraints on the temperature of the core-mantle boundary[116].

If Zerr and Boehler's work turned out to be wrong, as theorists currently suspect, one

of the most popular current models of the core-mantle boundary and as a result of the temperature profile throughout much of the earth would have to be substantially revised.

The aim of this chapter is twofold. First of all, MgO, will be used as a testing ground for the polarizable and distortable-ion interatomic potentials which we have discussed in chapter 3. We will use the parametrization scheme of chapter 4 and show how we can achieve a marked improvement in accuracy over simpler force-fields whilst still retaining the ability to simulate much larger systems than are possible with *ab initio* methods. Secondly, we tackle the problem of the melting slope of MgO using a combination of molecular dynamics with our improved effective force-field and total energy calculations within density functional theory.

6.2 Testing Potentials for MgO

In this section various different functional forms for the interatomic potential will be tested. The criterion that we use to determine the quality of a functional form is its ability to fit the *ab initio* data, as described in chapter 4. We will confine ourselves to testing the usefulness of three different types of potential :

1. A pairwise short-range interaction potential of the form

$$U_{IJ}(R_{IJ}) = B_{IJ}e^{-\alpha_{IJ}R_{IJ}} - \frac{C_{IJ}}{R_{IJ}^6} - \frac{E_{IJ}}{R_{IJ}^{N_{IJ}}} \tag{6.1}$$

   where $B_{IJ}, \alpha_{IJ}, C_{IJ}, E_{IJ}, N_{IJ}$ are all parameters to be optimized.

2. A polarizable-ion potential including short-range polarization, as discussed in section 3.7.1. Only the oxygen ion is considered polarizable.

3. A distortable-ion potential, as discussed in sections 3.7.2 and 3.7.3. The interaction energy between ions I and J is given by

$$U_{IJ}(L_{IJ}) = A_{IJ}e^{-\alpha_{IJ}L_{IJ}} + B_{IJ}e^{-\beta_{IJ}L_{IJ}} \tag{6.2}$$

   and the functions f_{IJ},$\sigma_I^{(0)}$, and $\sigma_{IJ}^{(1)}$ are given the same forms as in equations 3.48, 3.46 and 3.50 respectively, i.e.

$$f_{IJ} = C_{IJ}^{(1)}e^{-C_{IJ}^{(2)}R_{IJ}} \tag{6.3}$$

$$\sigma_I^{(0)}(\rho_I^{(0)}) = C_I^{(3)}\ln(\rho_I^{(0)}) \tag{6.4}$$

$$\sigma_{IJ}^{(1)} = C_{IJ}^{(4)}\ln\left(\frac{\rho_{IJ}^{(1)}}{\rho_I^{(0)}}\right) \tag{6.5}$$

   where C_1 from equation 3.50 has been merged into the pre-exponential factors A_{IJ} and B_{IJ}. The parameters to be optimized are A_{IJ}, α_{IJ}, B_{IJ}, β_{IJ}, $C_{IJ}^{(1)}$, $C_{IJ}^{(2)}$, $C_I^{(3)}$,$C_{IJ}^{(4)}$. The values $R_a = 8.5$ a.u and $R_b = 10$ a.u. were used in the decay function g_{IJ}.

Using a scheme which was slightly modified with respect to the one outlined in section 4.2, five force-fields were constructed using five different parametrizations. In addition to the ingredients mentioned, all five included the point charge-electrostatic potential with the charge on an ion as a parameter. The potentials created were

A. A pair-potential : short-range pair potential, parametrized in the crystal at ambient conditions.

B. A polarizable potential : short-range pair potential, with polarizable anions, parametrized in the crystal at ambient conditions.

C. A distortable-ion potential : distortable-ion potential, parametrized in the crystal at ambient conditions.

D. The full model : distortable-ion potential, with polarizable anions, parametrized in the crystal at ambient conditions.

E. The full model : distortable-ion potential, with polarizable anions, parametrized in the liquid at 3000 K.

Each of these potentials was tested by its ability to fit three different sets of *ab initio* data. Using the full model, which consists of a distortable-ion potential with anion polarization and point charges, three potentials have been created using the self-consistent procedure of section 4.2. These three potentials were optimized at zero pressure for (i) the liquid at 3000 K (ii) the crystal at 2000 K and (iii) the crystal at 300 K respectively. Each of these three potentials was used to create atomic configurations at the conditions for which it was optimised. These configurations are considered to be as representative of the true system as we have the ability to create.

The five potentials A to E were parametrized using the *ab initio* data at the correct conditions and each potential was evaluated not only by the values of ΔF, ΔS, and ΔE achieved during parametrization, but also by their ability to fit the *ab initio* data from the other two sets of conditions. For example, potential A was parametrized at 300 K, and then its ability to fit the *ab initio* data in the crystal at 2000 K and the liquid at 3000 K was also tested. Due to the fact that for stress and energies it was not possible to parametrize using an extremely large *ab initio* data set (we were limited by the computational cost of optimisation to 10 configurations), the numbers quoted are the fit to 10 configurations at the same conditions but which were *not* used in the minimization of $\Gamma(\{\eta\})$. In all cases the error in the stress was evaluated relative to a pressure $B = 140$ GPa which is close to the experimental bulk modulus at ambient conditions of 150 GPa.

The results are summarized in table 6.1. We cannot guarantee that we have found the global minimum in each case during optimization as simulated annealing had to be done at a rather rapid quench rate. The simulated annealing was followed by Powell minimization[72]. In each case, the total minimization time was the same (10 days on a single processor) and therefore more economical force-fields are likely to be better minimized than less economical ones.

A number of things can clearly be seen from table 6.1. First of all, not surprisingly, the distortable-ion model on its own is quite bad. This is probably because of the shortness of

Table 6.1: The fit to the *ab initio* data for the different potential forms

	300K crystal			2000K crystal			3000K Liquid		
	ΔF	ΔS	ΔE	ΔF	ΔS	ΔE	ΔF	ΔS	ΔE
A	9.3	5.0	25.5	13.7	3.3	15.5	25.1	4.8	52.4
B	6.9	5.2	23.8	9.0	6.2	17.8	17.5	5.6	23.6
C	10.4	39.1	5.9	13.6	51.7	164.8	32.2	58.2	69.2
D	3.4	0.6	3.0	6.8	0.3	9.8	17.1	0.3	10.5
E	12.8	0.1	59.0	10.2	0.1	18.9	9.6	0.0	17.7

the range of its interactions. Ions further away from each other than 10 a.u. interact only via the coulomb force between their charges. At 300 K, the full model is clearly better than all other forms. It also transfers very well up to higher temperatures and to the liquid. The pair-potential, although working quite well for the crystal, does not transfer well to the liquid. The polarizable model yields results which are intermediate in quality between the pair-potential and the full model. The results are a clear illustration of the fact that by adding more physics into the form of an effective potential one can create force-fields with, not only an improved ability to fit the *ab initio* data, but also a much improved transferability between different phases and conditions.

The poor fit of potential E to the energy differences in the crystal at ambient conditions is because the energy differences in the liquid and high temperature solid are much greater than those at lower temperatures. The absolute value of the error in the energy differences is the same at low temperature and high temperature but ΔE is the error relative to the root-mean-squared value, which for the crystal is very small.

Phonon Frequencies

Having established that our inclusion of many-body effects has improved the potential form with respect to the pair potential, at least according to the criterion that we have adopted, we now look at its ability to model the vibrational spectrum of MgO. We note once again that the DFT scheme to which the potential was fit gives a very good description of phonon frequencies at ambient conditions [6]. In order to get some perspective about the kind of accuracy that has been achieved in the past with other models we look at the results of simulations using a "Variational Induced Breathing" (VIB) model[119, 109]. The reason for comparison with this model is that it is the most highly evolved of a class of models of Gordon-Kim type [120]. In these models, the crystal charge density is modelled as a superposition of ionic charge densities. The total energy and forces are then calculated using Kohn-Sham theory [3]. Since the isolated O^{2-} ion is not stable, it must be stabilised in some manner. In the VIB model this is done by surrounding the ion with a sphere of +2 charge (called a "Watson sphere") , the radius of which is varied so as to minimize the total energy of the crystal. This non-empirical model is useful for comparison because models of this type have been extensively applied to MgO[119, 109, 121, 112, 111], and in particular to study the melting of MgO[112, 111, 121]. It is these theoretical melting curves that we would like to improve upon in section 6.4. A comparison of the results of

the VIB model with those of self-consistent DFT calculations is useful since it illustrates the importance of aspherical distortions which, if the fully ionic picture is correct, is the primary difference between them. As can be seen from the phonon dispersion curves

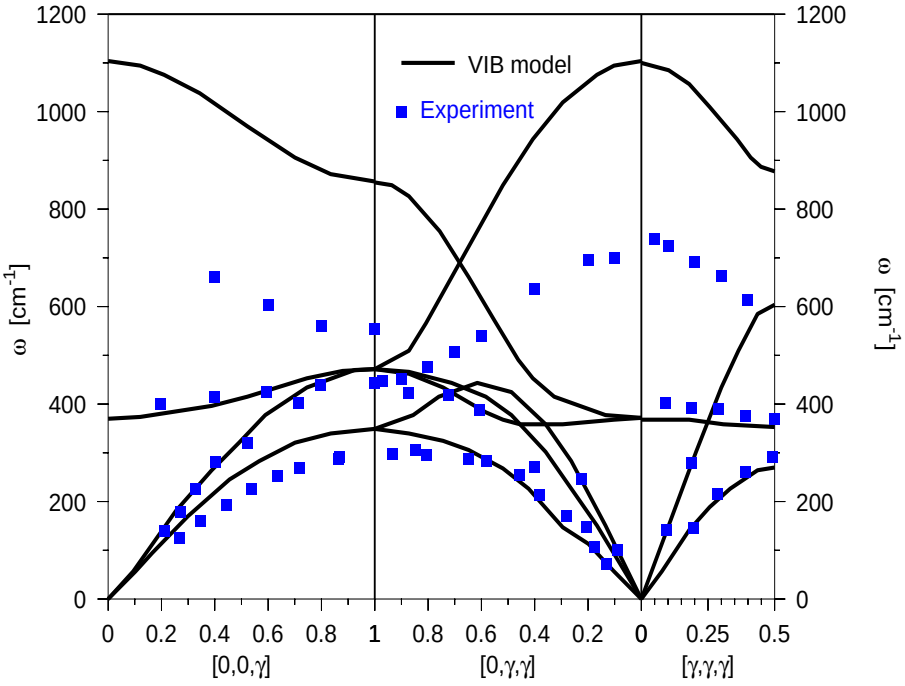

Figure 6.3: The phonon dispersions of MgO as calculated with the variational-induced breathing model[109] compared with experiment[62]

(figure 6.3) the level of agreement with experiment is quite poor for some of the phonon modes. Since the self-consistent DFT results are in very close agreement with experiment, this highlights the inadequacy of models which do not allow for aspherical ionic distortions. The most striking disagreement with experiment is in the longitudinal optical (LO) phonons. LO phonons induce a long-range electric field in the crystal which opposes the motion of the ions and therefore raises the energy of the phonon mode. In the real crystal, electrons screen out some of the effect of this electric field. The screening mechanism is mainly that of ionic polarization but may also include contributions from charge transfer between ions. Since this is not present in the VIB model, the electric field is too high and the LO frequencies are correspondingly higher. It is precisely this effect which prompted the development of the shell model and subsequent methods of treating ionic polarization.

We now turn to our model of interionic interactions to see how well it performs in the calculation of the phonon frequencies. The method that we use to calculate the phonon frequencies is derived from the fluctuation-dissipation theorem [122]. The phonon frequencies are calculated from the positions of the peaks in the spectra of the spatial Fourier components of longitudinal and transverse charge and mass current correlation

functions, for wavevectors along the high-symmetry directions of the crystal[57].

$$C^{\mathrm{Long}}(\mathbf{k},t) = \langle (\sum_{I=1}^{N} (-X^I(t) \imath \mathbf{k} \cdot \mathbf{v}^I(t) e^{-\imath \mathbf{k} \cdot \mathbf{r}^I(t)})) (\sum_{J=1}^{N} (-X^J(0) \imath \mathbf{k} \cdot \mathbf{v}^J(0) e^{-\imath \mathbf{k} \cdot \mathbf{r}^J(0)})) \rangle \quad (6.6)$$

$$C^{\mathrm{Trans}}(\mathbf{k},t) = \langle (\sum_{I=1}^{N} (-X^I(t) \imath \mathbf{k} \times \mathbf{v}^I(t) e^{-\imath \mathbf{k} \cdot \mathbf{r}^I(t)})) (\sum_{J=1}^{N} (-X^J(0) \imath \mathbf{k} \times \mathbf{v}^J(0) e^{-\imath \mathbf{k} \cdot \mathbf{r}^J(0)})) \rangle \quad (6.7)$$

where $\mathbf{v}^I(t)$ is the velocity of ion I at time t and $X^I(t)$ is the charge of species I for the optic modes and the mass of species I for the acoustic modes. $\mathbf{k}$ is a wavevector which is commensurate with the size of the simulation cell.

We performed an MD simulation on a system of 512 atoms using the full-model, optimised in the crystal at 300 K. The current correlation functions were calculated on a time domain of length 2.9 ps which was averaged over a simulation of length 20 ps. The phonon dispersions that we get are shown in figure 6.4. We get an extremely close fit to both the experimental and the self-consistent DFT data. The chief discrepancies are in the optical modes which are systematically underestimated. The longitudical optical mode in particular is underestimated near the zone center. Although we do not calculate the mode frequences at $\Gamma = (0,0,0)$, as this would require an infinitely large simulation cell with the method that we are using, it looks as though the LO-TO phonon splitting is slightly underestimated. In our parametrization procedure we have used a small cell to perform the *ab initio* calculations and so the long-range interactions which are important for dispersion near the $\Gamma-$point are not included. Our hope is that by modelling correctly the electrostatics at shorter range, we get a potential which, when used in a larger simulation cell, can accurately model the long range electrostatic interactions. This is not guaranteed however and is likely to work only if we include all relevant screening mechanisms in our functional form. The incorrect LO-TO phonon splitting suggests that our description of the electrostatics is incomplete. This is not surprising since dipole polarization is only one of many screening mechanisms. It may be that charge-transfer between ions is important. However, a comparison with the results of reference[55] is suggestive of it being due to the fact that we haven't included the affects of higher-order multipoles. Our Car-Parrinello simulations and static DFT calculations (see section 2.4) showed that there was very close to a complete transfer of 2 electrons from the magnesium to the oxygen ions at high pressure. However, the charge on the oxygen ion in this potential (and all other potentials that we have fit) is ~ 1.5 - considerably less than this. Although the degree of ionicity is certainly less at zero pressure where the LDA band gap is lowered by $20-30\%$ (to ~ 5 eV) it is unlikely to have reduced to this extent. Under the assumption that, within our model, short-range interactions and electrostatics describe completely separate aspects of the potential-energy surface (we do not know the extent to which this is true) the minimization routine fits the charge and the polarizability so as to best approximate the electrostatics of the crystal. The lack of higher order multipoles means that it must choose a compromise between purely dipole screening, in which the polarizability α and the charge q take their "true" values, and uniform screening in which the charge is simply reduced by a factor equal to the dielectric constant and the polarizability is zero. In

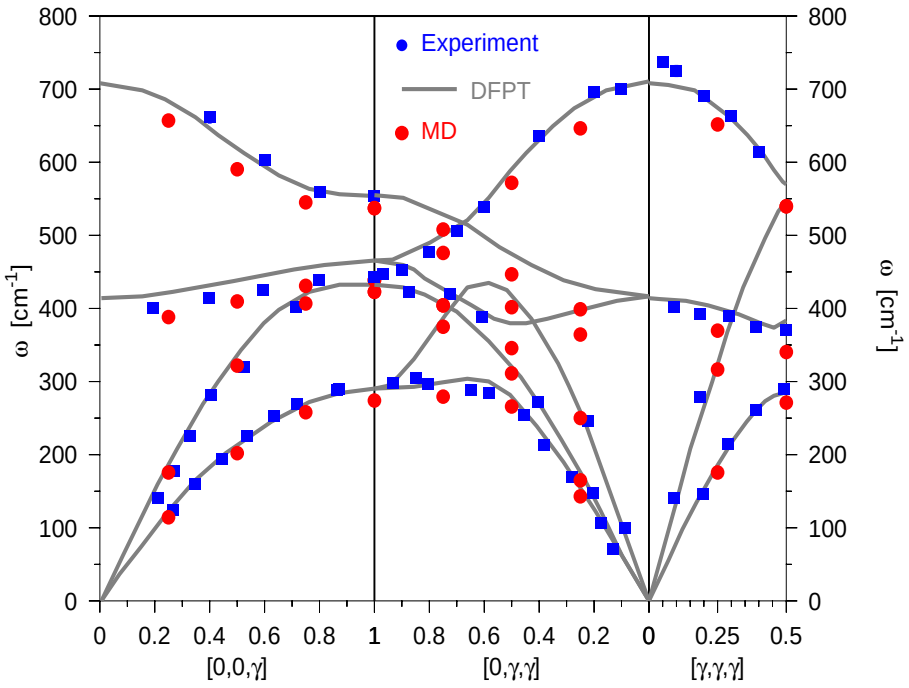

Figure 6.4: The phonon dispersions of MgO as calculated with the full polarizable and distortable-ion model parametrized in the crystal under ambient conditions compared with experiment[62] and with the density functional perturbation theory results of Karki *et al.*[6]

reference[55] they use formal ionic charges and include both quadrupoles and dipoles and they get better agreement with experiment. Nevertheless, the description of the electrostatics that we have is significantly better than any other effective potential that we are aware of (including the non-empirical Gordon-Kim models), and quadrupoles would add considerably to the computational expense of the model.

Density

We now look at the density as a function of pressure and temperature for this potential. As can be seen from figure 6.5, the MD simulations are in excellent agreement with experiment. The density as a function of pressure from the MD simulations are even in slightly better agreement with experiment than the DFT scheme of Karki *et al.*[6], particularly at high pressure. Although we have fit the stress so that it fits almost exactly the stress from DFT calculations using the same pseudopotentials as Karki *et al.*, our DFT calculations are not identical. We sample the Brillouin zone in a different way and we use a much higher plane wave cutoff. The cutoff used by Karki *et al.* is only barely converged at zero pressure and so it is possible that their calculations disimprove under pressure.

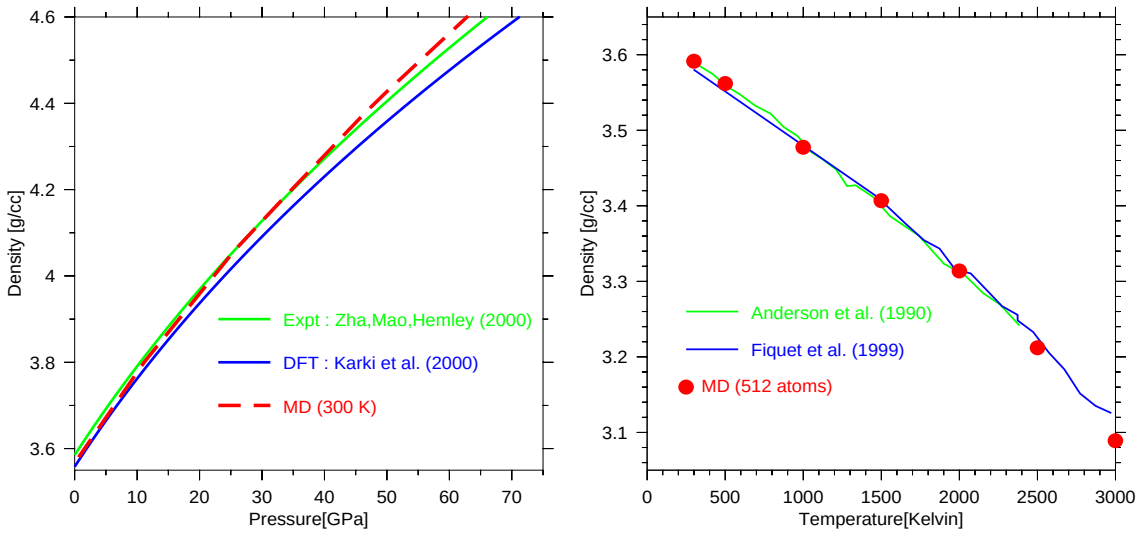

Figure 6.5: The density of MgO as a function of a) pressure (at 300 K) and compared to experiment[125] and density functional perturbation theory calculations [6]; b) temperature (at zero pressure) compared to experiment[123, 124]. MD simulations used the full model potential parametrized at ambient conditions and simulation cells containing 512 atoms.

6.3 The Distortable-Ion Model Revisited

As discussed in section 3.7.3, we do not impose the distortable-ion model on the system. We have parametrized the force-field using simulated annealing which was begun at a high temperature. This means that, although we have supplied a functional form which is capable of including distortable-ion behaviour, the minimization routine is free to do with this form whatever is best for reproducing *ab initio* forces. The options that are open to the minimization routine are

- to disable all variable-radius functionality, and therefore to model the interionic forces with a double exponential of the interionic distance R_{IJ}. It would be optimal to do this if the way in which we model distortions is completely unphysical.

- to enable only the compressible-ion part of the model, i.e. that which is analogous to the model of Wilson *et al*[47], thereby allowing only spherically symmetric anion distortions. It would be optimal for it to do this if the way in which we model aspherical distortions is unphysical but our description of spherical distortions is reasonable.

- to enable only the asymmetric part of the model and to disable purely spherically-symmetric distortions. This is optimal if our reasoning that aspherical distortions are energetically equivalent to spherical ones is true and the form of the model is reasonable.

- to partially enable either or both types of distortions as the best compromise between rigid-ion behaviour, breathing-ion behaviour and distortable-ion behaviour if all three of the models fail to varying degrees and in different ways to reproduce the *ab initio* potential energy surface.

The parametrization process is therefore itself a test of the distortable-ion model. We now look at what, precisely this parametrization process has done by examining the radius of an oxygen ion in the direction of a neighbouring magnesium ion for one of our potentials (potential F which is discussed in detail in section 6.4). The test is performed in the crystal at 3000K. The local radii of the anions consist of an arbitrary constant, which may be merged into the constant coefficient of the exponential force between ions, and the true variations of the radii due to changing environment. We look at the quantities $\sigma_{IJ} - \overline{\sigma_{IJ}}$, $\sigma_{IJ}^{(1)} - \overline{\sigma_{IJ}^{(1)}}$, and $\sigma_{I}^{(0)} - \overline{\sigma_{I}^{(0)}}$ for anion I and cation J where $\overline{\sigma_{IJ}}$,$\overline{\sigma_{IJ}^{(1)}}$ and $\overline{\sigma_{I}^{(0)}}$ are averages over a long trajectory. These quantities therefore are the non-constant parts of the different contributions to the radius of ion I in the direction of J (Recall that $\sigma_{IJ} = \sigma_{I}^{(0)} + \sigma_{IJ}^{(1)}$ where $\sigma_{I}^{(0)}$ includes only spherically-symmetric distortions and $\sigma_{IJ}^{(1)}$ includes aspherical distortions).

The results are shown in figure 6.6 and the variation in the value of L_{IJ}, as defined by equation 3.30, along the same trajectory is shown for comparison. As can be seen, the local radius is dominated by the effect of the *aspherical* part of the distortable-ion model. The spherical part makes a significantly smaller contribution. This clearly vindicates our extension of the compressible-ion model to include aspherical distortions. The variation in the radius is very small compared to the variation in L_{IJ} and so we look at what contribution this makes to the forces between the ions. Looking at the forces in a pairwise way is not entirely justified given the many-body nature of the potential, however it seems natural to look at the quantities

$$Q_{IJ}^{(1)} = 100 \times \frac{\frac{\partial U_{IJ}(L_{IJ})}{\partial L_{IJ}} - \frac{\partial U_{IJ}(R_{IJ} - \overline{\sigma_{IJ}} - \overline{\sigma_{JI}})}{\partial R_{IJ}}}{F_{IJ}^{\text{r.m.s.}}} \tag{6.8}$$

and

$$Q_{IJ}^{(2)} = 100 \times \frac{\frac{\partial U_{IJ}(L_{IJ})}{\partial L_{IJ}} - \frac{\partial U_{IJ}(R_{IJ} - \overline{\sigma_{IJ}} - \overline{\sigma_{JI}})}{\partial R_{IJ}}}{\frac{\partial U_{IJ}(L_{IJ})}{\partial L_{IJ}}} \tag{6.9}$$

where $F_{IJ}^{\text{r.m.s.}}$ is the root mean-squared value (averaged over time) of the *total* force on anion I (i.e. from all atoms and from both electrostatic and non-electrostatic contributions) projected onto the line joining the centers of I and J. These quantities are plotted in figure 6.7. $Q^{(1)}$ is a way of looking at the impact of instantaneous variations of the membrane radii on the total force on the ion. $Q^{(2)}$ is a way of looking at the impact of instantaneous variations of the membrane radii on just the *short-range* part of the force between ions I and J. If the radius the ion is constant, then $Q^{(1)} = Q^{(2)} = 0$.

It is difficult to know how one should best compare forces, or judge the impact of individual contributions to the forces. However, inspection of these two quantities strongly suggests that, with the parameters of the model chosen by the minimization routine, the variation of the anion's radius has a significant impact on dynamics.

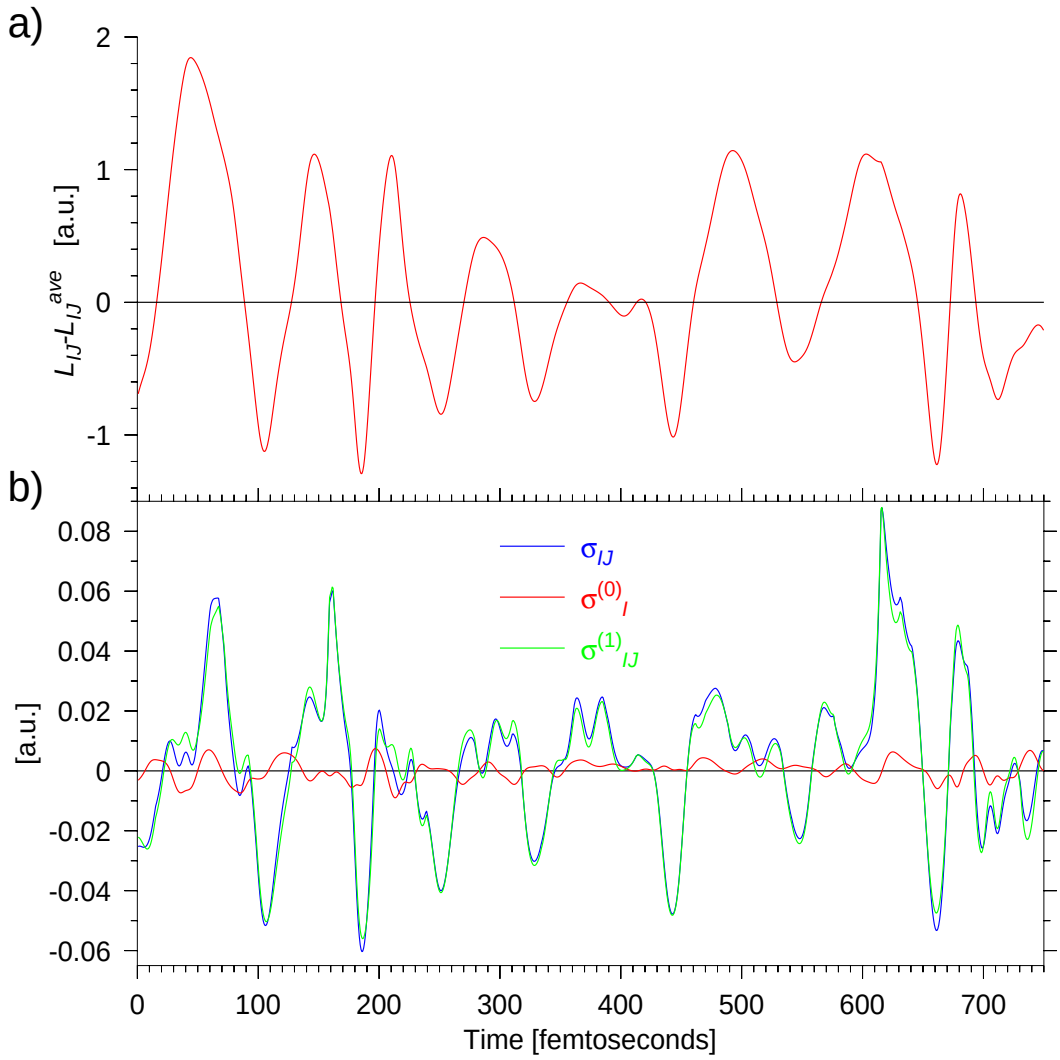

Figure 6.6: a) $L_{IJ} - \overline{L_{IJ}}$ as a function of time, where $\overline{L_{IJ}} \approx 4.66$ a.u. is the average over the trajectory of L_{IJ}, the inter-*membrane* distance (see section 3.7.2). b) $\sigma_{IJ} - \overline{\sigma_{IJ}}$,$\sigma^{(1)}_{IJ} - \overline{\sigma^{(1)}_{IJ}}$, and $\sigma^{(0)}_{I} - \overline{\sigma^{(0)}_{I}}$. I and J are neighbouring anion and cation respectively.

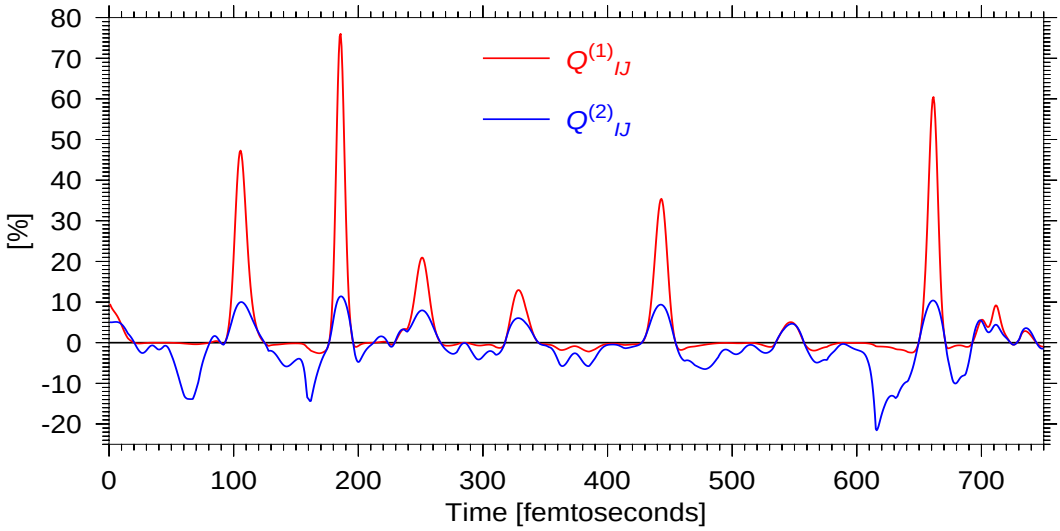

Figure 6.7: $Q^{(1)}_{IJ}$ and $Q^{(2)}_{IJ}$ (see equations 6.8 and 6.9)as a function of time along the same trajectory shown in figure 6.6

So, the above discussion shows that the minimization routine finds it optimal to allow fully aspherical distortions of the anions which impact significantly on the interatomic forces. This, coupled with the overall ability of the model to fit *ab initio* data would strongly suggest that the distortable-ion model works and is a valuable addition to the force-field. However, it is very likely that it could be improved with research into the various functional forms on which it depends.

6.4 The Melting Line of MgO

As mentioned in the introduction to this chapter, there is considerable debate about the melting temperature of MgO as a function of pressure. In this section we attempt to calculate the derivative of the melting temperature as a function of pressure using a combination of classical MD simulations, ground-state DFT calculations and Car-Parrinello MD simulations. The method that we use to find the zero-pressure slope is to use the Clausius-Clapeyron equation

$$\frac{dT_m}{dP} = T_m \frac{\Delta V}{\Delta H} \tag{6.10}$$

which relates the derivative of the coexistence curve between the solid and the liquid to the change in enthalpy ΔH and volume ΔV between the phases. At zero pressure the change in enthalpy is simply equal to the change in the internal energy ΔU. The failure of previous theoretical models to agree with each other and with experiment makes it important for us to eliminate as many sources of error as possible from our calculation. Ideally we would like to eliminate all sources of uncertainty except for those inherent in the DFT calculations, i.e. the uncertainty due to the use of approximations to the exchange-correlation energy.

Table 6.2: The fit to the LDA *ab initio* data for the liquid (F) and solid (G) potentials used in the calculation of the melting slope.

	3000K Crystal			3000K Liquid		
	ΔF	ΔS	ΔE	ΔF	ΔS	ΔE
F	9.6	0.1	10.8	10.4	0.2	10.2
G	6.2	0.3	10.6	44.0	2.3	54.0

Table 6.3: The fit to the PBE *ab initio* data for the liquid (F) and solid (G) potentials used in the calculation of the melting slope.

	3000K Crystal			3000K Liquid		
	ΔF	ΔS	ΔE	ΔF	ΔS	ΔE
F	10.6	1.3	12.0	10.8	0.9	12.2
G	6.6	1.6	11.2	45.0	1.5	56.1

In order to calculate the melting slope we need to calculate the melting temperature T_m, the volume at the melting temperature in the solid (V_s) and the liquid (V_l) and the potential energy at the melting temperature in the solid (U_s) and the liquid (U_l). In order to maximise the accuracy of our MD simulations we parametrize two separate potentials, one for the liquid at 3000 K (potential "F") and one for the solid at 3000 K (potential "G") . Each potential consists of a polarizable-ion part, point charge electrostatics, and distortable-ion short-range interactions. The distortable-ion self-energy in this case is given by equation 3.49. The values $R_a = 7.0$ a.u. and $R_b = 8.0$ were used in the decay function g_{IJ}. The parameters of these potentials are given in appendix **??**. The ability of each of these potentials to fit *ab initio* data from the solid the liquid at 3000 K was tested. We have also performed calculations on the same configurations using the state-of-the-art generalized-gradient approximation to exchange and correlation of Perdew, Burke and Ernzerhoff (PBE)[74]. The results are summmarized in tables 6.2 and 6.3 It was found that the potential which was parametrized on the solid at 3000 K could not be used at higher temperatures or in the liquid. The reason for this is that the iterative procedure which was used to calculate $\sigma_I^{(0)}$ and $\sigma_{IJ}^{(1)}$, due to the form of the self-energy used, did not converge for this potential under these conditions. This is the reason for the poor fit to the liquid *ab initio* data in table 6.2. There were no such problems for the potential which was parametrized on the liquid. The solid potential is therefore used mainly in order to test the *functional form* of potential which differs from that previously used. It also is used to verify that experimental data on thermal expansivity does not differ strongly at higher temperatures from extrapolation of low temperature behaviour.

We would like to test the ability of the potentials to reproduce experimentally known properties of MgO. We begin by looking at the ability of the potential parametrized in the solid to describe the phonon dispersion at ambient conditions. The results are shown in figure 6.8. One should not expect results which are as good as those for a potential which is parametrized at ambient conditions, and so the results are extremely good. There is very good agreement with both experiment and the DFPT results of Karki *et al.*. As

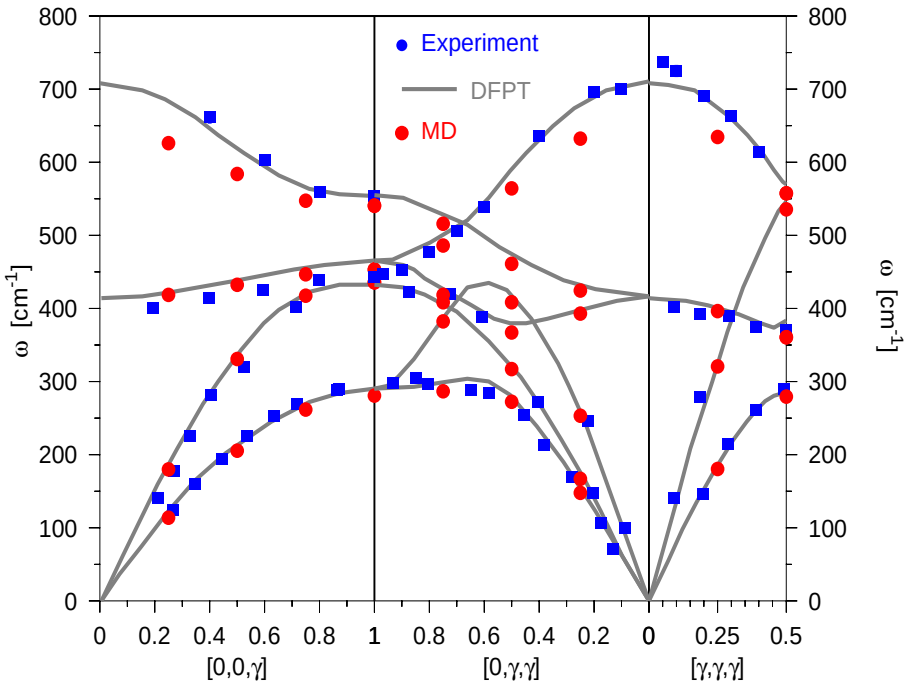

Figure 6.8: The phonon dispersions of MgO as calculated with the full polarizable and distortable-ion model parametrized in the crystal under ambient conditions compared with experiment[62] and with the density functional perturbation theory results of Karki *et al.*[6]

before, the worst agreement is for the long-wavelength LO phonons, and once again this is probably due to our incomplete description of electronic screening. It may also be that the very high symmetry of the relatively cold crystal makes polarization energetically unfavourable, and so the polarizability appropriate for a hot crystal is larger. A too-large polarizability, as discussed earler, should manifest itself in the phonon curves as a lowering of the energy of the long-wavelength LO phonon modes. However, in general the results seem even better than those of figure 6.4 and the ability of both potentials to reproduce *ab initio* energy differences is very satisfying and suggests that the form of the distortable-ion self-energy used may be better than a simple exponential.

As in the case of silica, there is little or no experimental data on liquid MgO and so we compare the structure of the liquid with the structure obtained in Car-Parrinello simulations. We would like to be as sure as possible that the liquid that we have created has a reasonable structure. We have performed CPMD of liquid MgO (using a small fictitious mass, $\mu_0 = 100$ a.u., and applying all the precautions and corrections described in chapter 2). The Car-Parrinello simulations, once corrected according to the rigid-ion approximation, still showed errors in the forces of $\sim 12.5\%$. This is even higher than the errors in the forces using our effective potential. Nevertheless, agreement between the two approaches would indicate the probability that both are right. The Car-Parrinello simulations were continued from a long classical simulation with potential F. Following

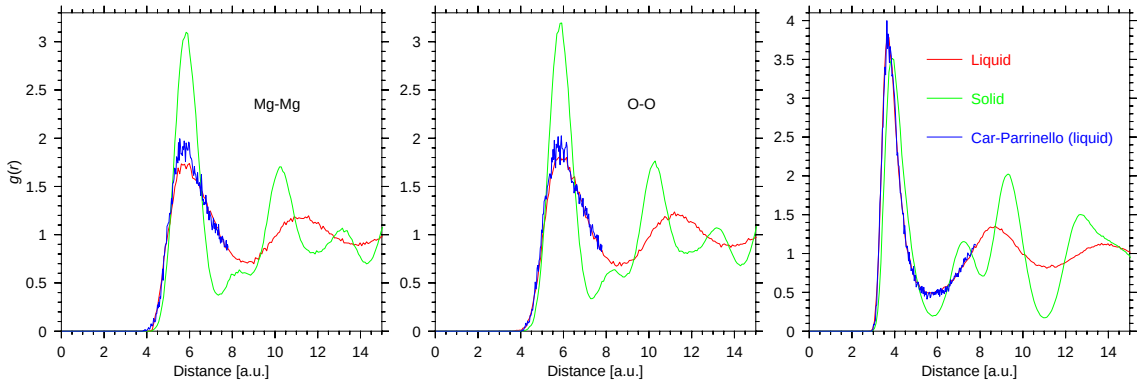

Figure 6.9: The pair-correlation functions of liquid MgO at $\sim$ 3100 K and zero pressure as calculated with our effective potential and from a Car-Parrinello simulation.

2 picoseconds of equilibration with CPMD the pair-correlation functions were calculated on a further 1.5 picosecond trajectory. This time is not sufficient to get accurate density averages (2 different simulations at pressures of $\sim$ 0 GPa and $\sim$ 0.5 GPa both yielded the same average density), however we can check that the structural features are the same as were obtained with our effective potential. The high rate of diffusion should mean that the liquid has had ample time to relax structurally. In figure 6.9 the Mg-O pair-correlation functions for the Car-Parrinello and effective potential liquids at 3050 K and the effective potential solid at 3100K are plotted. There is remarkable agreement between the CPMD results and our classical simulations indicating that the liquid is well reproduced The comparison with the solid pair-correlation function shows that there is a substantial difference in structure between solid and liquid. We see a change in the average coordination from 6 to $\sim$ 5. This change in structure is consistent with what is generally expected in ionic melts[126, 127] and it is consistent with a large volume change between solid and liquid. Ubbelohde[126] has argued that the coordination and volume change on melting is correlated with the polarizability of the anions. Compensating electrostatic forces in the crystal are responsible for larger interionic distances than occur in the melt. This can clearly be seen by the displacement inward of the first peak in the Mg-O pair-correlation function in the melt as compared to the crystal (figure 6.9). It is the strong attraction between anion and cation which is responsible for this. However, a large ionic polarizability weakens this attraction due to screening leading to increased Mg-O distances, a coordination number closer to six and a structure and hence volume more similar to that in the solid. Cohen and Gong[112], found a coordination number of around 4.5, and a volume difference $\Delta V/V_s \sim 30\%$ (V_s = volume in the solid at the melting point), using the *non-polarizable* PIB model. Our model attributes a sizeable polarizability ($\sim$ 14.3 a.u.) to the oxygen ion and we find $\Delta V/V_s \sim 20\%$.

Melting Temperature

We first try to calculate the zero pressure melting temperature T_m. The method that we use to do this is the "2-phase" method [128, 129, 115]. Solid and liquid configurations

which have been pre-equilibrated at the desired temperature and pressure are "stuck together"[1] to form a supercell in which there is a solid-liquid interface. If the temperature is higher than the melting temperature, the solid portion should begin to melt and the interface moves so as to increase the amount of liquid. If the temperature is lower than the melting temperature, the liquid at the interface begins to crystallize and the solid portion increases. Crystallization generates latent heat which raises the temperature of the simulation cell. Melting, on the other hand, absorbs latent heat thereby lowering the temperature of the simulation cell. At temperatures much higher than T_m, the system melts completely and at temperatures much lower than T_m the system crystallizes completely (see figure 6.10). In principle it is possible to bracket T_m in this way and this has been the approach of Belonoshko and Dubrovinsky in their calculation of the melting line of MgO. However, we have found that, within quite a large range of starting temperatures (between $\sim$ 2800 K and $\sim$ 3300 K), the temperature performs large fluctuations about T_m in which the system is by turns crystallizing and melting. If full crystallization or melting does not occur these oscillations can persist for a long time and therefore in order to get a rough idea of the melting temperature, following an initial equilibration period we have averaged the temperature over these oscillations. The average temperature depends on the relative sizes of the solid and liquid portions of the coexistence cell via the specific heat capacities of the solid and the liquid. This means that different simulations give different average temperatures depending on the initial conditions of the simulation. It is also true that, if equilibrium between solid and liquid occurs such that either phase is under-represented, finite-size effects may play a role. In order to get a rough estimate of T_m, we have performed a number of different 2-phase simulations and discarded those in which only a small fraction of the cell was either solid or liquid.

Simulations were performed at constant pressure[96] and were begun from configurations that were already very close (within $\sim$ 0.5 GPa) to zero pressure. Clearly, one cannot use two different potentials in the same simulation and so, due to the convergence problem of the solid-parametrized potential, we have performed the two-phase simulations with the liquid potential. A simulation cell containing 1024 atoms was used. Previous investigations[115, 113] have concluded that for systems of more than a few hundred atoms, the finite size effects are negligible.

Simulations which were initially at 2800 K and 3300 K transformed completely into crystal and melt respectively. In five further simulations, solid and liquid were observed to coexist for a long time. Following 20 ps of equilibration the temperature was averaged over a further 15 ps for each simulation. Averages of 2974 K, 2984 K, 3025 K, 3038 K and 3042 K were found for these simulations giving an overall average of 3013 K.

There is some controversy regarding the melting temperature at zero pressure with values of T_m ranging from about 3000 K to about 3250 K[110, 130]. Zerr and Boehler [110] measured the temperature to be 3040 ± 100 K which is close to previous measurements[131, 132], and in excellent agreement with all of our average temperatures. However, recent work[130] suggests that the correct value may be 3250 ± 20 K. Even an error of $\sim$ 250 K

[1] This involves performing a few steps of steepest-descent minimization on the atoms very close to the interface between solid and liquid in order to prevent large increases in the kinetic energy and/or non-convergent polarization due to unphysical ionic separations.

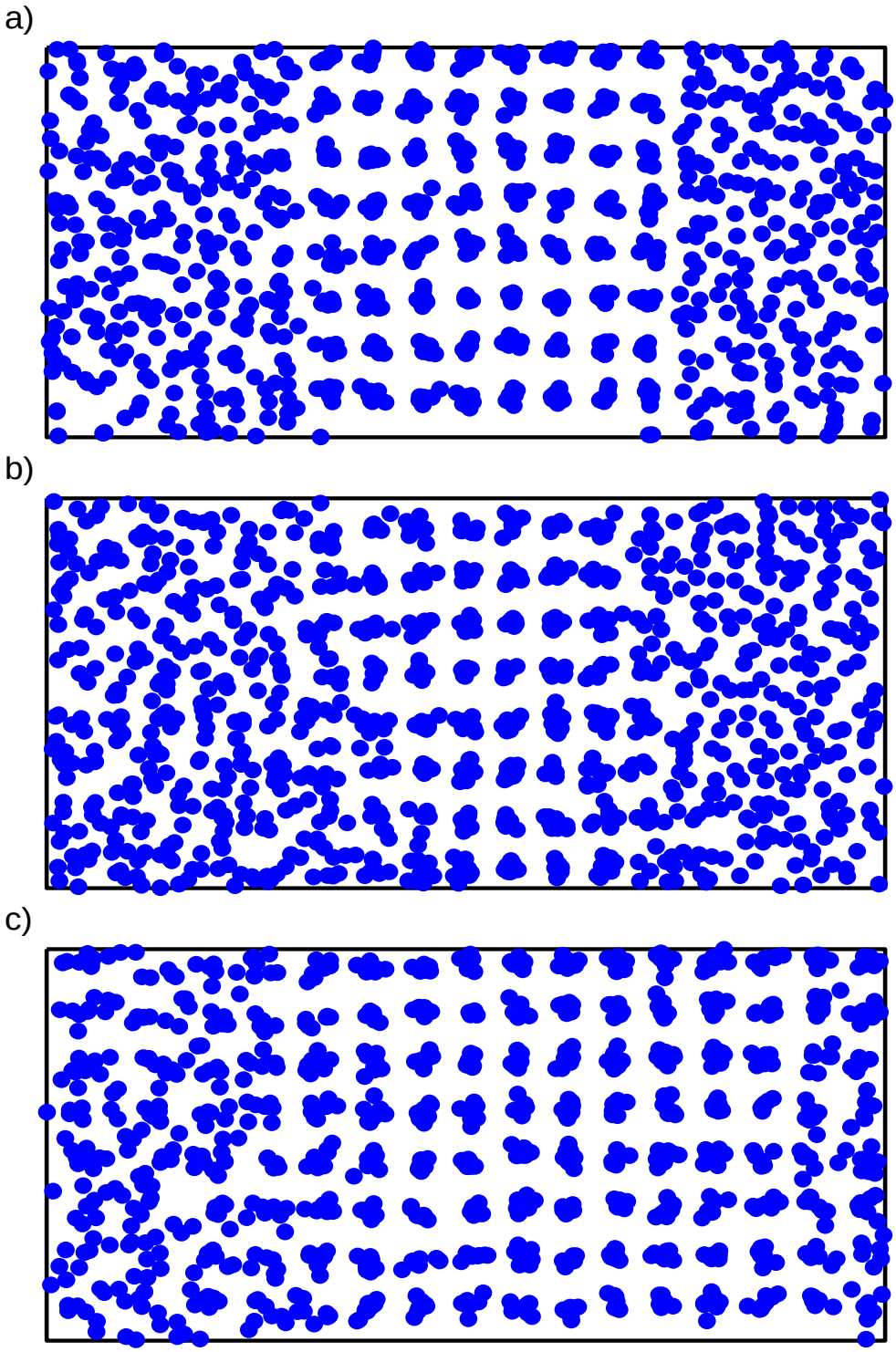

Figure 6.10: The 2-phase melting procedure. a) The simulation cell at the beginning containing 512 atoms of crystalline MgO and 512 atoms of liquid MgO periodically repeated; b) $T > T_m$. The liquid portion has grown at the expense of the solid portion. The interfaces are not as clear as in a) but the center of the cell still shows signs of order, indicating crystallinity while liquid makes up a large portion of the cell on either side; c) $T < T_m$, some of the liquid portion has crystallized. The edges of the cell are still clearly liquid but much of the cell looks relatively ordered.

in our calculated melting temperature is good considering the level of agreement which can generally be obtained using *ab initio* methods[25]. Since we are primarily interested in the melting slope dT_m/dP, and since a 10% level of accuracy would still vastly improve on the current uncertainty of the slope, we have chosen a value $T_m \sim 3100$ K at which to calculate the energy differences and the volume.

Volume and Energy Differences

In order to calculate the volumes in the liquid and solid, we first would like to test that our potentials reproduce the experimental temperature and pressure dependence of the volume in the solid. Since our *ab initio* simulations will be done in cells containing 64 atoms, we also check that finite size effects are not too great. The convergence problem for the solid potential that was mentioned previously has meant that at 3100 K it was not possible to run for a long time. Eventually convergence failed and the simulation had to be abandoned. This was only a problem in the solid at temperatures very close to the melting temperature. For this reason, we have not succeeded in running a simulation near T_m for long enough to get a completely reliable average of the density. We have therefore checked the volume at this temperature using the liquid potential.

The temperature dependence of density is a property which is quite a challenge for effective potentials because thermal expansion depends on the *second* derivatives of the potential energy with respect to ionic positions. In figure 6.11 we plot the equilibrium volume as a function of temperature for system sizes of 512, 216 and 64 atoms. The results are in excellent agreement with experiment. What is most striking is the fact that the finite size effects are very small. We find similar results for the silica potential in chapter 5. It has been shown in other simulations[55, 67] that finite size effects for ionic systems can be considerable. It may be that because we treat the polarization in a realistic way (by fitting to *ab initio* data) the long range electrostatic effects are effectively screened. This is an important quality of our potentials since they are significantly slower to evaluate than pair-potentials and the fact that one can use smaller systems for many applications alleviates some of this burden.

Figure 6.12 shows the equation of state for the 512 atom system compared to experiment and to the DFT results of Karki *et al.*[6]. Once again, the results at low pressures are in excellent agreement with experiment. At higher pressures ($> 20 - 30$ GPa.) the agreement is not as good as was found in figure 6.5 due to the lower radial cutoff for the decay function, however since we are interested in the melting slope at low pressure, this is of little consequence.

We now calculate the volume in the liquid and the solid at zero pressure for temperatures near the melting temperature T_m. The liquid potential was used to calculate the pressure at constant volume for a range of densities (near the zero pressure equilibrium volume) and temperatures (near T_m) using simulation cells containing 512 atoms. From these we extracted the volume as a function of temperature at zero pressure. For the solid, constant pressure simulations were performed in order to extract the equilibrium densities. The results are shown in figure 6.13. It can be seen that the volume difference is not strongly dependent on temperature and that the use of the liquid potential in the

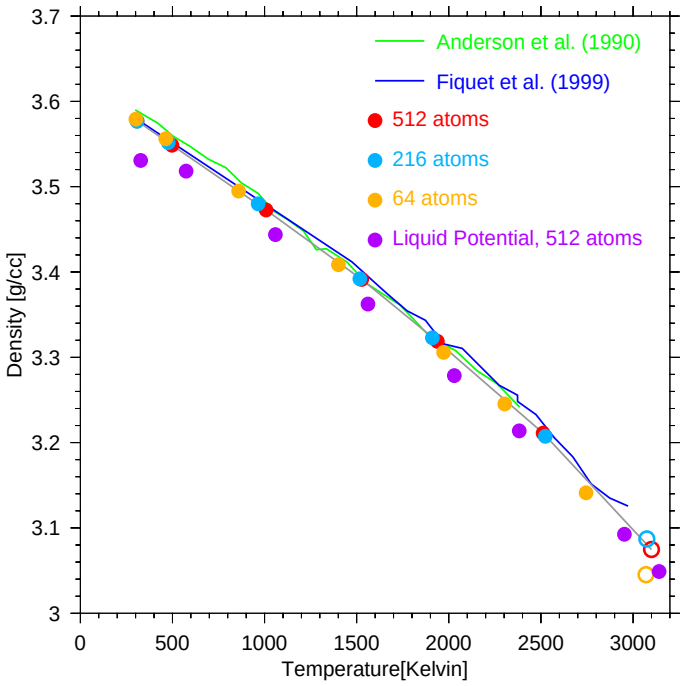

Figure 6.11: The density as a function of temperature compared to experiment[123, 124] for the solid potential with different simulation cell sizes and for the liquid potential. Open symbols indicate that simulations were too short to guarantee reliable averages of the density.

solid is probably justified given the level of agreement with the unconverged data points from the solid potential relative to the difference in volume between solid and liquid. The variation of the volume change ΔV with temperature is quite small (the difference between 2950 K and 3250 K is about 7.2%) and the difference between the (unconverged) results from the solid potential is very small ($\sim 2.6\%$).

We have extracted the average potential energy in the liquid and the solid from the same simulations in which we obtained the densities. The results are shown in figure 6.4. The energy difference between solid and liquid, like the density difference, has a negligible temperature dependence.

The melting slope that we get from these simulations is primarily dependent on the choice of the melting temperature T_m used in equation 6.10 and this dependence is shown in figure 6.15. We get a slope of between 145 K GPa^{-1} and 170 K GPa^{-1} depending on the value of T_m. If we stick to the value of T_m that we have estimated in our 2-phase simulations, the slope is 149.3 K GPa^{-1}. This differs by more than a factor of 4 from the experimental slope of Zerr and Boehler[110] . It is also greater than some of the more recent theoretically determined slopes. For example, Cohen and Weitz found a value of ~ 114 K GPa^{-1}[111] and Strachan*et al* a value of ~ 88 K GPa^{-1}[114].

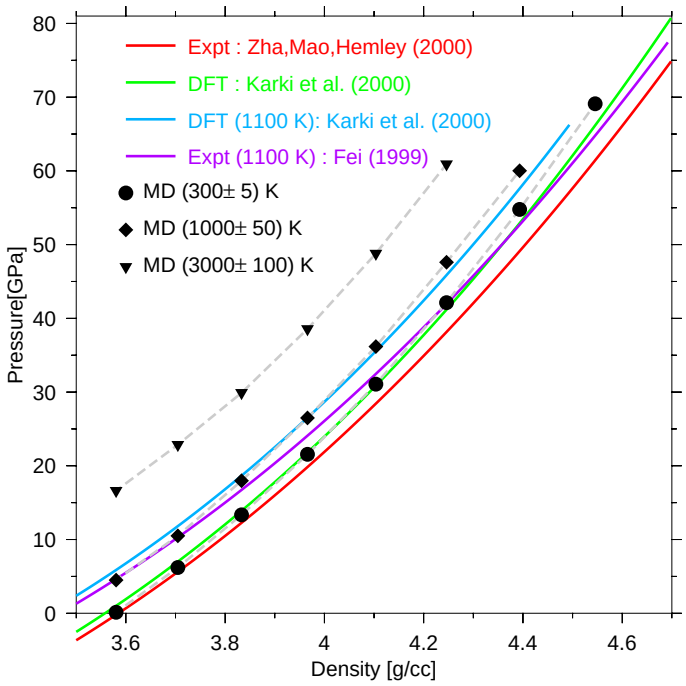

Figure 6.12: The equation of state of the solid-parametrized potential compared to experiment[133, 125] and to density functional perturbation theory[6]

6.4.1 Correcting the melting slope with *ab initio* calculations

The ability of our force-field to fit *ab initio* data suggests that the slope that we have obtained should be very close to the "true" *LDA* result. However, we would like to check that this is the case and correct any errors in the slope to bring it closer to the LDA value. We consider possible errors in the energy differences and volume differences separately. Using our effective potential, long simulations of the solid and the liquid were performed at 3070 K. From each of these simulations 20 well-separated snapshots were extracted and DFT total energy calculations performed on these configurations.

A source of error which it is not possible for us to control is the error inherent in the use of an approximate exchange-correlation functional. Although there is no clear trend for bulk systems as regards which approximate exchange-correlation functional gives the best structural properties, it has been suggested on a number of occasions[97, 25, 134] that generalized gradient approximations improve upon *total energies* with respect to the LDA and that it is possible that for this reason GGAs can significantly improve melting temperatures calculated with DFT[25, 134]. A comparison of properties calculated with different exchange-correlation functional give a hint as to the magnitude of the error due to the use of approximate exchange-correlation functionals. For these reasons, aswell as performing total energy calculations using the LDA, we have performed total energy calculations with the GGA functional of Perdew, Burke and Ezrenhoff[74].

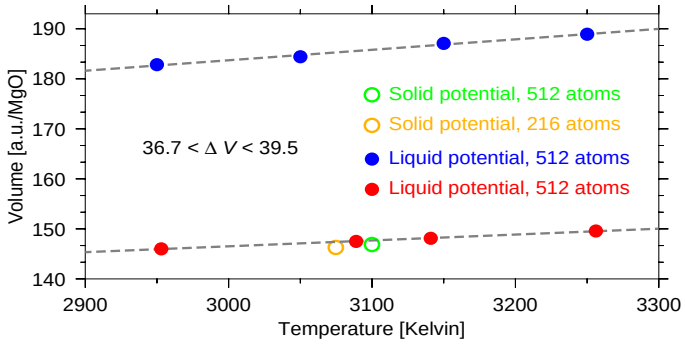

Figure 6.13: The equilibrium volume of the solid and the liquid at zero pressure as a function of temperature. The unconverged values from simulations using the solid-parametrized potential are included for comparison. The dashed lines are a fit to the data and their slightly different slopes account for the range of ΔV indicated.

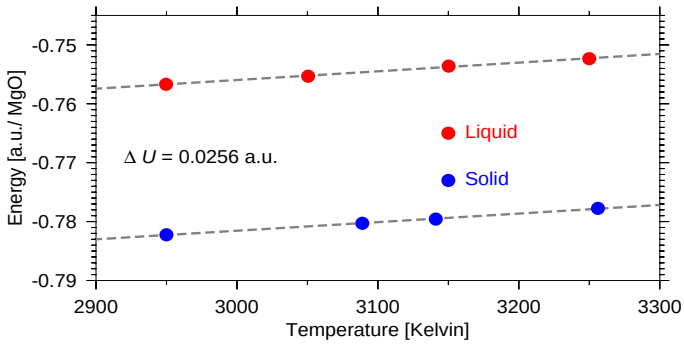

Figure 6.14: The average energy at zero pressure of the solid and the liquid as a function of temperature from our MD simulations. The dashed lines are regression lines the slopes of which differ by only $\sim 1\%$.

Correcting Volume Differences

A possible source of error in our calculated melting slope is that both the solid and the liquid were found to be extremely compressible at temperatures close to the melting temperature. For example, at 3100 K, for our effective potential, the liquid compresses by about 0.12 gcm^{-3} per GPa of applied pressure whereas the solid compresses by only about 0.047 gcm^{-3} per GPa. Our potential reproduces the LDA stress of the liquid and solid within about 0.3 GPa and 0.15 GPa respectively, on average. For the GGA these numbers are 1.3 GPa for the liquid and 1.8 GPa for the solid. The potential does not systematically underestimate or overestimate the internal pressure with respect to the LDA however. We have looked at the average internal pressure on the 20 liquid configurations and the 20 solid configurations with the effective potential and with LDA and GGA. The results are shown in table 6.4. From this table it is clear that, with respect to the LDA, the errors in the volume are very small, both for the solid and for the liquid. The effect of these small differences in pressure is a change in the melting slope of about $\sim 0.5\%$ and so may be

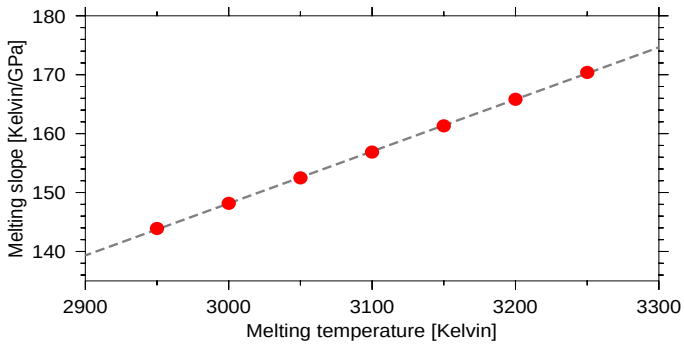

Figure 6.15: The calculated slope of the melting curve as a function of the zero pressure melting temperature T_m. A fit to the calculated points gives the line $y = 0.08831x - 116.782$.

Table 6.4: The average internal pressure (in GPa) on the sample solid and liquid configurations evaluated with LDA, GGA and the effective (liquid-parametrized) potential.

	LDA	Potential	GGA
Solid	-2.84	-2.90	0.26
Liquid	-3.30	-3.29	-1.17

neglected.

A point of some concern considering the high compressibility of both solid and liquid at temperatures near the melting temperature is that the extent to which the potential underestimates the pressure relative to the GGA is different in the solid than in the liquid. This indicates that there may be a difference in the GGA ΔV with respect to the one we have calculated with the LDA. However, in order to do a proper comparison we would need to find ΔV with a GGA-optimized potential because it is possible that some of the stress differences is attributable to atomic configurations which were created with an LDA-optimized potential and which are therefore unnatural within a GGA description. The total change in volume with respect to the LDA also depends on the thermal stress and the compressibility both of which are different in the solid and the liquid. All of these factors mean that it is very difficult for us to estimate what ΔV is for the PBE functional. A crude estimate (which is most likely to be an overestimate due to the calculation of stress on LDA conifgurations) may be obtained using the pressure differences of table 6.4 and the compressibilities of the effective potential. This gives $\Delta V_{PBE} = 52.3$ at 3100 K, an increase of $\sim 37\%$.

We conclude that a very important source of error with our method of calculating the melting slope is related to the ability of approximate exchange-correlation functionals to predict volumes and solid-liquid volume differences to a high accuracy. Although we can get volume differences which are practically identical to those that would be obtained *ab initio* with the functional used in the potential fit, different functionals may give different volume differences.

Correcting Energy Differences

In testing our potential we found errors in energy differences (within a given phase) of 10 to 12% (see tables 6.2 and 6.3). Here we look at the error in the energy difference *between* phases relative to the LDA and the GGA using our effective potential.

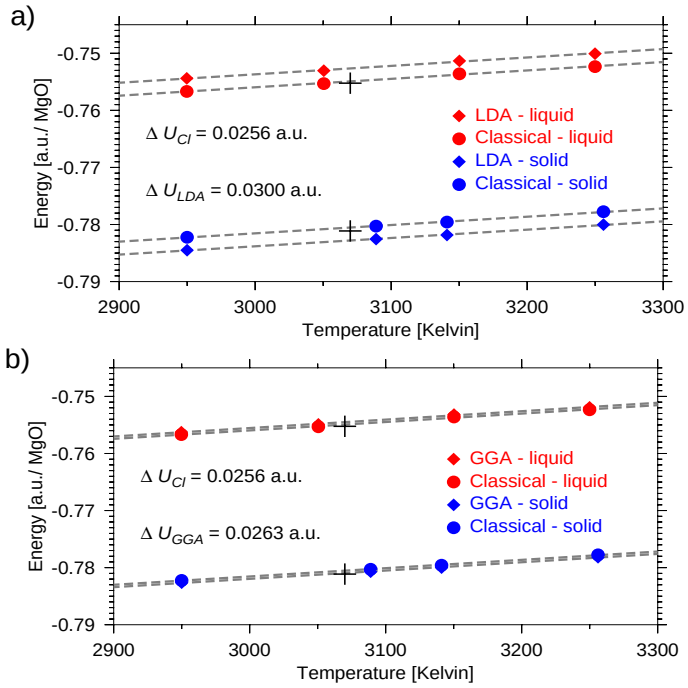

Figure 6.16: The average energy at zero pressure of the solid and the liquid as a function of temperature from our MD simulations, and these energies once corrected using a) LDA DFT calculations and b) GGA DFT calculations. The crosses show the average energy (calculated with the effective potential) in the 20 configurations on which *ab initio* calculations were performed.

The average difference between the *ab initio* energy and the energy from the classical potential ($\Delta_U = U_{\text{a.i.}} - U_{\text{cl}}$) were calculated for both the solid (Δ_U^S) and the liquid(Δ_U^L). The energy as a function of temperature was corrected using the ab initio data by adding the quantity $\Delta_U^S - \frac{1}{2}(\Delta_U^S + \Delta_U^L)$ to the energies of the solid and the quantity $\Delta_U^L - \frac{1}{2}(\Delta_U^S + \Delta_U^L)$ to the energies of the liquid. The results for the LDA and the GGA are given in figures 6.4.1 and 6.4.1 respectively. The fact that we have added the same correction at all temperatures is justified by the observation that the temperature dependence of the energies is very weak.

Although the LDA makes a significant difference ($\sim$ 17%) to the energy difference between solid and liquid (ΔU), the GGA gives almost precisely the same result (within 3%) as our effective potential.

The fact that the average of the energy over the configurations on which the DFT calculations were performed is very close to the average energy from the MD simulations at the same temperature (3070K) is very important. Not only does it suggest that the

number of configurations used is sufficient to obtain meaningful corrections to ΔU, it also means that the finite-size effects are small since the cell size in these configurations was only 64 atoms.

Correcting T_m

We can correct, to first order, the errors in the melting temperature calculated with our potential using the following relationship[135]

$$\frac{\Delta T_m}{T_m} = \frac{\langle U_l^{ai} - U_l^{ep} \rangle_{ep} - \langle U_s^{ai} - U_s^{ep} \rangle_{ep}}{\langle U_l^{ep} \rangle_{ep} - \langle U_s^{ep} \rangle_{ep}} \tag{6.11}$$

where the superscripts '*ai*' and '*ep*' indicate that a quantity has been calculated *ab initio* or with our effective potential, respectively and $\langle \cdots \rangle_{ep}$ indicates an average over a trajectory generated with the effective potential. The corrections can be extracted from the calculations that we have already performed and which are plotted in figure 6.4.1. The LDA melting temperature is $\sim 17\%$ larger at $T_m^{\mathrm{LDA}} = 3531$ K and the GGA melting temperature is 2.7% larger at $T_m^{\mathrm{PBE}} = 3095$ K.

The Melting Slope

We now look at the melting slope as corrected using the DFT calculations and as calculated with our effective potential (EP). We choose the intermediate value $T_m = 3100$K at which to calculate the slopes since T_m is overestimated with the LDA and since all our em ab initio calculations have been performed at close to this temperature. We get

$$m_{\mathrm{LDA}} = 133.86 \ \mathrm{K\ GPa^{-1}} \tag{6.12}$$

$$m_{\mathrm{PBE}} = 209.53 \ \mathrm{K\ GPa^{-1}} \tag{6.13}$$

$$m_{\mathrm{EP}} = 156.87 \ \mathrm{K\ GPa^{-1}} \tag{6.14}$$

These slopes are plotted in figure 6.17. If we calculate what the melting slope in the LDA approximation should be, using the corrected value of $T_m^{\mathrm{LDA}} = 3531$ K, we get $m_{\mathrm{LDA}} = 168.3$ K GPa^{-1}, in closer agreement with the PBE result. However, it is not at all certain that the volumes as a function of pressure in the solid and the liquid can be extrapolated linearly as we have done, or whether energy differences remain constant up to such a high temperature. Even with this correction there is still a large difference in the values of m_{LDA} and m_{PBE} and this shows the level of uncertainty in our calculations which is attributable to the exchange-correlation functional. However even this level of uncertainty cannot explain the huge discrepancy between our results and experiment.

6.5 Discussion

In this chapter we have applied the distortable-ion potential introduced in chapter 3 to MgO and clearly demonstrated its ability to accurately reproduce the *ab initio* potential energy surface. We have then applied this model to the long-standing controversy surrounding the pressure dependence of the MgO melting temperature.

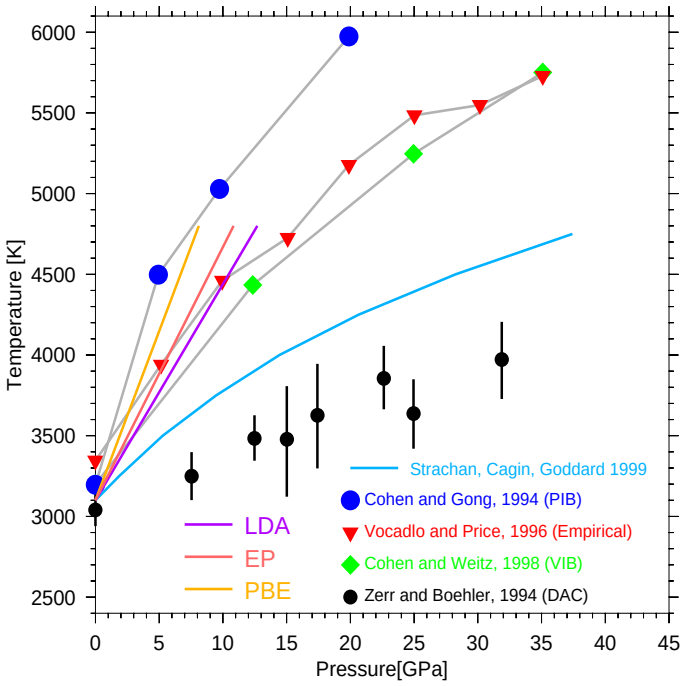

Figure 6.17: The melting temperature of MgO as a function of pressure from experiment[110] and from simulations using the variational induced breathing (VIB) model[111], the potential induced breathing model[112], and the effective potentials of Vocadlo and Price [113] and Strachan,Cagin and Goddard [114]. The melting slopes that we obtain at $T_m = 3100$ K, from our combination of classical MD and DFT calculations are also shown.

We find a melting slope that differs very strongly from the experimental slope. However, we have basically eliminated all our errors except for those inherent in the *ab initio* calculations, i.e. those due to the use of approximate exchange-correlation functionals. The errors due to the approximate exchange-correlation functionals is very large and illustrates the large impact this quantity can have on a calculation. However, while we have shown that different functionals give different melting slopes (by up to 40 or 50%), our theoretical results differ with experiment by a factor of between ~ 4 and ~ 6. It is unlikely that this disagreement is simply due to the exchange-correlation functional.

The melting slope depends on the volume change between solid and liquid and the energy difference between solid and liquid. We have obtained very good agreement with lower temperature data on the volume of the solid as a function of temperature and so is is unlikely that we are substantially underestimating the volume in the solid at higher temperatures. There is no experimental data to compare with in the liquid, however our results compare very well with Car-Parrinello simulations and with what is generally expected from an ionic system of this type. The change in volume that we see is, if anything, small compared to similar compounds (such as LiF) and compared to some previous simulations of MgO[111].

It is also unlikely,that there is a large error in our calculation of total energies. Since

LDA and PBE both gave similar results (within $\sim 15\%$), this would probably require that the structure of the liquid is not representative of the true system. However, the pair-correlation functions that we calculate are in very good agreement with those from CPMD and so this scenario is unlikely.

The discrepancy may be due to an error in the experiment. This possibility has been suggested previously[111, 115, 127]. It may also be that the exchange-correlation functionals that we have used are incapable of modelling some exotic feature of the electronic structure of liquid MgO. This is very unlikely given the ability of DFT to describe properties of the solid[6] and the quality of DFT calculations in general.

The most likely scenario is that the slope of the melting curve is initially very steep, but that it flattens out very quickly, perhaps due to a liquid structure which changes rapidly under pressure to being much more similar to the solid. Pair-correlation functions have been calculated at high pressure[115] and qualitatively similar differences between liquid and solid as we have seen here were found. However, the potential used in these calculations was quite crude and did not include the effect of polarization. Polarization has the tendency to reduce structural changes between solid and liquid[126].

The discrepancy with experiment remains a mystery and suggests that a repeat of the experiment may be in order. Our future theoretical work will investigate the melting temperature at higher pressures in order to check if the discrepancy is due to a rapidly decreasing slope at low pressures.

Chapter 7

Discussion and Conclusions

In this thesis an attempt has been made to find a way in which thermodynamic properties of ionic systems can be predicted with a reasonable degree of accuracy from molecular dynamics simulations. We use the combination of effective parameter-based force-fields and *ab initio* simulations. The high quality of the results that we have obtained for structural and thermodynamic properties of silica and MgO suggest that once a suitable functional form for a force-field is available, the use of *ab initio* parametrization can greatly improve the ability of the force-field to reproduce experimental data.

We use a slightly modified form of a previously proposed *ab initio* parametrization process[69, 70] which has the advantage that one can make very specific and non-trivial statements about potentials created : It can be said that for any atomic configuration created with the potential under specified thermodynamic conditions, the forces are, on average, within X% of those calculated *ab initio*[1], the stress components within Y%, and the energy-differences between configurations within Z%.

However, our experience with the BKS [88] force-field for silica (see chapter 5) has shown us that unless the functional form is physically appropriate for the system at hand this method of parametrization fails to improve upon the ability of the potential to reproduce experimental data. *The form of the potential is crucial to the success of the method.* For ionic systems electrostatics dominate the interionic forces, and by including ionic polarization one can greatly improve the ability of the force-field to model structural properties.

Energetics and dynamics are more difficult to model. Although the positions of minima in the potential energy surface seem to be mainly determined by electrostatics, the energy barriers between minima and the details of the surface that contribute to dynamics also depend strongly on other factors. We have described in chapter 3 the various approaches that have been taken in the past to modelling such effects as anion "breathing" and distortion. These involve translating this complicated quantum-mechanical electronic behaviour into a simplified phenomenological picture. This phenomenological approach is necessary in order to formulate force-fields which are economical and capable of approximating interactions between ions.

[1] For a specified *ab-initio* calculation. Pseudopotentials, basis sets, sampling techniques and exchange-correlation functionals must all be specified.

For MgO we have aspired to modelling features of the ions' potential energy surface which govern dynamics and energetics and been quite successful if one is to judge by such quantities as phonon dispersion relations and thermal expansion. A force-field has been proposed which is mathematically equivalent yet superior from a computational point of view to a commonly used method of modelling anion breathing effects[47]. This model has been extended to include aspherical distortions in a way which seems plausible *assuming the effectiveness of the compressible-ion model.* This "distortable-ion" model depends on a number of constituent functions. We have postulated forms for these functions in order to perform the preliminary testing of the model. We have not researched these forms in any detail. This is an important endeavour if this potential is to be used in the future. Our tests have shown that the model is indeed an improvement over simple pair potentials despite the lack of research into its constituent functions, indicating that further improvement could be achieved by investigating the optimal form of these functions.

In order to be able to confidently model dynamics such as diffusion or temperature-induced soft-mode phase transitions it is vital to have a potential which accurately reproduces energy barriers. Within our parametrization procedure, which, due to the sheer quantity of data involved, is mainly focussed on forces, it is difficult to see how this may be achieved except by making the functional form more realistic. The distortable-ion potential presented is one quite general framework within which this may be achieved. It is attractive due to the generality of its form, its non-reliance on an extended Lagrangian formalism and its computational speed. It is also easy to envisage extensions to the model such as the inclusion of a self-consistent procedure for the local radii, σ_{IJ}, or an extension beyond the dependence of forces only on the distance between ions *along their line of centers.* However further testing is necessary.

A very important open question remains if one is to use the parametrization scheme of chapter 4 or judge the value of a force-field on the basis of its ability to reproduce forces in an averaged way as we have done thoughout this thesis : How do errors in the forces manifest themselves in thermodynamic properties ? It is very unlikely that there is a general answer to this question. It is also very unlikely that the only thing that matters is the average error in the force on an ion. Small, rare and subtle forces may have the ability to make qualitative differences to a system. We have not tackled this problem and it is certainly one that needs attention.

It has clearly been shown in this thesis that one can achieve high accuracy in many quantities with effective force-fields. We have applied the method proposed to study an important outstanding problem in geophysics : the melting line of MgO. In this case we demonstrate how accurate force-fields and *ab initio* methods can be used together to reduce the uncertainty to close to that inherent in the *ab initio* method.

Acknowledgments

I would like to thank my advisor, Sandro Scandolo, for teaching me so much about physics. His door was always open, it was fun working with him, and he didn't lose patience when anybody else would have.

I want to thank my parents for providing me with every opportunity I needed to get this far and for always being there if I needed them.

I want to thank Roberto Car for giving me the opportunity to work in his group at Princeton University where I found myself a part of a very stimulating and enjoyable environment. Thanks also to all the people there who helped in my work and play.

Many people over four years were very helpful and contributed significantly to this thesis. Those that spring to mind are Alessandro Laio for helping me as I was starting out; Erio Tosatti for answering my occasional questions; Andrea Trombettoni and Gabriele Cipriani for acting as surrogate advisors when Sandro and I were on different continents...it was invaluable to have somebody to bounce ideas off; Carlo Cavazzoni is, for good reason, one of the most-thanked people in SISSA theses and he generously gave his time to me whenever I asked for his help; Mike Payne and Nicola Marzari helped me by carefully reading the work on the Car-Parrinello method and providing some valuable suggestions; Young-gui Yoon took on the unenviable task of deciphering my code and then gave it back to me, parallelized. I know I've forgotten somebody important. I want to generally thank SISSA and the SISSA condensed matter theory sector for pushing me so hard and for providing an environment from which one emerges a better scientist.

An exhaustive list of the friends who have made my life enjoyable over the last four years would insult whoever I forgot, so I'll just thank Mohinish for dinner.

Finally, thanks to Lia.

Bibliography

[1] J. Bardeen, L. N. Cooper, and J. R. Schrieffer Phys. Rev. 108, 1175-1204 (1957) ; Phys. Rev. 106, 162-164 (1957) .

[2] P. Hohenberg and W. Kohn, Phys. Rev. **136**, B864 (1964).

[3] W. Kohn and L. Sham, Phys. Rev. **140**, A1133 (1965).

[4] R. Car and M. Parrinello, Phys. Rev. Lett. **55**, 2471 (1985).

[5] B. B. Karki, R. M. Wentzcovitch, S. de Gironcoli and S. Baroni, Science **286**, 1705 (1999).

[6] B. B. Karki, R. M. Wentzcovitch, S. de Gironcoli and S. Baroni, Phys. Rev. B **61**, 8793 (2000).

[7] B. B. Karki, R. M. Wentzcovitch, S. de Gironcoli and S. Baroni, Phys. Rev. B **62**, 14750 (2000).

[8] M. C. Payne, J. D. Joannopoulos, D. C. Allan, M. P. Teter and D. H. Vanderbilt, Phys. Rev. Lett. , **56**, 2656 (1986).

[9] M. P. Teter, M. C. Payne and D. C. Allan, Phys. Rev. B **40**, 12255 (1989)

[10] M. C. Payne, M. P. Teter, D. C. Allan, T. A. Arias, and J. D. Joannopoulos Rev. Mod. Phys. **64**, 1045 (1992).

[11] G. Kresse and J. Hafner, Phys. Rev. B **47**, 558 (1993).

[12] G. Pastore, E. Smargiassi and F. Buda, Phys. Rev. A **44**, 6334 (1991)

[13] D. Marx and J. Hütter, *Modern Methods and Algorithms of Quantum Chemistry*, Proceedings, John von Neumann Institute for Computing, Jüli ch, **3**, 329 (2000).

[14] F. A. Bornemann and C. Schütte, Numer. Math. **78**, 359 (1998).

[15] P. E. Blöchl and M. Parrinello, Phys. Rev. B **45**, 9413 (1992).

[16] P. E. Blöchl Phys. Rev. B **65**, 104303 (2002).

[17] G. Galli and M. Parrinello, in *Computer Simulations in Materials Science*, p. 282, eds. M. Meyer and V. Pontikis (Kluwer, Dordrecht, 1991).

[18] P. E. Blöchl, Phys. Rev. B **50** 17953 (1994).

[19] S. Nosé, Mol. Phys. **52**, 255 (1984).

[20] J. Kohanoff, Comput. Mater. Sci. **2**, 221 (1994).

[21] S. Scandolo *et al*, Phys. Rev. Lett. **74**, 4015 (1995).

[22] N. Trouiller and J. L. Martins, Phys. Rev. **B 43**, 1993 (1991)

[23] F. Tassone, F. Mauri and R. Car, Phys. Rev. B **50**, 10561 (1994).

[24] D. K. Remler and P. A. Madden, Mol. Phys. **70**, 921 (1990).

[25] O. Sugino and R. Car, Phys. Rev. Lett. **74**, 1823 (1995).

[26] O.Schütt, P. Pavone, W. Windl, K. Karch, and D. Strauch, Phys. Rev. B **50**, 3746 (1994).

[27] C. Lee, D. Vanderbilt, K. Laasonen, R. Car, and M. Parrinello, Phys. Rev. B **47**, 4863 (1993)

[28] K. Laasonen, M. Sprik, M. Parrinello, and R. Car, J. Chem. Phys.**99**, 9080 (1993).

[29] M. Sprik, J. Hütter, and M. Parrinello, J. Chem. Phys.**105**, 1142 (1996).

[30] P. L. Silvestrelli and M. Parrinello, J. Chem. Phys.**111**, 3572 (1999).

[31] M. Sprik, J. Phys. : Condens. Matter **12**, A161 (2000).

[32] S. Izvekov and G. A. Voth, J. Chem. Phys.**116**, 10372 (2002).

[33] G.B. Bachelet, D.R. Hamann, and M. Schlüter, Phys. Rev. B **26**, 4199 (1982).

[34] F. Gygi, Phys. Rev B **48**, 11692 (1993).

[35] A. D. Becke, Phys. Rev. A **38**, 3098 (1988); C. Lee, W. Yang, and R. C. Parr, Phys. Rev. B **37** , 785 (1988).

[36] D. M. Ceperley and B. J. Alder, Phys. Rev. Lett. **45**, 566 (1980).

[37] J. Perdew and A. Zunger, Phys. Rev. B **23**, 5048 (1981).

[38] M. J. L. Sangster and M. Dixon Adv. Phys. **23**, 247, (1976).

[39] M. Born. and J. E. Mayer Z. Phys., **75**, 1 (1932).

[40] S. W. de Leeuw, J. W. Perram and E. R. Smith Proc. R. Soc. Lond. A **373**, 27 (1980).

[41] W. Shockley, Phys. Rev. **73** 1273 (1948).

[42] G. D. Mahan, Solid State Ionics **1**, 29 (1980).

[43] B. G. Dick and A. W. Overhauser, Phys. Rev. **112**. 90 (1958).

[44] W. Cochran, Phys. Rev. Lett. **2**, 495 (1959); Crit. Rev. Solid State

[45] M. Stoneham, J. Harding and T. Harker MRS Bulletin **21**, 29 (1996). Sci. **2**, 1 (1971).

[46] U. Schröder, Solid State Comm. **4**, 347 (1966).

[47] M. Wilson, P. A. Madden, N. C. Pyper, and L. H. Harding J. Chem. Phys. **104**, 8068 (1996).

[48] M. Sprik and M. L. Klein J. Chem. Phys. **89**, 7556 (1988).

[49] M. Sprik J. Phys. Chem. **95**, 2283 (1991).

[50] M. Wilson and P. A. Madden, J. Phys. : Condens. Matt. **5**, 2687 (1993); **6**, A151 (1994).

[51] P. Jemmer, M. Wilson, P. A. Madden, and P. W. Fowler J. Chem. Phys. **111**, 2083 (1999).

[52] A. Rowley, P. Jemmer, M. Wilson and P. A. Madden J. Chem. Phys. **108**, 10209 (1998).

[53] A. K. Rappé and W. A. Goddard III J. Phys. Chem. **95**, 3358 (1991).

[54] K. T. Tang and J. P. Toennies J. Chem. Phys. **80**, 3727 (1984).

[55] A. Aguado, L. Bernasconi and P. A. Madden Chem. Phys. Lett. **356**, 437 (2002).

[56] A. Toukmaji, C. Sagui, J. Board and T. Darden J. Chem. Phys. **113**, 10913 (2000).

[57] M. Wilson, B. J. Costa-Cabral and P. A. Madden , J. Phys. Chem. **100**, 1227 (1996)

[58] P. W. Fowler and P. A. Madden, Phys. Rev. B **31**, 5443 (1985).

[59] M. Born and H. Kun, *Dynamical Theory of Crystal Lattices* (Oxford University Press, Oxford 1969).

[60] D. G. Isaak, O. L. Anderson, and T. Goto, Phys. Chem. Miner. **16**, 704 (1989).

[61] H. Oda, O. L. Anderson, D. G. Isaak, and I. Suzuki, Phys. Chem. Miner. **19**, 96 (1 992).

[62] M. J. L. Sangster, J. Phys. Chem. Solids **34**, 355 (1973).

[63] H. Kornfeld, Z. Phys. **22**, 27)1924).

[64] A. Toukmaji, C. Sagui, J. Board and T. Darden J. Chem. Phys.**113**, 10913 (2000).

[65] F. H. Stillinger and C. W. David J. Chem. Phys.**69**, 1473 (1978).

[66] J. A. C. Rullmann and P. Th. van Duijen Mol. Phys. **63**, 451 (1988).

[67] M. Matsui J. Chem. Phys.**108**, 3304 (1998).

[68] N. A. Marks, M. W. Finnis, J. H. Harding, and N. C. Pyper J. Chem. Phys.**114**, 4406 (2001).

[69] F. Ercolessi and J.B Adams, Europhys. Lett. **26**, 583 (1994)

[70] A. Laio, S. Bernard , G. L. Chiarotti , S. Scandolo , E. Tosatti , Science **287**, 1027 (2000) ; A. Laio, Ph.D Thesis, SISSA, Trieste (1999), available to download at : http://www.sissa.it/cm/thesis/1999/laio.ps.gz .

[71] S. Kirkpatrick, C. D. Gelatt, and M. P. Vecchi, Science, **220**, 671-680, (1983).

[72] W. H. Press, W. T. Vetterling, B. P. Flannery, and S. A. Teukolsky, *Numerical Recipes in Fortran 77 and Fortran 90 : the art of scientific and parall el computing, 2nd Ed.* , Camb. Univ. Press (1996).

[73] J. P. Perdew, in *Electronic Structure of Solids '91*, edited by P. Ziesche and H. Eschrig (Akademie Verlag, Berlin, 1991), p. 11.

[74] J. P. Perdew, K. Burke, and M. Ernzerhof Phys. Rev. Lett. **77**, 3865 (1996).

[75] J. Ihm, A. Zunger, and M. L. Cohen, J. Phys. C **4**, 4409 (1979).

[76] W. E. Pickett, Comp. Phys. Rep. **9**, 115 (1989).

[77] J. P. Perdew Phys. Rev. B **33**, 8822 (1986); A. D. Becke Phys. Rev. A **38**, 3098 (1988).

[78] P. A. Cox, *The Electronic Structure and Chemistry of Solids* (Oxford University Press, Oxford, 1987), p. 6.

[79] L. V. Woodcock, C. A. Angell, P. Cheeseman, J. Chem. Phys. **65**, 1565 (1976).

[80] P. Vashishta, R. K. Kalia, J. P. Rino, I. Ebbsjo, Phys. Rev. B. **41** 12197 (1990).

[81] J. R. Chelikowsky, H. E. King Jr., and J. Glinnemann Phys. Rev. B **41**, 10866 (1990).

[82] L. Stixrude and M. S. T. Bukowinski Phys. Rev. B **44**, 2523 (1991).

[83] Chem. Soc. Rev. **25**, 339 (1996).

[84] E. Demiralp, T. Cagin, W. A. Goddard III , Phys. Rev. Lett. **82**, 1708 (1999).

[85] Wilson M., Madden P.A., Hemmati M., Angell C.A., Phys. Rev. Lett **77**, 4023 (1996).

[86] A. Pasquarello and R. Car, Phys. Rev. Lett. **79**, 1766 (1997).

[87] S. Tsuneyuki, M. Tsukada, H. Aoki, Y. Matsui, Phys. Rev. Lett. **61**, 869 (1988)

[88] B. W. H. van Beest, G. J. Kramer, R. A. van Santen, Phys. Rev. Lett. **64** , 1955 , (1990).

[89] See, for example : B. Coluzzi and P. Verrocchio, J. Chem. Phys. **116**, 3789 (2002) ; E. La Nave , H. E. Stanley , F. Sciortino, Phys. Rev. Lett. **88**, 035501 (2002).; J. Horbach and W. Kob, Phys. Rev. B. **60**, 3169 (1999).

[90] A. Trave, P. Tangney, S. Scandolo, A. Pasquarello, R. Car, Phys. Rev. Lett. (submitted).

[91] G.J. Kramer, N. P. Farragher, B. W. H. vanBeest, R. A. van Santen, Phys. Rev. B.

[92] G. A. Gaetani, P.D. Asimow, E. M. Stolper, Geochimica et Cosmochimica Acta

[93] I. Kushiro, J. Geophys. Res **73**, 619 (1976).

[94] S. Tsuneyuki and Y. Matsui, Phys. Rev. Lett. **74**, 3197 (1995).

[95] V. Swamy, S. K. Saxena, B. Sundman, J. Zhang, J. Geophys. Res. **99**, 11787 (1994).

[96] M. Parrinello and A. Rahman, J. Chem. Phys.**76**, 2662 (1982).

[97] D. R. Hamann, Phys. Rev. Lett. **76**, 660 (1996).

[98] A. Trave, Ph.D. Thesis, University of Geneva (2001).

[99] J.L. Barrat , J. Badro , P. Gillet , Molecular Simulation **20** , 17 (1997).

[100] L. Levien, C. T. Prewitt, D. J.Weidner, Am. Mineral. **65** 920 (1980).

[101] W. W. Schmahl, I. P. Swainson, M. T. Dove, A. Graeme-Barber, Zeit. fur Kristall. **201** 125 (1992).

[102] L. Levien, C. T. Prewitt, D. J.Weidner, Am. Mineral. **66** 324 (1981).

[103] N. R. Keskar and J. R. Chelikowsky, Phys. Rev. B **46**, 1 (1992).

[104] J. Horbach and W. Kob, Phys. Rev. B **60**, 3169 (1999).

[105] G. Urbain, Y. Bottinga, and P. Richet, Geochim. Cosmochim. Acta **46**, 1061 (1982).

[106] N. Binggeli, N. Troullier, José Luís Martins, and James R. Chelikowsky, Phys. Rev. B **44**, 4771-4777 (1991).

[107] T. S. Duffy, R. J. Hemley, and H.-k. Mao Phys. Rev. Lett. **74**, 1371-1374 (1995).

[108] D. L. Anderson, *Theory of the Earth* (Blackwell Scientific, Boston, 1989).

[109] A. Chizmeshya, F. M. Zimmermann, R. A. LaViolette, and G. H. Wolf, Phys. Rev. B **50**, 15559 (1994).

[110] A. Zerr and R. Boehler, Nature **371**, 506 (1994).

[111] R. E. Cohen amd J. Weitz, *High Pressure-Temperature Research : Properties of Earth and Planetary Minerals*, edited by M. H. Manghnani and T. Yagi (AGU, Washington, D. C. 1998), p. 185.

[112] R. E. Cohen and Z. Gong, Phys. Rev. B **50**, 12301 (1994).

[113] L. Vocadlo and G. D. Price, Phys. Chem. Minerals, **23**, 42 (1996).

[114] A. Strachan, T. Cagin and W. A. Goddard III, Phys. Rev. B bf 60, 15084 (1999).

[115] A. B. Belonoshko and L. S. Dubrovinsky, Am. Mineral. **81**, 303 (1996).

[116] R. Boehler, Rev. of Geophysics **38**, 221 (2000).

[117] L. Wen and D. V. Helmberger, Science **279**, 1701 (1998).

[118] A. Zerr and R. Boehler, Science **262**, 553 (1993).

[119] G. H. Wolf and M. S. T Bukowinsky, Phys. Chem. Minerals **15**, 209 (1988).

[120] R. G. Gordon and Y. S. Kim, J. Chem. Phys.**56**, 3122 (1972).

[121] R. E. Cohen, L. L. Boyer, and M. J. Mehl, Phys. Rev. B **35**, 5749 (1987).

[122] D. Chandler, *Introduction to Modern Statistical Mechanics*, Oxford. Univ. Press. (1987), Chapter 8.

[123] O. L. Anderson, K Zou, J. Phys. Chem. Ref. Data **19** 69 (1990).

[124] G. Fiquet, P. Richtet, G. Montagnac, Phys. Chem. Miner. **103**, 27 (1999).

[125] C. S. Zha, H. K. Mao, R. J. Hemley, Proc. Nat. Acad. Sc. **97**, 13494 (2000).

[126] A. R. Ubbelohde, *The Molten State of Matter* (Wiley, 1978).

[127] A. R. Belonoshko, R. Ahuja, and B. Johansson, Phys. Rev. B **61**, 11928 (2000).

[128] F. Ercolessi, O. Tomagnini, S. Iarlori, and E. Tosatti, in *Nanosources and Manipulation of Atoms under High Fields and Temperatures : Application s*, edited by Vu Thien Binh, N. Garcia, and K. Dransfeld, NATO ASI Series E, **235** (Kluwer. Dordrecht, 1993), p.185.

[129] J. R. Morris, C. Z. Wang, K. M. Ho, and C. T. Chan, Phys. Rev. B **49**, 3109 (1994).

[130] C. Ronchi and M. Sheindlin, J. App. Phys. **90**, 3325 (2001), and references therei n.

[131] R. N. McNally, F. I. Peters, and P. H. Ribbe, J. Am. Ceram. Soc. **44**, 491 (1961).

[132] B. Riley, Rev. Hautes Temp. Refract. **3**, 327 (1966)

[133] Y. Fei, Am. Mineral. **84** 272 (1999).

[134] X. Wang and R. Car, private communication.

[135] D. Alfe, M. J. Gillan, and G. D. Price, J. Chem. Phys.**116**, 6172 (2002).

99